

Metallicity-dependent nucleosynthetic yields of Type Ia supernovae originating from double detonations of sub- M_{Ch} white dwarfs

Sabrina Gronow^{1,2,*,}, Benoit Côté^{3,4,5}, Florian Lach^{1,2}, Ivo R. Seitenzahl⁶, Christine E. Collins^{7,8}, Stuart A. Sim⁷, and Friedrich K. Röpke^{2,9}

¹ Zentrum für Astronomie der Universität Heidelberg, Astronomisches Rechen-Institut, Mönchhofstr. 12-14, 69120 Heidelberg, Germany

² Heidelberger Institut für Theoretische Studien, Schloss-Wolfsbrunnenweg 35, 69118 Heidelberg, Germany

³ Konkoly Observatory, Research Centre for Astronomy and Earth Sciences, Eötvös Loránd Research Network (ELKH), Konkoly Thege Miklós út 15-17, H-1121 Budapest, Hungary

⁴ ELTE Eötvös Loránd University, Institute of Physics, Budapest, 1117, Pázmány Péter Sétány 1/A, Hungary

⁵ Joint Institute for Nuclear Astrophysics - Center for the Evolution of the Elements, USA

⁶ School of Science, University of New South Wales, Canberra, ACT 2600, Australia

⁷ Astrophysics Research Center, School of Mathematics and Physics, Queen's University Belfast, Belfast BT7 1NN, Northern Ireland, UK

⁸ GSI Helmholtzzentrum für Schwerionenforschung, Planckstraße 1, 64291 Darmstadt, Germany

⁹ Zentrum für Astronomie der Universität Heidelberg, Institut für theoretische Astrophysik, Philosophenweg 12, 69120 Heidelberg, Germany

... ; ...

ABSTRACT

Double detonations in sub-Chandrasekhar mass carbon-oxygen white dwarfs with helium shell are a potential explosion mechanism for a Type Ia supernova. It comprises a shell detonation and subsequent core detonation. The focus of our study is on the effect of the progenitor metallicity on the nucleosynthetic yields. For this, we compute and analyse a set of eleven different models with varying core and shell masses at four different metallicities each. This results in a total of 44 models at metallicities between $0.01 Z_{\odot}$ and $3 Z_{\odot}$. Our models show a strong impact of the metallicity in the high density regime. The presence of ^{22}Ne causes a neutron-excess which shifts the production from ^{56}Ni to stable isotopes such as ^{54}Fe and ^{58}Ni in the α -rich freeze-out regime. The isotopes of the metallicity implementation further serve as seed nuclei for additional reactions in the shell detonation. Most significantly, the production of ^{55}Mn increases with metallicity confirming the results of previous work. A comparison of elemental ratios relative to iron shows a relatively good match to solar values for some models. Super-solar values are reached for Mn at $3 Z_{\odot}$ and solar values in some models at Z_{\odot} . This indicates that the required contribution of Type Ia supernovae originating from Chandrasekhar mass WDs can be lower than estimated in previous work to reach solar values of [Mn/Fe] at [Fe/H]=0. Our galactic chemical evolution models suggest that Type Ia supernovae from sub-Chandrasekhar mass white dwarfs, along with core-collapse supernovae, could account for more than 80% of the solar Mn abundance. Using metallicity-dependent Type Ia supernova yields helps to reproduce the upward trend of [Mn/Fe] as a function of metallicity for the solar neighborhood. These chemical evolution predictions, however, depend on the massive star yields adopted in the calculations.

Key words. Methods: numerical – Nuclear reactions, nucleosynthesis, abundances – Stars: abundances – supernovae: general – white dwarfs

1. Introduction

The nucleosynthetic yields from thermonuclear explosions of carbon-oxygen white dwarfs (CO WDs) depend sensitively on the WD mass and explosion mechanism. Studies on these were carried out by Iwamoto et al. (1999); Brachwitz et al. (2000); Leung & Nomoto (2018); Bravo et al. (2019); Bravo (2019); Leung & Nomoto (2020); Lach et al. (2020) and Gronow et al. (2021) among others. Here, we focus on a further parameter, namely the metallicity of the WD, which originates from the metallicity of the zero-age main sequence progenitor star and leads to a neutron-excess in the WD material. An enhancement of neutrons can be achieved in different ways depending on the total mass of

the WD. In Chandrasekhar mass (M_{Ch}) WDs it originates from the initial metallicity, and, most importantly, from electron capture in high-density regions. This second effect is not found in sub- M_{Ch} WDs as high enough densities are not reached. Instead the metallicity leads to an initial neutron-excess still present when entering the α -rich freeze-out regime. The decrease in the electron fraction Y_e increases the production of neutron-rich iron group elements (IGEs) (Thielemann et al. 1986).

Nuclear statistical equilibrium (NSE) is not reached in the He detonation of a sub- M_{Ch} CO WD with He shell and heavy elements are produced via α -captures. In this density regime the nucleosynthetic yields are affected by the available seed nuclei of the metallicity implementation (Hashimoto et al. 1983; Khokhlov & Érgma 1985; Lach et al. 2020). A neutron-excess is present due to the metallicity and supports the formation of neutron-rich isotopes.

* e-mail: sabrinagronow2@gmail.com, Fellow of the International Max Planck Research School for Astronomy and Cosmic Physics at Heidelberg University (IMPRS-HD)

A metallicity-dependence of the nucleosynthetic yields is expected from observations. Höflich et al. (1998) find that small changes in the spectra can be attributed to the metallicity of the WD. They also find that the effect on the color is stronger and depends on redshift. This is the case as the spectrum is transferred to different color bands at varying redshifts. Other effects are investigated by Umeda et al. (1999) and Iwamoto et al. (1999) who find that a change in metallicity (and therefore a change in Y_e) influences the amount of ^{54}Fe , ^{56}Ni , and ^{58}Ni produced in the explosion. Furthermore, Timmes et al. (2003) attribute some variations found in observations of peak luminosities to different metallicities of the exploding WD. This is in agreement with work by Mazzali & Podsiadlowski (2006) and Bravo et al. (2010). Mazzali & Podsiadlowski (2006) investigate the $(^{54}\text{Fe} + ^{58}\text{Ni}) / ^{56}\text{Ni}$ ratio as a source of the scatter in the light curves and find that their bolometric light curves are fainter with higher ratios (differences of 0.25 mag). Their values for the luminosity decrease over 15 days after peak, Δm_{15} , compare well with observations. In addition, Timmes et al. (2003) derive a linear relation between the metallicity and ^{56}Ni mass produced in the explosion. It is apparent in their models of M_{Ch} WDs at $1/3 Z_{\odot}$ to $3 Z_{\odot}$ that the amount of produced ^{56}Ni decreases by 25% going to higher metallicity. A determination of the metallicity from SN observations is attempted by Lentz et al. (2000) and Taubenberger et al. (2008), though they are affected by large uncertainties originating from the imprecision of the observations themselves as well as potential degeneracies between metallicity and other effects on the spectra.

SNe Ia play a key role in galactic chemical evolution (GCE) (e.g., Greggio & Renzini 1983; Matteucci & Greggio 1986; Kobayashi et al. 1998; Lach et al. 2020). The nucleosynthetic yields which are found in explosion simulations are crucial input parameters for GCE models. Comparing GCE predictions with the composition of the Milky Way and other galaxies helps to constrain the explosion mechanism and identify the importance of various proposed SN Ia progenitors. Previous GCE studies suggested that multiple SN Ia channels should have contributed to the synthesis of Mn (e.g., Seitenzahl et al. 2013a; Cescutti & Kobayashi 2017), including a possible $\sim 25 - 75\%$ contribution from sub- M_{Ch} explosions in the solar neighbourhood (e.g., Seitenzahl et al. 2013a; Kobayashi et al. 2020; Eitner et al. 2020). Additional GCE studies suggested that chemical evolution trends derived from spectroscopy are better reproduced with models that include metallicity-dependent SN Ia yields (e.g., Kobayashi et al. 1998; Cescutti et al. 2008; North et al. 2012). Work by de los Reyes et al. (2020) suggests that the dominant progenitors are sub- M_{Ch} WDs at early times shifting to M_{Ch} WDs at later times based on their comparison of data from dwarf spheroidal galaxies with extended star formation history to theoretical models.

We investigate the dependence of the nucleosynthetic yields of thermonuclear explosions of sub- M_{Ch} CO WDs with He shell on the metallicity of the progenitor star as a follow-up study to the work presented in Gronow et al. (2021). The simulations of Gronow et al. (2021) follow a double detonation of the WD. In this scenario a He detonation is ignited at the base of the shell due to thermal instabilities. It causes a second, core detonation when the shock wave converges off-center in the core (converging shock mechanism), or when the He detonation wave converges at the antipode to its ignition spot (scissors mechanism). In a third scenario, a carbon detonation is ignited at the core-shell interface directly after He ignition (edge-lit mechanism). Gronow et al. (2021) compute a set of models exploring different core and He shell masses at solar metallicity. On the basis of

these models three more metallicity values of the WD are examined in this work spanning the range from $0.01 Z_{\odot}$ to $3 Z_{\odot}$. This work is one of the first to cover the parameter space for sub- M_{Ch} CO WDs with He shell (see also Leung & Nomoto 2020). Other work (e.g., Sim et al. 2010; Shen et al. 2018) investigates pure detonations of sub- M_{Ch} CO WDs.

The methods and model setup are described in Section 2. The results of the nucleosynthesis calculations are presented in Section 3 including a comparison of elemental ratios relative to iron to solar values. In Section 4 the results are compared to previous works. We discuss the implication of our SN Ia yields in a GCE context in Section 5. Conclusions are drawn in Section 6.

2. Methods and Model setup

In our hydrodynamic simulations of explosions of CO WDs with He shells, the metallicity is represented by ^{14}N and ^{22}Ne . During the evolution of the WD progenitor star and its companion ^{14}N is formed in hydrogen burning via the CNO cycle from pre-existing C, N, and O at zero-age main sequence. In subsequent He burning of the WD progenitor, it is converted to ^{22}Ne via $^{14}\text{N}(\alpha, \gamma)^{18}\text{F}(\beta^+, \nu_e)^{18}\text{O}(\alpha, \gamma)^{22}\text{Ne}$. There, the metallicity of the progenitor star ends up as ^{14}N in the He shell and ^{22}Ne in the CO core. A homogeneous distribution of ^{22}Ne is employed in the core. This is a reasonable assumption as sedimentation of ^{22}Ne in the rather extended sub- M_{Ch} WDs is not expected to have a significant effect (see Bildsten & Hall 2001; Deloye & Bildsten 2002; García-Berro et al. 2008).

In a postprocessing step, we increased the number of species included to represent the metallicity in order to obtain detailed nucleosynthetic yields. In our simulations the isotopes coming from the implementation of the metallicity influence the final yields.

Our study is based on results of the hydrodynamics simulations of Gronow et al. (2021). Their explosion simulations were carried out with the AREPO code (Springel 2010) in 3D. Details on the method can be found in Gronow et al. (2021) and references therein. The models cover a range of different core and shell masses. The core mass of their models is between $0.8 M_{\odot}$ and $1.1 M_{\odot}$ with shell masses of $0.02 M_{\odot}$ to $0.1 M_{\odot}$.

We used the temperature and density evolution of the two million tracer particles from their explosion simulations (Gronow et al. 2021). These tracers had a random distribution in the initial WD which sampled the mass distribution of the WD and represented equal fractions of the material. They allow us to determine detailed nucleosynthetic yields and the ejecta structure of the SN Ia explosion models (Travaglio et al. 2004). The evolution of the temperature and density of tracers which were initially located in the He shell and CO core of Model M10_03_1 are shown in Figure 1 in red and blue, respectively. The tracers were chosen at random while, nevertheless, representing a typical evolution of tracers in these regions. The peaks in the profiles illustrate well that the He detonation reached the tracer particle in the He shell in the first 0.4 s before the C detonation had an impact on the tracer particle in the core. Following this, the tracer particle from the He shell exhibits another rise in temperature and density as a shock wave originating from the C detonation reaches its position. Gronow et al. (2021) carried out a postprocessing step involving a large nuclear reaction network consisting of 384 isotopes. The models in their study assumed solar metallicity of the zero-age main sequence progenitor star.

We followed up on this by re-calculating the postprocessing step using the parameters of the hydrodynamic sim-

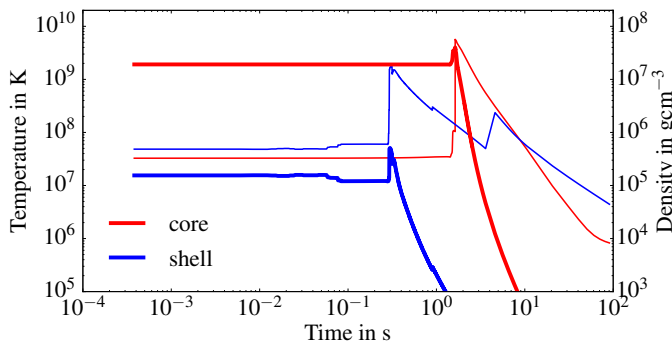


Fig. 1: Temperature (thin lines) and density (thick lines) evolution of a shell (blue) and core (red) tracer particle of Model M10_03_1.

ulations which are listed in Tables 1 and 2 of Gronow et al. (2021), and Gronow et al. (2020) for Models M2a and M2a_pp. Our additional models assume three different metallicities, 0.01, 0.1, and $3 Z_{\odot}$. For this, we scaled the solar abundances given by Asplund et al. (2009). However, according to Prantzos et al. (2018) at sub-solar metallicity we kept the abundance ratios of the α -elements fixed (i.e., $[C/Fe]=0.18$, $[O/Fe]=0.47$, $[Mg/Fe]=0.27$, $[Si/Fe]=0.37$, $[S/Fe]=0.35$, $[Ar/Fe]=0.35$, $[Ca/Fe]=0.33$, $[Ti/Fe]=0.23$) which is motivated by observations of low-metallicity stars. Similar to Gronow et al. (2021), we used this set of elements to represent metallicity in the postprocessing step along with the initial profile of the composition. In the initial profile of the hydrodynamic simulations, the metallicity was set by including ^{14}N and ^{22}Ne in the shell and core, respectively (see Gronow et al. 2021). We point out that some core material was mixed into the shell during the relaxation step (see Gronow et al. 2020 and Gronow et al. 2021 for a detailed description of the relaxation step) adding some ^{12}C and ^{22}Ne to the shell. A total of 384 species was followed in the postprocessing step. In the same way as Gronow et al. (2021) and following the methods in Pakmor et al. (2012), the REACLIB data base (Rauscher & Thielemann 2000) in its 2014 version was used. Weak reaction rates were taken from Langanke & Martínez-Pinedo (2001).

Major differences between our approach and a full re-calculation of the hydrodynamics were not expected. This was the case since the changes in the ^{14}N and ^{22}Ne abundances at the different metallicities do not alter the energy release in the hydrodynamic simulations significantly. It is different to deflagrations where the buoyancy, and therefore Rayleigh-Taylor instabilities, depend on Y_e . In contrast to detonations, the propagation of a deflagration front is thus affected by the metallicity (e.g., Meakin et al. 2009). The assumption we made here is confirmed by the comparison of the models presented in Table 1. Model M2a is taken from Gronow et al. (2020). The model was calculated at zero metallicity and has a total mass of $1.05 M_{\odot}$ with a He shell of $0.07 M_{\odot}$ at He ignition. Model M10_05_1, on the other hand, has a similar mass configuration, though it was calculated at solar metallicity (Model M10_05 in Gronow et al. 2021). Model M2a_pp is the same model as Model M2a, but the postprocessing step was calculated with solar metallicity instead of zero metallicity. An inspection of the abundances of Models M2a_pp and M10_05_1 at $t = 100$ s after He detonation ignition shows that the results of the postprocessing step with varying metallicities are in reasonable good agreement with a full re-calculation of the hydrodynamic model. The maximum difference in the yields produced in the core detonation is only

10%, while the maximum difference is 50% in the He detonation (excluding ^{12}C in both). However, differences in the yields produced in the He detonation can in part be attributed to the slightly different setups of Model M2a (and therefore Model M2a_pp) and Model M10_05_1 at the beginning of the relaxation simulation, with the differences in the total and shell masses being less than 1% (see Gronow et al. 2021 for an explanation of the difference). Generally, the contribution of the yields from the He detonation to the total nucleosynthetic yields are small compared to those of the core detonation. Our approach is thus sufficient to derive nucleosynthetic yields for GCE studies. It saves significant computational costs as additional 3D hydrodynamical simulations of the explosion do not need to be carried out. There might, nevertheless, be slight differences visible in the observables because they are sensitive to the products of the He shell detonation (Höflich et al. 1996; Nugent et al. 1997; Kromer et al. 2010).

Our models are named based on the initial core mass (first two digits), the initial shell mass (two digits) and metallicity relative to solar. Models M08_10_r and M09_10_r of Gronow et al. (2021) are renamed to M08_10 and M09_10, respectively, for simplicity. The use of names such as M10_05 refers to all models with an initial core mass of $1.0 M_{\odot}$ and shell mass of $0.05 M_{\odot}$, therefore combining names of four models at different metallicity. The nucleosynthesis yields of the models will be uploaded to the supernova archive HESMA¹ (Kromer et al. 2017).

3. Metallicity-dependent nucleosynthetic yields

In the following, we discuss the effect different metallicities have on the nucleosynthetic yields. For a comparison of the models at different masses (e.g., all M10_10 and M09_05 models) as well as a discussion of the differences in the detonation ignition mechanism of the various models we refer to Gronow et al. (2021). The nucleosynthetic yields are affected by the modeling of the C detonation. The shock strength depends on its propagation history. Because C detonations cannot be spatially resolved in SN simulations, substantial modeling effort is necessary to settle this issue, which is beyond the scope of this work. The relations of the nucleosynthetic yields of the models found by Gronow et al. (2021) are the same for the models at the other metallicities. Our analysis focuses on manganese as well as iron and nickel. These elements originate in most part from SNe Ia (Timmes et al. 1995; McWilliam 1997; Kobayashi et al. 2020), or are a main product of a SN Ia explosion.

Tables 1 to 12 list the nucleosynthetic yields of selected isotopes for all models at $t = 100$ s after He detonation ignition. They are given separately for the He detonation and core detonation. The distinction is based on the initial He mass fraction of the cell a tracer is associated with, thus cells with an initial He mass fraction larger than 0.01 are considered to be part of the shell. The abundances of the models at solar metallicity are taken from Gronow et al. (2021) with additional values given for ^{54}Fe , ^{55}Fe , and ^{58}Ni . The yields of Model M2a are taken from Gronow et al. (2020) and are extended by ^{52}Fe , ^{54}Fe , ^{55}Fe , ^{55}Mn , ^{55}Co , and ^{58}Ni .

Detailed nucleosynthetic yields for the models at 0.01, 0.1, and $3 Z_{\odot}$ are given in the appendix in Tables A.1 to A.22. The yields of the solar metallicity models are included in Gronow et al. (2021). Tables A.1 to A.11 list the abundances of stable nuclides, radioactive nuclides with lifetime longer than 2 Gyr at

¹ <https://hesma.h-its.org>

Table 1: Final abundances for Model M2a⁽¹⁾, M2a_pp, and M10_05_1⁽²⁾.

	He detonation			core detonation		
	M2a ⁽¹⁾	M2a_pp	M10_05_1 ⁽²⁾	M2a ⁽¹⁾	M2a_pp	M10_05_1 ⁽²⁾
	[M _⊙]	[M _⊙]	[M _⊙]	[M _⊙]	[M _⊙]	[M _⊙]
⁴ He	2.3×10^{-2}	2.2×10^{-2}	2.0×10^{-2}	5.0×10^{-3}	4.2×10^{-3}	4.6×10^{-3}
¹² C	1.0×10^{-4}	1.0×10^{-4}	4.0×10^{-5}	8.9×10^{-4}	8.6×10^{-4}	4.4×10^{-4}
¹⁶ O	7.4×10^{-3}	6.8×10^{-3}	9.3×10^{-3}	5.2×10^{-2}	5.6×10^{-2}	6.1×10^{-2}
²⁸ Si	8.9×10^{-3}	9.6×10^{-3}	1.3×10^{-2}	1.6×10^{-1}	1.7×10^{-1}	1.6×10^{-1}
³² S	3.2×10^{-3}	3.6×10^{-3}	4.9×10^{-3}	1.1×10^{-1}	1.0×10^{-1}	9.6×10^{-2}
⁴⁰ Ca	3.6×10^{-3}	3.5×10^{-3}	4.3×10^{-3}	2.3×10^{-2}	1.8×10^{-2}	1.7×10^{-2}
⁴⁴ Ti	7.0×10^{-4}	7.1×10^{-4}	7.9×10^{-4}	2.8×10^{-5}	2.2×10^{-5}	2.1×10^{-5}
⁴⁸ Cr	1.6×10^{-3}	1.6×10^{-3}	2.1×10^{-3}	4.8×10^{-4}	3.7×10^{-4}	3.6×10^{-4}
⁵² Fe	3.2×10^{-3}	3.2×10^{-3}	4.1×10^{-3}	1.0×10^{-2}	8.0×10^{-3}	7.8×10^{-3}
⁵⁴ Fe	2.6×10^{-5}	3.2×10^{-5}	4.2×10^{-5}	9.2×10^{-5}	2.4×10^{-2}	2.2×10^{-2}
⁵⁵ Fe	5.3×10^{-7}	5.7×10^{-7}	7.6×10^{-7}	6.0×10^{-7}	4.9×10^{-5}	5.0×10^{-5}
⁵⁵ Mn	1.6×10^{-7}	5.8×10^{-8}	5.9×10^{-8}	6.4×10^{-10}	4.3×10^{-8}	4.4×10^{-8}
⁵⁵ Co	3.8×10^{-4}	3.9×10^{-4}	4.8×10^{-4}	1.1×10^{-4}	4.1×10^{-3}	4.0×10^{-3}
⁵⁶ Ni	1.2×10^{-2}	1.2×10^{-2}	8.2×10^{-3}	5.7×10^{-1}	5.3×10^{-1}	5.4×10^{-1}
⁵⁸ Ni	2.3×10^{-4}	2.4×10^{-4}	1.2×10^{-4}	8.9×10^{-4}	1.7×10^{-2}	1.8×10^{-2}

References. (1) Gronow et al. (2020), (2) Gronow et al. (2021)

Table 2: Final abundances for Model M10_05_001, M10_05_01, and M10_05_3.

	He detonation			core detonation		
	M10_05_001	M10_05_01	M10_05_3	M10_05_001	M10_05_01	M10_05_3
	[M _⊙]	[M _⊙]	[M _⊙]	[M _⊙]	[M _⊙]	[M _⊙]
⁴ He	2.0×10^{-2}	2.0×10^{-2}	1.9×10^{-2}	5.0×10^{-3}	5.0×10^{-3}	3.3×10^{-3}
¹² C	4.0×10^{-5}	4.0×10^{-5}	4.0×10^{-5}	4.4×10^{-4}	4.4×10^{-4}	4.3×10^{-4}
¹⁶ O	9.2×10^{-3}	9.2×10^{-3}	9.7×10^{-3}	6.0×10^{-2}	6.0×10^{-2}	6.1×10^{-2}
²⁸ Si	1.3×10^{-2}	1.3×10^{-2}	1.3×10^{-2}	1.6×10^{-1}	1.6×10^{-1}	1.6×10^{-1}
³² S	5.0×10^{-3}	5.0×10^{-3}	4.9×10^{-3}	9.9×10^{-2}	9.9×10^{-2}	8.4×10^{-2}
⁴⁰ Ca	4.3×10^{-3}	4.3×10^{-3}	4.3×10^{-3}	1.8×10^{-2}	1.8×10^{-2}	1.3×10^{-2}
⁴⁴ Ti	7.8×10^{-4}	7.8×10^{-4}	8.1×10^{-4}	2.4×10^{-5}	2.4×10^{-5}	1.4×10^{-5}
⁴⁸ Cr	2.1×10^{-3}	2.1×10^{-3}	2.1×10^{-3}	4.0×10^{-4}	4.0×10^{-4}	2.8×10^{-4}
⁵² Fe	4.0×10^{-3}	4.0×10^{-3}	4.4×10^{-3}	8.4×10^{-3}	8.4×10^{-3}	6.4×10^{-3}
⁵⁴ Fe	3.5×10^{-5}	3.5×10^{-5}	5.0×10^{-5}	1.2×10^{-2}	1.2×10^{-2}	5.4×10^{-2}
⁵⁵ Fe	4.1×10^{-7}	4.2×10^{-7}	1.1×10^{-6}	1.8×10^{-5}	1.7×10^{-5}	3.5×10^{-4}
⁵⁵ Mn	3.3×10^{-10}	2.9×10^{-9}	8.7×10^{-8}	4.2×10^{-9}	7.4×10^{-9}	3.3×10^{-7}
⁵⁵ Co	4.8×10^{-4}	4.8×10^{-4}	4.9×10^{-4}	3.0×10^{-3}	2.9×10^{-3}	6.4×10^{-3}
⁵⁶ Ni	8.3×10^{-3}	8.3×10^{-3}	8.1×10^{-3}	5.6×10^{-1}	5.6×10^{-1}	4.8×10^{-1}
⁵⁸ Ni	1.0×10^{-4}	1.0×10^{-4}	1.4×10^{-4}	9.6×10^{-3}	9.4×10^{-3}	4.9×10^{-2}

time $t = 100$ s, and radioactive nuclides with shorter lifetime decayed to stability. The nucleosynthetic yields of some radioactive nuclides with lifetime shorter than 2 Gyr at $t = 100$ s are given in Tables A.12 to A.22. Each table lists the abundances for one hydrodynamic explosion model at different metallicities. The tables are only available in electronic form at the CDS.

3.1. Nucleosynthesis in SNe Ia

The nucleosynthesis in SN Ia explosions can be described as that of explosive silicon (Si) burning with carbon and oxygen serving as fuel. Woosley et al. (1973) distinguish three different

burning regimes: incomplete Si burning, α -rich freeze-out and normal freeze-out from NSE. Details of the burning regimes and their leading reactions are also discussed by Lach et al. (2020). Figure 1 in Lach et al. (2020) illustrates the burning regimes in the $T_{\text{peak}} - \rho_{\text{peak}}$ - plane following Woosley et al. (1973) for explosive Si burning. The burning regimes are also marked in our Figures 2, 3, and 4 by shaded boundaries.

In double detonations of sub-M_{Ch} CO WDs, explosive He burning is taking place as well (Khokhlov 1984; Khokhlov & Érgma 1985). It is, however, clear by comparing Figure 1 of Khokhlov (1984) (see also Khokhlov & Érgma 1985)

Table 3: Final abundances for Model M10_10_001, M10_10_01, M10_10_1, and M10_10_3.

	He detonation				core detonation			
	M10_10_001 [M _⊙]	M10_10_01 [M _⊙]	M10_10_1 ⁽²⁾ [M _⊙]	M10_10_3 [M _⊙]	M10_10_001 [M _⊙]	M10_10_01 [M _⊙]	M10_10_1 ⁽²⁾ [M _⊙]	M10_10_3 [M _⊙]
⁴ He	2.1×10^{-2}	2.1×10^{-2}	2.1×10^{-2}	2.0×10^{-2}	7.1×10^{-3}	7.1×10^{-3}	6.5×10^{-3}	4.5×10^{-3}
¹² C	7.4×10^{-6}	7.3×10^{-6}	1.1×10^{-5}	7.5×10^{-6}	2.5×10^{-6}	2.5×10^{-6}	1.7×10^{-5}	1.1×10^{-6}
¹⁶ O	3.0×10^{-3}	3.0×10^{-3}	3.1×10^{-3}	3.2×10^{-3}	2.7×10^{-3}	2.7×10^{-3}	2.7×10^{-3}	2.7×10^{-3}
²⁸ Si	3.7×10^{-2}	3.7×10^{-2}	3.7×10^{-2}	3.8×10^{-2}	7.3×10^{-2}	7.3×10^{-2}	7.3×10^{-2}	7.3×10^{-2}
³² S	1.6×10^{-2}	1.6×10^{-2}	1.6×10^{-2}	1.6×10^{-2}	5.6×10^{-2}	5.6×10^{-2}	5.4×10^{-2}	4.8×10^{-2}
⁴⁰ Ca	3.4×10^{-3}	3.4×10^{-3}	3.4×10^{-3}	3.5×10^{-3}	1.4×10^{-2}	1.4×10^{-2}	1.3×10^{-2}	1.1×10^{-2}
⁴⁴ Ti	2.7×10^{-4}	2.7×10^{-4}	2.7×10^{-4}	2.8×10^{-4}	2.0×10^{-5}	2.0×10^{-5}	1.8×10^{-5}	1.2×10^{-5}
⁴⁸ Cr	5.3×10^{-4}	5.3×10^{-4}	5.5×10^{-4}	6.0×10^{-4}	4.1×10^{-4}	4.1×10^{-4}	3.8×10^{-4}	3.0×10^{-4}
⁵² Fe	2.0×10^{-3}	2.0×10^{-3}	2.0×10^{-3}	2.0×10^{-3}	9.3×10^{-3}	9.3×10^{-3}	8.7×10^{-3}	7.2×10^{-3}
⁵⁴ Fe	9.4×10^{-4}	9.5×10^{-4}	1.1×10^{-3}	1.1×10^{-3}	1.0×10^{-2}	1.0×10^{-2}	2.3×10^{-2}	4.9×10^{-2}
⁵⁵ Fe	1.8×10^{-6}	1.8×10^{-6}	3.1×10^{-6}	3.7×10^{-6}	3.2×10^{-6}	3.0×10^{-6}	8.0×10^{-6}	8.6×10^{-5}
⁵⁵ Mn	9.9×10^{-10}	3.6×10^{-9}	6.1×10^{-8}	8.6×10^{-8}	1.5×10^{-9}	1.4×10^{-9}	9.1×10^{-8}	9.2×10^{-8}
⁵⁵ Co	2.5×10^{-4}	2.5×10^{-4}	2.7×10^{-4}	2.7×10^{-4}	3.2×10^{-3}	3.1×10^{-3}	4.4×10^{-3}	7.2×10^{-3}
⁵⁶ Ni	4.0×10^{-2}	3.9×10^{-2}	3.9×10^{-2}	3.9×10^{-2}	7.4×10^{-1}	7.5×10^{-1}	7.2×10^{-1}	6.5×10^{-1}
⁵⁸ Ni	5.7×10^{-4}	5.7×10^{-4}	5.7×10^{-4}	5.4×10^{-4}	1.4×10^{-2}	1.4×10^{-2}	3.2×10^{-2}	6.8×10^{-2}

References. (2) Gronow et al. (2021)

Table 4: Final abundances for Model M10_03_001, M10_03_01, M10_03_1, and M10_03_3.

	He detonation				core detonation			
	M10_03_001 [M _⊙]	M10_03_01 [M _⊙]	M10_03_1 ⁽²⁾ [M _⊙]	M10_03_3 [M _⊙]	M10_03_001 [M _⊙]	M10_03_01 [M _⊙]	M10_03_1 ⁽²⁾ [M _⊙]	M10_03_3 [M _⊙]
⁴ He	1.3×10^{-2}	1.3×10^{-2}	1.3×10^{-2}	1.2×10^{-2}	5.5×10^{-3}	5.5×10^{-3}	5.1×10^{-3}	3.6×10^{-3}
¹² C	7.7×10^{-4}	7.7×10^{-4}	7.6×10^{-4}	7.5×10^{-4}	1.2×10^{-3}	1.2×10^{-3}	1.2×10^{-3}	1.2×10^{-3}
¹⁶ O	6.6×10^{-3}	6.6×10^{-3}	6.8×10^{-3}	7.1×10^{-3}	4.8×10^{-2}	4.8×10^{-2}	4.9×10^{-2}	4.9×10^{-2}
²⁸ Si	8.9×10^{-3}	8.9×10^{-3}	8.9×10^{-3}	9.0×10^{-3}	1.5×10^{-1}	1.5×10^{-1}	1.5×10^{-1}	1.5×10^{-1}
³² S	3.7×10^{-3}	3.7×10^{-3}	3.7×10^{-3}	3.7×10^{-3}	9.4×10^{-2}	9.4×10^{-2}	9.1×10^{-2}	8.0×10^{-2}
⁴⁰ Ca	3.2×10^{-3}	3.2×10^{-3}	3.3×10^{-3}	3.5×10^{-3}	1.8×10^{-2}	1.8×10^{-2}	1.6×10^{-2}	1.3×10^{-2}
⁴⁴ Ti	1.0×10^{-3}	1.0×10^{-3}	1.1×10^{-3}	1.2×10^{-3}	2.0×10^{-5}	2.0×10^{-5}	1.8×10^{-5}	1.2×10^{-5}
⁴⁸ Cr	1.7×10^{-3}	1.7×10^{-3}	1.7×10^{-3}	1.5×10^{-3}	4.0×10^{-4}	4.0×10^{-4}	3.7×10^{-4}	2.8×10^{-4}
⁵² Fe	7.3×10^{-4}	7.2×10^{-4}	6.5×10^{-4}	5.1×10^{-4}	8.7×10^{-3}	8.7×10^{-3}	8.1×10^{-3}	6.7×10^{-3}
⁵⁴ Fe	4.7×10^{-6}	4.7×10^{-6}	6.2×10^{-6}	5.3×10^{-6}	1.2×10^{-2}	1.2×10^{-2}	2.7×10^{-2}	5.4×10^{-2}
⁵⁵ Fe	5.6×10^{-8}	6.2×10^{-8}	2.1×10^{-7}	3.3×10^{-7}	1.7×10^{-5}	1.7×10^{-5}	4.8×10^{-5}	3.3×10^{-4}
⁵⁵ Mn	3.4×10^{-10}	3.4×10^{-9}	7.3×10^{-8}	1.1×10^{-7}	3.5×10^{-9}	4.4×10^{-9}	3.8×10^{-8}	2.7×10^{-7}
⁵⁵ Co	1.7×10^{-5}	1.7×10^{-5}	1.7×10^{-5}	1.4×10^{-5}	3.1×10^{-3}	3.0×10^{-3}	4.2×10^{-3}	6.6×10^{-3}
⁵⁶ Ni	6.9×10^{-5}	6.8×10^{-5}	6.0×10^{-5}	4.2×10^{-5}	6.1×10^{-1}	6.1×10^{-1}	5.9×10^{-1}	5.3×10^{-1}
⁵⁸ Ni	2.3×10^{-6}	2.6×10^{-6}	1.4×10^{-5}	2.2×10^{-5}	1.0×10^{-2}	1.1×10^{-2}	2.5×10^{-2}	5.5×10^{-2}

References. (2) Gronow et al. (2021)

to our figures that NSE is not reached in the He detonation of our models.

3.2. Low and intermediate mass elements

The models show a varying impact of the metallicity on the nucleosynthetic yields produced in the He and core detonations. This is the case because its impact is different at higher densities present in the core. As described in Section 1, the metallicity causes a neutron-excess in the core while the isotopes of the metallicity implementation (¹⁴N and ²²Ne among others) serve as seed nuclei for the reactions in the He detonation and in the low density regime of the core (see Shen & Moore 2014, for a discussion of the effect on the detonation speed). The latter ef-

The generally low central density in sub-M_{Ch} CO WDs is an important parameter for the nucleosynthesis as it implies that the regime of normal freeze-out from NSE is not reached. Instead, IGEs are produced in α -rich freeze-out and incomplete Si burning in the core detonation, and in the burning of the He detonation.

Table 5: Final abundances for Model M10_02_001, M10_02_01, M10_02_1, and M10_02_3.

	He detonation				core detonation			
	M10_02_001 [M _⊙]	M10_02_01 [M _⊙]	M10_02_1 ⁽²⁾ [M _⊙]	M10_02_3 [M _⊙]	M10_02_001 [M _⊙]	M10_02_01 [M _⊙]	M10_02_1 ⁽²⁾ [M _⊙]	M10_02_3 [M _⊙]
⁴ He	1.4×10^{-2}	1.4×10^{-2}	1.3×10^{-2}	1.3×10^{-2}	4.2×10^{-3}	4.2×10^{-3}	3.8×10^{-3}	2.7×10^{-3}
¹² C	1.7×10^{-3}	1.7×10^{-3}	1.7×10^{-3}	1.6×10^{-3}	2.0×10^{-3}	2.0×10^{-3}	1.9×10^{-3}	1.9×10^{-3}
¹⁶ O	1.8×10^{-3}	1.8×10^{-3}	1.9×10^{-3}	2.0×10^{-3}	5.7×10^{-2}	5.7×10^{-2}	5.7×10^{-2}	5.8×10^{-2}
²⁸ Si	2.9×10^{-3}	2.9×10^{-3}	2.9×10^{-3}	3.0×10^{-3}	1.7×10^{-1}	1.7×10^{-1}	1.7×10^{-1}	1.7×10^{-1}
³² S	1.6×10^{-3}	1.6×10^{-3}	1.6×10^{-3}	1.7×10^{-3}	1.1×10^{-1}	1.1×10^{-1}	1.0×10^{-1}	9.0×10^{-2}
⁴⁰ Ca	2.3×10^{-3}	2.3×10^{-3}	2.4×10^{-3}	2.5×10^{-3}	2.0×10^{-2}	2.0×10^{-2}	1.8×10^{-2}	1.4×10^{-2}
⁴⁴ Ti	5.7×10^{-4}	5.7×10^{-4}	5.7×10^{-4}	5.5×10^{-4}	2.0×10^{-5}	2.0×10^{-5}	1.8×10^{-5}	1.3×10^{-5}
⁴⁸ Cr	2.5×10^{-4}	2.5×10^{-4}	2.3×10^{-4}	1.9×10^{-4}	4.3×10^{-4}	4.3×10^{-4}	3.9×10^{-4}	3.1×10^{-4}
⁵² Fe	2.9×10^{-5}	2.9×10^{-5}	2.5×10^{-5}	1.9×10^{-5}	9.5×10^{-3}	9.5×10^{-3}	8.8×10^{-3}	7.2×10^{-3}
⁵⁴ Fe	5.0×10^{-7}	5.3×10^{-7}	1.3×10^{-6}	1.6×10^{-6}	1.4×10^{-2}	1.4×10^{-2}	2.5×10^{-2}	6.0×10^{-2}
⁵⁵ Fe	1.1×10^{-8}	1.4×10^{-8}	9.2×10^{-8}	1.5×10^{-7}	1.9×10^{-5}	1.8×10^{-5}	5.3×10^{-5}	3.7×10^{-4}
⁵⁵ Mn	4.6×10^{-10}	4.7×10^{-9}	9.9×10^{-8}	1.4×10^{-7}	3.8×10^{-9}	4.7×10^{-9}	4.4×10^{-8}	3.1×10^{-7}
⁵⁵ Co	1.3×10^{-6}	1.3×10^{-6}	1.5×10^{-6}	1.3×10^{-6}	3.3×10^{-3}	3.3×10^{-3}	4.5×10^{-3}	7.1×10^{-3}
⁵⁶ Ni	1.8×10^{-6}	1.8×10^{-6}	1.9×10^{-6}	1.8×10^{-6}	5.6×10^{-1}	5.6×10^{-1}	5.4×10^{-1}	4.9×10^{-1}
⁵⁸ Ni	9.2×10^{-8}	2.5×10^{-7}	5.8×10^{-6}	9.7×10^{-6}	8.9×10^{-3}	8.7×10^{-3}	1.7×10^{-2}	4.6×10^{-2}

References. (2) Gronow et al. (2021)

Table 6: Final abundances for Model M09_10_001, M09_10_01, M09_10_1, and M09_10_3.

	He detonation				core detonation			
	M09_10_001 [M _⊙]	M09_10_01 [M _⊙]	M09_10_1 ⁽²⁾ [M _⊙]	M09_10_3 [M _⊙]	M09_10_001 [M _⊙]	M09_10_01 [M _⊙]	M09_10_1 ⁽²⁾ [M _⊙]	M09_10_3 [M _⊙]
⁴ He	3.2×10^{-2}	3.2×10^{-2}	3.2×10^{-2}	3.1×10^{-2}	4.2×10^{-3}	4.2×10^{-3}	3.9×10^{-3}	2.8×10^{-3}
¹² C	3.8×10^{-5}	3.8×10^{-5}	3.9×10^{-5}	3.8×10^{-5}	1.4×10^{-4}	1.3×10^{-4}	1.3×10^{-4}	1.3×10^{-4}
¹⁶ O	8.4×10^{-3}	8.4×10^{-3}	8.5×10^{-3}	8.8×10^{-3}	5.5×10^{-2}	5.5×10^{-2}	5.5×10^{-2}	5.6×10^{-2}
²⁸ Si	1.3×10^{-2}	1.3×10^{-2}	1.3×10^{-2}	1.3×10^{-2}	1.5×10^{-1}	1.5×10^{-1}	1.6×10^{-1}	1.5×10^{-1}
³² S	4.4×10^{-3}	4.3×10^{-3}	4.3×10^{-3}	4.3×10^{-3}	9.5×10^{-2}	9.5×10^{-2}	9.2×10^{-2}	8.1×10^{-2}
⁴⁰ Ca	4.7×10^{-3}	4.7×10^{-3}	4.7×10^{-3}	4.8×10^{-3}	1.7×10^{-2}	1.7×10^{-2}	1.6×10^{-2}	1.3×10^{-2}
⁴⁴ Ti	8.7×10^{-4}	8.7×10^{-4}	8.9×10^{-4}	9.1×10^{-4}	1.8×10^{-5}	1.8×10^{-5}	1.6×10^{-5}	1.2×10^{-5}
⁴⁸ Cr	1.9×10^{-3}	1.9×10^{-3}	1.9×10^{-3}	2.0×10^{-3}	3.7×10^{-4}	3.7×10^{-4}	3.4×10^{-4}	2.6×10^{-4}
⁵² Fe	4.0×10^{-3}	4.0×10^{-3}	4.0×10^{-3}	4.1×10^{-3}	8.1×10^{-3}	8.1×10^{-3}	7.5×10^{-3}	6.1×10^{-3}
⁵⁴ Fe	4.0×10^{-5}	4.1×10^{-5}	5.0×10^{-5}	6.0×10^{-5}	1.2×10^{-2}	1.2×10^{-2}	2.2×10^{-2}	5.2×10^{-2}
⁵⁵ Fe	3.7×10^{-7}	3.9×10^{-7}	8.5×10^{-7}	1.2×10^{-6}	1.7×10^{-5}	1.7×10^{-5}	4.7×10^{-5}	3.3×10^{-4}
⁵⁵ Mn	3.5×10^{-10}	3.0×10^{-9}	6.2×10^{-8}	9.0×10^{-8}	7.8×10^{-9}	1.4×10^{-8}	4.5×10^{-8}	3.0×10^{-7}
⁵⁵ Co	3.7×10^{-4}	3.7×10^{-4}	3.7×10^{-4}	3.8×10^{-4}	2.9×10^{-3}	2.8×10^{-3}	3.9×10^{-3}	6.2×10^{-3}
⁵⁶ Ni	2.6×10^{-2}	2.6×10^{-2}	2.6×10^{-2}	2.6×10^{-2}	4.9×10^{-1}	4.9×10^{-1}	4.8×10^{-1}	4.3×10^{-1}
⁵⁸ Ni	6.7×10^{-4}	6.7×10^{-4}	6.6×10^{-4}	6.4×10^{-4}	8.2×10^{-3}	8.0×10^{-3}	1.6×10^{-2}	4.1×10^{-2}

References. (2) Gronow et al. (2021)

fect is important for the production of IMEs as they are mostly produced in the incomplete Si burning regime at maximum densities lower than about 2.5×10^7 g cm⁻³. In the He detonation no or only little influence of the metallicity is observed on the abundances of elements lighter or equal to ⁴⁴Ti. This is also the case for ¹²C, ¹⁶O, and ²⁸Si in the ejecta of the core detonation. The behavior is expected for the fuel of the detonation (C and O) because the detonation propagation is not affected by the metallicity as stated above. Also, IMEs such as ²⁸Si are not produced in NSE. However, it is obvious from the yields produced in the core detonation that an increase in metallicity decreases the ⁴He

abundance, which is a product in the α -rich freeze-out. With increasing neutronization the reaction ⁴He(α n, γ)⁹Be(α ,n)¹²C commences and even becomes dominant in comparison to the triple- α reaction (Howard et al. 1993; Hix & Thielemann 1999) supporting the burning of ⁴He.

3.3. Manganese

⁵⁵Mn is the only stable isotope of manganese. It is produced directly in incomplete Si burning and by the decay of ⁵⁵Co via

Table 7: Final abundances for Model M09_05_001, M09_05_01, M09_05_1, and M09_05_3.

	He detonation				core detonation			
	M09_05_001 [M _⊙]	M09_05_01 [M _⊙]	M09_05_1 ⁽²⁾ [M _⊙]	M09_05_3 [M _⊙]	M09_05_001 [M _⊙]	M09_05_01 [M _⊙]	M09_05_1 ⁽²⁾ [M _⊙]	M09_05_3 [M _⊙]
⁴ He	2.6 × 10 ⁻²	2.6 × 10 ⁻²	2.5 × 10 ⁻²	2.5 × 10 ⁻²	2.1 × 10 ⁻³	2.1 × 10 ⁻³	1.9 × 10 ⁻³	1.3 × 10 ⁻³
¹² C	4.4 × 10 ⁻⁴	4.4 × 10 ⁻⁴	4.3 × 10 ⁻⁴	4.3 × 10 ⁻⁴	2.7 × 10 ⁻³	2.7 × 10 ⁻³	2.6 × 10 ⁻³	2.6 × 10 ⁻³
¹⁶ O	7.1 × 10 ⁻³	7.1 × 10 ⁻³	7.3 × 10 ⁻³	7.6 × 10 ⁻³	7.7 × 10 ⁻²	7.7 × 10 ⁻²	7.8 × 10 ⁻²	7.9 × 10 ⁻²
²⁸ Si	1.0 × 10 ⁻²	1.0 × 10 ⁻²	1.0 × 10 ⁻²	1.0 × 10 ⁻²	1.9 × 10 ⁻¹	1.9 × 10 ⁻¹	1.9 × 10 ⁻¹	1.9 × 10 ⁻¹
³² S	4.5 × 10 ⁻³	4.5 × 10 ⁻³	4.4 × 10 ⁻³	4.5 × 10 ⁻³	1.1 × 10 ⁻¹	1.1 × 10 ⁻¹	1.1 × 10 ⁻¹	9.7 × 10 ⁻²
⁴⁰ Ca	5.1 × 10 ⁻³	5.1 × 10 ⁻³	5.1 × 10 ⁻³	5.2 × 10 ⁻³	2.0 × 10 ⁻²	2.0 × 10 ⁻²	1.8 × 10 ⁻²	1.4 × 10 ⁻²
⁴⁴ Ti	2.0 × 10 ⁻³	2.0 × 10 ⁻³	2.0 × 10 ⁻³	2.1 × 10 ⁻³	1.7 × 10 ⁻⁵	1.7 × 10 ⁻⁵	1.5 × 10 ⁻⁵	1.1 × 10 ⁻⁵
⁴⁸ Cr	4.5 × 10 ⁻³	4.5 × 10 ⁻³	4.6 × 10 ⁻³	5.0 × 10 ⁻³	4.0 × 10 ⁻⁴	4.0 × 10 ⁻⁴	3.7 × 10 ⁻⁴	2.8 × 10 ⁻⁴
⁵² Fe	5.1 × 10 ⁻³	5.1 × 10 ⁻³	5.1 × 10 ⁻³	5.3 × 10 ⁻³	8.8 × 10 ⁻³	8.8 × 10 ⁻³	8.1 × 10 ⁻³	6.6 × 10 ⁻³
⁵⁴ Fe	8.3 × 10 ⁻⁵	8.3 × 10 ⁻⁵	9.1 × 10 ⁻⁵	9.7 × 10 ⁻⁵	1.4 × 10 ⁻²	1.4 × 10 ⁻²	2.5 × 10 ⁻²	5.9 × 10 ⁻²
⁵⁵ Fe	1.1 × 10 ⁻⁶	1.1 × 10 ⁻⁶	1.4 × 10 ⁻⁶	1.6 × 10 ⁻⁶	2.2 × 10 ⁻⁵	2.1 × 10 ⁻⁵	6.1 × 10 ⁻⁵	4.2 × 10 ⁻⁴
⁵⁵ Mn	3.3 × 10 ⁻¹⁰	3.2 × 10 ⁻⁹	6.8 × 10 ⁻⁸	1.0 × 10 ⁻⁷	4.4 × 10 ⁻⁹	5.9 × 10 ⁻⁹	5.7 × 10 ⁻⁸	3.9 × 10 ⁻⁷
⁵⁵ Co	4.1 × 10 ⁻⁴	4.1 × 10 ⁻⁴	4.1 × 10 ⁻⁴	3.9 × 10 ⁻⁴	3.1 × 10 ⁻³	3.1 × 10 ⁻³	4.2 × 10 ⁻³	6.5 × 10 ⁻³
⁵⁶ Ni	2.1 × 10 ⁻³	2.1 × 10 ⁻³	2.0 × 10 ⁻³	1.7 × 10 ⁻³	4.0 × 10 ⁻¹	4.0 × 10 ⁻¹	3.8 × 10 ⁻¹	3.4 × 10 ⁻¹
⁵⁸ Ni	7.3 × 10 ⁻⁵	7.4 × 10 ⁻⁵	1.0 × 10 ⁻⁴	1.1 × 10 ⁻⁴	5.5 × 10 ⁻³	5.4 × 10 ⁻³	1.0 × 10 ⁻²	2.7 × 10 ⁻²

References. (2) Gronow et al. (2021)

Table 8: Final abundances for Model M09_03_001, M09_03_01, M09_03_1, and M09_03_3.

	He detonation				core detonation			
	M09_03_001 [M _⊙]	M09_03_01 [M _⊙]	M09_03_1 ⁽²⁾ [M _⊙]	M09_03_3 [M _⊙]	M09_03_001 [M _⊙]	M09_03_01 [M _⊙]	M09_03_1 ⁽²⁾ [M _⊙]	M09_03_3 [M _⊙]
⁴ He	1.5 × 10 ⁻²	1.5 × 10 ⁻²	1.5 × 10 ⁻²	1.4 × 10 ⁻²	6.7 × 10 ⁻⁴	6.8 × 10 ⁻⁴	5.8 × 10 ⁻⁴	3.3 × 10 ⁻⁴
¹² C	3.5 × 10 ⁻³	3.5 × 10 ⁻³	3.5 × 10 ⁻³	3.4 × 10 ⁻³	4.9 × 10 ⁻³	4.9 × 10 ⁻³	4.9 × 10 ⁻³	4.7 × 10 ⁻³
¹⁶ O	3.8 × 10 ⁻³	3.8 × 10 ⁻³	3.9 × 10 ⁻³	4.2 × 10 ⁻³	9.2 × 10 ⁻²	9.2 × 10 ⁻²	9.2 × 10 ⁻²	9.3 × 10 ⁻²
²⁸ Si	5.8 × 10 ⁻³	5.8 × 10 ⁻³	5.8 × 10 ⁻³	5.9 × 10 ⁻³	2.2 × 10 ⁻¹	2.2 × 10 ⁻¹	2.2 × 10 ⁻¹	2.2 × 10 ⁻¹
³² S	2.7 × 10 ⁻³	2.7 × 10 ⁻³	2.8 × 10 ⁻³	2.9 × 10 ⁻³	1.3 × 10 ⁻¹	1.3 × 10 ⁻¹	1.3 × 10 ⁻¹	1.1 × 10 ⁻¹
⁴⁰ Ca	3.9 × 10 ⁻³	4.0 × 10 ⁻³	4.0 × 10 ⁻³	4.1 × 10 ⁻³	2.2 × 10 ⁻²	2.2 × 10 ⁻²	2.0 × 10 ⁻²	1.6 × 10 ⁻²
⁴⁴ Ti	7.5 × 10 ⁻⁴	7.5 × 10 ⁻⁴	7.2 × 10 ⁻⁴	6.5 × 10 ⁻⁴	1.6 × 10 ⁻⁵	1.6 × 10 ⁻⁵	1.4 × 10 ⁻⁵	1.1 × 10 ⁻⁵
⁴⁸ Cr	1.3 × 10 ⁻⁴	1.2 × 10 ⁻⁴	1.0 × 10 ⁻⁴	7.4 × 10 ⁻⁵	4.3 × 10 ⁻⁴	4.3 × 10 ⁻⁴	3.9 × 10 ⁻⁴	3.0 × 10 ⁻⁴
⁵² Fe	5.2 × 10 ⁻⁶	5.1 × 10 ⁻⁶	4.1 × 10 ⁻⁶	2.7 × 10 ⁻⁶	9.5 × 10 ⁻³	9.5 × 10 ⁻³	8.8 × 10 ⁻³	7.1 × 10 ⁻³
⁵⁴ Fe	1.5 × 10 ⁻⁷	1.9 × 10 ⁻⁷	1.0 × 10 ⁻⁶	1.4 × 10 ⁻⁶	1.6 × 10 ⁻²	1.5 × 10 ⁻²	2.8 × 10 ⁻²	6.6 × 10 ⁻²
⁵⁵ Fe	3.6 × 10 ⁻⁹	7.9 × 10 ⁻⁹	1.3 × 10 ⁻⁷	2.3 × 10 ⁻⁷	2.5 × 10 ⁻⁵	2.5 × 10 ⁻⁵	7.2 × 10 ⁻⁵	4.9 × 10 ⁻⁵
⁵⁵ Mn	6.1 × 10 ⁻¹⁰	6.2 × 10 ⁻⁹	1.3 × 10 ⁻⁷	1.9 × 10 ⁻⁷	9.6 × 10 ⁻⁹	8.0 × 10 ⁻⁹	7.6 × 10 ⁻⁸	4.8 × 10 ⁻⁷
⁵⁵ Co	2.6 × 10 ⁻⁷	2.6 × 10 ⁻⁷	4.3 × 10 ⁻⁷	5.3 × 10 ⁻⁷	3.3 × 10 ⁻³	3.3 × 10 ⁻³	4.5 × 10 ⁻³	7.0 × 10 ⁻³
⁵⁶ Ni	7.5 × 10 ⁻⁷	7.5 × 10 ⁻⁷	1.0 × 10 ⁻⁶	1.3 × 10 ⁻⁶	3.4 × 10 ⁻¹	3.4 × 10 ⁻¹	3.3 × 10 ⁻¹	2.9 × 10 ⁻¹
⁵⁸ Ni	5.0 × 10 ⁻⁸	2.4 × 10 ⁻⁷	7.4 × 10 ⁻⁶	1.3 × 10 ⁻⁵	3.8 × 10 ⁻³	3.7 × 10 ⁻³	7.0 × 10 ⁻³	1.8 × 10 ⁻²

References. (2) Gronow et al. (2021)

⁵⁵Fe. Since the abundance of ⁵⁵Mn usually is orders of magnitudes below that of ⁵⁵Co immediately after the explosive nuclear burning and prior to ⁵⁵Co decay, the production of Mn mainly depends on the ⁵⁵Co production (Truran et al. 1967). Lach et al. (2020) describe in more detail how the Mn production is influenced by different parameters in the double detonation scenario: the shell-core mass ratio, the density of the He shell and the metallicity. The metallicity-effect is discussed in the following while Lach et al. (2020) give a detailed account of the other effects.

In the He detonation, the impact of the metallicity increase on the ⁵⁵Co production is relatively weak. In contrast to that, the direct production of ⁵⁵Mn increases by one order of magnitude for each increase in metallicity (from 0.01 Z_⊙ to 0.1 Z_⊙ to 1 Z_⊙ to 3 Z_⊙). Nevertheless, it only reaches values close to those of ⁵⁵Co for Models M09_03_3 and M08_03_3. ⁵⁵Fe is more abundant than ⁵⁵Mn, and its dependence on metallicity is similarly weak as that of ⁵⁵Co as both are less neutron-rich than ⁵⁵Mn. The changes in the nucleosynthetic yields are a result of the presence of ¹⁴N and, in addition, ²²Ne, which was mixed into the shell during the relaxation step of the hydrodynamic simulation.

Table 9: Final abundances for Model M08_10_001, M08_10_01, M08_10_1, and M08_10_3.

	He detonation				core detonation			
	M08_10_001 [M _⊙]	M08_10_01 [M _⊙]	M08_10_1 ⁽²⁾ [M _⊙]	M08_10_3 [M _⊙]	M08_10_001 [M _⊙]	M08_10_01 [M _⊙]	M08_10_1 ⁽²⁾ [M _⊙]	M08_10_3 [M _⊙]
⁴ He	3.6×10^{-2}	3.6×10^{-2}	3.6×10^{-2}	3.4×10^{-2}	1.5×10^{-3}	1.5×10^{-3}	1.4×10^{-3}	9.9×10^{-4}
¹² C	1.2×10^{-4}	1.2×10^{-4}	1.2×10^{-4}	1.2×10^{-4}	1.1×10^{-3}	1.1×10^{-3}	1.1×10^{-3}	1.0×10^{-3}
¹⁶ O	9.1×10^{-3}	9.1×10^{-3}	9.3×10^{-3}	9.6×10^{-3}	8.0×10^{-2}	8.0×10^{-2}	8.1×10^{-2}	8.2×10^{-2}
²⁸ Si	1.3×10^{-2}	1.2×10^{-2}	1.3×10^{-2}	1.3×10^{-2}	1.9×10^{-1}	1.9×10^{-1}	1.9×10^{-1}	1.9×10^{-1}
³² S	5.6×10^{-3}	5.6×10^{-3}	5.5×10^{-3}	5.6×10^{-3}	1.1×10^{-1}	1.1×10^{-1}	1.1×10^{-1}	9.6×10^{-2}
⁴⁰ Ca	6.2×10^{-3}	6.2×10^{-3}	6.2×10^{-3}	6.3×10^{-3}	1.9×10^{-2}	1.9×10^{-2}	1.7×10^{-2}	1.4×10^{-2}
⁴⁴ Ti	1.8×10^{-3}	1.8×10^{-3}	1.8×10^{-3}	1.8×10^{-3}	1.5×10^{-5}	1.5×10^{-5}	1.4×10^{-5}	1.0×10^{-5}
⁴⁸ Cr	3.8×10^{-3}	3.8×10^{-3}	3.8×10^{-3}	3.9×10^{-3}	3.7×10^{-4}	3.7×10^{-4}	3.3×10^{-4}	2.6×10^{-4}
⁵² Fe	7.3×10^{-3}	7.4×10^{-3}	7.5×10^{-3}	7.9×10^{-3}	7.9×10^{-3}	7.9×10^{-3}	7.3×10^{-3}	6.0×10^{-3}
⁵⁴ Fe	6.3×10^{-5}	6.3×10^{-5}	7.3×10^{-5}	8.7×10^{-5}	1.3×10^{-2}	1.3×10^{-2}	2.3×10^{-2}	5.6×10^{-2}
⁵⁵ Fe	9.7×10^{-7}	9.9×10^{-7}	1.4×10^{-6}	1.7×10^{-6}	2.2×10^{-5}	2.1×10^{-5}	6.1×10^{-5}	4.3×10^{-4}
⁵⁵ Mn	3.3×10^{-10}	3.3×10^{-9}	6.4×10^{-8}	9.3×10^{-8}	3.3×10^{-8}	3.6×10^{-8}	6.8×10^{-8}	4.4×10^{-7}
⁵⁵ Co	9.2×10^{-4}	9.2×10^{-4}	9.4×10^{-4}	9.7×10^{-4}	2.8×10^{-3}	2.8×10^{-3}	3.8×10^{-3}	5.9×10^{-3}
⁵⁶ Ni	1.5×10^{-2}	1.5×10^{-2}	1.5×10^{-2}	1.5×10^{-2}	3.2×10^{-1}	3.2×10^{-1}	3.1×10^{-1}	2.8×10^{-1}
⁵⁸ Ni	1.7×10^{-4}	1.8×10^{-4}	2.1×10^{-4}	2.5×10^{-4}	4.2×10^{-3}	4.1×10^{-3}	7.8×10^{-3}	2.0×10^{-2}

References. (2) Gronow et al. (2021)

Table 10: Final abundances for Model M08_05_001, M08_05_01, M08_05_1, and M08_05_3.

	He detonation				core detonation			
	M08_05_001 [M _⊙]	M08_05_01 [M _⊙]	M08_05_1 ⁽²⁾ [M _⊙]	M08_05_3 [M _⊙]	M08_05_001 [M _⊙]	M08_05_01 [M _⊙]	M08_05_1 ⁽²⁾ [M _⊙]	M08_05_3 [M _⊙]
⁴ He	2.8×10^{-2}	2.8×10^{-2}	2.7×10^{-2}	2.6×10^{-2}	9.8×10^{-5}	9.8×10^{-5}	8.2×10^{-5}	4.6×10^{-5}
¹² C	2.3×10^{-3}	2.3×10^{-3}	2.3×10^{-3}	2.3×10^{-3}	7.5×10^{-3}	7.5×10^{-3}	7.5×10^{-3}	7.2×10^{-3}
¹⁶ O	6.1×10^{-3}	6.1×10^{-3}	6.3×10^{-3}	6.6×10^{-3}	1.2×10^{-1}	1.2×10^{-1}	1.2×10^{-1}	1.2×10^{-1}
²⁸ Si	9.2×10^{-3}	9.2×10^{-3}	9.3×10^{-3}	9.4×10^{-3}	2.3×10^{-1}	2.3×10^{-1}	2.3×10^{-1}	2.3×10^{-1}
³² S	4.7×10^{-3}	4.7×10^{-3}	4.7×10^{-3}	4.8×10^{-3}	1.3×10^{-1}	1.3×10^{-1}	1.3×10^{-1}	1.1×10^{-1}
⁴⁰ Ca	7.8×10^{-3}	7.9×10^{-3}	8.0×10^{-3}	8.5×10^{-3}	2.0×10^{-2}	2.0×10^{-2}	1.9×10^{-2}	1.4×10^{-2}
⁴⁴ Ti	2.6×10^{-3}	2.6×10^{-3}	2.7×10^{-3}	2.9×10^{-3}	1.3×10^{-5}	1.3×10^{-5}	1.2×10^{-5}	9.3×10^{-6}
⁴⁸ Cr	2.7×10^{-3}	2.7×10^{-3}	2.6×10^{-3}	2.4×10^{-3}	3.5×10^{-4}	3.5×10^{-4}	3.1×10^{-4}	2.4×10^{-4}
⁵² Fe	8.9×10^{-4}	8.8×10^{-4}	8.0×10^{-4}	6.4×10^{-4}	7.4×10^{-3}	7.4×10^{-3}	6.8×10^{-3}	5.4×10^{-3}
⁵⁴ Fe	8.7×10^{-6}	8.8×10^{-6}	1.1×10^{-5}	1.1×10^{-5}	1.4×10^{-2}	1.3×10^{-2}	2.4×10^{-2}	5.7×10^{-2}
⁵⁵ Fe	1.5×10^{-7}	1.6×10^{-7}	4.4×10^{-7}	6.4×10^{-7}	2.6×10^{-5}	2.6×10^{-5}	7.5×10^{-5}	5.2×10^{-4}
⁵⁵ Mn	4.7×10^{-10}	4.7×10^{-9}	1.0×10^{-7}	1.5×10^{-7}	5.5×10^{-9}	8.2×10^{-9}	9.9×10^{-8}	5.8×10^{-7}
⁵⁵ Co	3.0×10^{-5}	3.0×10^{-5}	3.1×10^{-5}	2.7×10^{-5}	2.6×10^{-3}	2.6×10^{-3}	3.5×10^{-3}	5.2×10^{-3}
⁵⁶ Ni	7.5×10^{-5}	7.4×10^{-5}	6.7×10^{-5}	5.0×10^{-5}	2.1×10^{-1}	2.1×10^{-1}	2.0×10^{-1}	1.8×10^{-1}
⁵⁸ Ni	2.6×10^{-6}	3.0×10^{-6}	1.9×10^{-5}	3.3×10^{-5}	1.8×10^{-3}	1.8×10^{-3}	3.3×10^{-3}	7.8×10^{-3}

References. (2) Gronow et al. (2021)

The most important effect the metallicity has is the resulting neutron excess and, therefore, lower Y_e (due to ^{22}Ne). This Y_e is approximately conserved during the duration of the explosive burning, which in the case described here happens at time scales that are too short for β -decays to change the electron fraction while densities are too low for electron capture reactions to drive Y_e lower. Effectively, the lower Y_e reduces the free proton abundance during freeze-out, which leads to a net decrease of the destruction of ^{55}Co via $^{55}\text{Co}(p,\gamma)^{56}\text{Ni}$ which is the key reaction governing the final yield of ^{55}Mn (see Table 13 of Bravo & Martínez-Pinedo 2012).

Figure 2 shows the tracer particle distribution of Models M10_03 at four different metallicities (increasing from left to right) with color-coded mass fraction of ^{55}Mn (top) and ^{55}Co (bottom). The trends in the nucleosynthetic yields of ^{55}Mn and ^{55}Co which are produced in the He detonation are visible. The tracer particles of the He detonation are shown in Figure 3 for comparison. Furthermore, Figure 2 illustrates that both isotopes, ^{55}Mn and ^{55}Co , are produced in incomplete Si burning. As discussed by Seitenzahl et al. (2013a), ^{55}Co is destroyed in α -rich freeze-out from NSE by $^{55}\text{Co}(p,\gamma)^{56}\text{Ni}$. The production of ^{55}Mn is, however, several orders of magnitude lower than that of ^{55}Co .

Table 11: Final abundances for Model M08_03_001, M08_03_01, M08_03_1, and M08_03_3.

	He detonation				core detonation			
	M08_03_001 [M _⊙]	M08_03_01 [M _⊙]	M08_03_1 ⁽²⁾ [M _⊙]	M08_03_3 [M _⊙]	M08_03_001 [M _⊙]	M08_03_01 [M _⊙]	M08_03_1 ⁽²⁾ [M _⊙]	M08_03_3 [M _⊙]
⁴ He	1.9×10^{-2}	1.9×10^{-2}	1.8×10^{-2}	1.8×10^{-2}	3.5×10^{-6}	3.5×10^{-6}	3.2×10^{-6}	2.5×10^{-6}
¹² C	3.4×10^{-3}	3.4×10^{-3}	3.3×10^{-3}	3.3×10^{-3}	1.3×10^{-2}	1.3×10^{-2}	1.2×10^{-2}	1.2×10^{-2}
¹⁶ O	2.5×10^{-3}	2.5×10^{-3}	2.6×10^{-3}	2.8×10^{-3}	1.4×10^{-1}	1.4×10^{-1}	1.4×10^{-1}	1.5×10^{-1}
²⁸ Si	4.2×10^{-3}	4.2×10^{-3}	4.2×10^{-3}	4.4×10^{-3}	2.6×10^{-1}	2.6×10^{-1}	2.6×10^{-1}	2.5×10^{-1}
³² S	2.3×10^{-3}	2.3×10^{-3}	2.4×10^{-3}	2.6×10^{-3}	1.4×10^{-1}	1.4×10^{-1}	1.4×10^{-1}	1.2×10^{-1}
⁴⁰ Ca	3.1×10^{-3}	3.1×10^{-3}	3.1×10^{-3}	3.0×10^{-3}	2.2×10^{-2}	2.2×10^{-2}	1.9×10^{-2}	1.5×10^{-2}
⁴⁴ Ti	2.3×10^{-4}	2.2×10^{-4}	2.2×10^{-4}	1.9×10^{-4}	1.3×10^{-5}	1.3×10^{-5}	1.2×10^{-5}	8.9×10^{-6}
⁴⁸ Cr	8.2×10^{-6}	8.1×10^{-6}	7.2×10^{-6}	6.0×10^{-6}	3.2×10^{-4}	3.2×10^{-4}	2.9×10^{-4}	2.1×10^{-4}
⁵² Fe	8.6×10^{-7}	8.6×10^{-7}	8.8×10^{-7}	9.6×10^{-7}	6.2×10^{-3}	6.2×10^{-3}	5.6×10^{-3}	4.5×10^{-3}
⁵⁴ Fe	2.2×10^{-8}	7.5×10^{-8}	1.3×10^{-6}	1.9×10^{-6}	1.3×10^{-2}	1.3×10^{-2}	2.4×10^{-2}	5.4×10^{-2}
⁵⁵ Fe	6.4×10^{-10}	4.0×10^{-9}	9.5×10^{-8}	1.7×10^{-7}	3.0×10^{-5}	2.9×10^{-5}	8.6×10^{-5}	5.9×10^{-4}
⁵⁵ Mn	8.4×10^{-10}	8.5×10^{-9}	1.8×10^{-7}	2.6×10^{-7}	6.3×10^{-9}	2.0×10^{-8}	2.0×10^{-7}	8.1×10^{-7}
⁵⁵ Co	1.1×10^{-7}	1.1×10^{-7}	2.8×10^{-7}	4.3×10^{-7}	2.2×10^{-3}	2.1×10^{-3}	2.8×10^{-3}	4.0×10^{-3}
⁵⁶ Ni	8.0×10^{-7}	8.1×10^{-7}	9.9×10^{-7}	1.2×10^{-6}	1.4×10^{-1}	1.4×10^{-1}	1.3×10^{-1}	1.1×10^{-1}
⁵⁸ Ni	4.3×10^{-8}	1.9×10^{-7}	5.5×10^{-6}	9.2×10^{-6}	1.1×10^{-3}	1.1×10^{-3}	2.0×10^{-3}	4.6×10^{-3}

References. (2) Gronow et al. (2021)

Table 12: Final abundances for Model M11_05_001, M11_05_01, M11_05_1, and M11_05_3.

	He detonation				core detonation			
	M11_05_001 [M _⊙]	M11_05_01 [M _⊙]	M11_05_1 ⁽²⁾ [M _⊙]	M11_05_3 [M _⊙]	M11_05_001 [M _⊙]	M11_05_01 [M _⊙]	M11_05_1 ⁽²⁾ [M _⊙]	M11_05_3 [M _⊙]
⁴ He	1.1×10^{-2}	1.1×10^{-2}	1.0×10^{-2}	9.9×10^{-3}	9.2×10^{-3}	9.2×10^{-3}	8.4×10^{-3}	5.7×10^{-3}
¹² C	5.2×10^{-6}	5.3×10^{-6}	5.7×10^{-6}	5.7×10^{-6}	3.1×10^{-6}	3.1×10^{-6}	2.5×10^{-6}	1.2×10^{-6}
¹⁶ O	3.7×10^{-3}	3.7×10^{-3}	3.8×10^{-3}	4.0×10^{-3}	7.5×10^{-4}	7.5×10^{-4}	7.5×10^{-4}	7.6×10^{-4}
²⁸ Si	5.5×10^{-2}	5.6×10^{-2}	5.6×10^{-2}	5.6×10^{-2}	4.5×10^{-2}	4.5×10^{-2}	4.6×10^{-2}	4.4×10^{-2}
³² S	2.5×10^{-2}	2.4×10^{-2}	2.4×10^{-2}	2.5×10^{-2}	3.8×10^{-2}	3.8×10^{-2}	3.7×10^{-2}	3.4×10^{-2}
⁴⁰ Ca	5.7×10^{-3}	5.7×10^{-3}	5.7×10^{-3}	5.8×10^{-3}	1.1×10^{-2}	1.1×10^{-2}	1.0×10^{-2}	9.1×10^{-3}
⁴⁴ Ti	1.5×10^{-4}	1.5×10^{-4}	1.6×10^{-4}	1.7×10^{-4}	2.0×10^{-5}	2.1×10^{-5}	1.7×10^{-5}	1.2×10^{-5}
⁴⁸ Cr	7.2×10^{-4}	7.2×10^{-4}	7.4×10^{-4}	8.0×10^{-4}	3.5×10^{-4}	3.5×10^{-4}	3.2×10^{-4}	2.6×10^{-4}
⁵² Fe	2.0×10^{-3}	2.0×10^{-3}	2.1×10^{-3}	2.2×10^{-3}	7.8×10^{-3}	7.8×10^{-3}	7.3×10^{-3}	6.1×10^{-3}
⁵⁴ Fe	1.5×10^{-3}	1.5×10^{-3}	1.7×10^{-3}	1.8×10^{-3}	8.0×10^{-3}	7.8×10^{-3}	1.5×10^{-2}	3.8×10^{-2}
⁵⁵ Fe	4.5×10^{-6}	4.6×10^{-6}	6.9×10^{-6}	8.0×10^{-6}	1.8×10^{-6}	1.9×10^{-6}	4.5×10^{-6}	3.4×10^{-5}
⁵⁵ Mn	1.6×10^{-9}	4.1×10^{-9}	6.4×10^{-8}	9.2×10^{-8}	3.3×10^{-10}	7.4×10^{-10}	5.7×10^{-8}	6.6×10^{-8}
⁵⁵ Co	2.1×10^{-4}	2.1×10^{-4}	2.2×10^{-4}	2.2×10^{-4}	2.6×10^{-3}	2.6×10^{-3}	3.7×10^{-3}	6.1×10^{-3}
⁵⁶ Ni	1.2×10^{-2}	1.2×10^{-2}	1.2×10^{-2}	1.1×10^{-2}	8.5×10^{-1}	8.5×10^{-1}	8.3×10^{-1}	7.5×10^{-1}
⁵⁸ Ni	1.9×10^{-4}	1.9×10^{-4}	2.0×10^{-4}	2.1×10^{-4}	1.8×10^{-2}	1.8×10^{-2}	3.0×10^{-2}	8.1×10^{-2}

References. (2) Gronow et al. (2021)

The amount of ⁵⁵Co produced in the core detonation doubles from lowest to highest assumed metallicity, while the production of ⁵⁵Mn shows a steeper increase with metallicity. The increase in ⁵⁵Co is visible in the bottom panel of Figure 2: more ⁵⁵Co is produced in the lower temperature and density regime. The presence of ²²Ne has the same effect on the nucleosynthesis of the core detonation as on the He detonation (²²Ne was mixed into the shell during the relaxation) since the isotopes are produced in the same temperature and density region in both cases. Generally, in both the He and core detonations, it is visible that the presence of ²²Ne, and with that the metallicity of the progenitor

star, has a strong impact on the production of Mn as suggested by Seitenzahl et al. (2013a).

Manganese is an element that is mostly produced in SNe Ia with core-collapse (CC) SNe contributing to the total production as well. It is not sufficiently known yet what the origin of the solar [Mn/Fe] is. Different explosion scenarios of SNe Ia are usually considered to explain the rise in [Mn/Fe] at [Fe/H] ≥ -1 to solar values (Matteucci & Greggio 1986; Cescutti & Kobayashi 2017; Eitner et al. 2020; Kobayashi et al. 2020) seen in observations (Gratton & Sneden 1988, 1991). Seitenzahl et al. (2013a) state that a source with a super-solar ratio of [Mn/Fe] is needed to

explain this trend. Their comparison of the Mn production from different progenitor models leads them to conclude that at least 50 % of SNe Ia originate from near- M_{Ch} WD explosions. They argue that this is the case because normal freeze-out is necessary to reach a high enough production of ^{55}Co so that [Mn/Fe] becomes super-solar. The production in incomplete Si burning is not sufficient for this. However, normal freeze-out can only be achieved in near- M_{Ch} WDs which have high enough central densities.

[Seitenzahl et al. \(2013a\)](#) examine WD mergers in their study to represent explosions of sub- M_{Ch} WDs and investigate a metallicity-dependence for the near- M_{Ch} WD explosion models. They argue that gravitational settling is needed in order for ^{22}Ne to be sufficiently abundant in the high density regions to alter the direct ^{55}Mn production. Since the effect is small for near- M_{Ch} WDs, it is neglected for sub- M_{Ch} WD. In our models, we presume a homogeneous distribution of ^{22}Ne in the core under the assumptions that it was produced homogeneously during the evolution of the zero-age main sequence progenitor star and that gravitational settling has a minor effect. This leads to the presence of ^{22}Ne affecting the Mn production in the high density regime. Our study shows that [Mn/Fe] of all models significantly increases with higher metallicity. This also applies to [Mn/Fe] originating from the core detonation. Accordingly, all models have a super-solar [Mn/Fe] value at $3 Z_{\odot}$ (see bottom panel in Figure 7). The contribution of progenitors with super-solar metallicity to the solar Mn over Fe ratio at [Fe/H]= 0 is not well known. They do not contribute to the ratio at that point in one-zone galactic evolution models. [Lach et al. \(2020\)](#) show that [Mn/Fe] is significantly super-solar in the nucleosynthetic yields of the shell detonation increasing the total Mn over Fe ratio. Thus showing that the He detonation plays an important role for the total [Mn/Fe]. A comparison of the ^{55}Mn and ^{55}Co yields originating from the shell and core detonation of Models M08_10, M08_05, and M08_03 (Tables 9, 10, and 11) confirms that the contribution of the shell detonation becomes more relevant at higher shell masses. The relation is the same among other models with equal core mass.

We point out that [Seitenzahl et al. \(2013a\)](#) use CC SN yields provided by [Woosley & Weaver \(1995\)](#) in their GCE model. These have a strong influence on the predicted evolution of [Mn/Fe] over [Fe/H]. They are similar to those by [Nomoto et al. \(2013, N13\)](#). The chemical evolution calculations presented in [Seitenzahl et al. \(2013a\)](#) would potentially lead to a less stiff requirement for M_{Ch} WD explosions if CC SN yields by [Limongi & Chieffi \(2018, LC18\)](#) were used.

The effect of core-shell mixing on [Mn/Fe] is investigated by a comparison of Models M08_10 by [Gronow et al. \(2021\)](#). While one of the models has the core and shell compositions obtained after the relaxation step, the mixing is reset in the other model (see [Gronow et al. 2021](#) for a detailed description of both models). The models have solar metallicity. [Mn/Fe] is about 0.2 in both cases with a difference of a few percent indicating that the mixing caused by the relaxation only has a small effect on the value. Variations in the ^{55}Mn production are minor as well. Some admixture of C into the shell in the initial transition region rather already influences the yields as described in [Yoon et al. \(2004\)](#) and [Gronow et al. \(2020\)](#).

3.4. Iron and nickel

^{56}Ni is the main product of a SN Ia explosion. Thus, the iron abundances is high as well after the decay of ^{56}Ni . Among those elements the isotopes ^{54}Fe and ^{58}Ni are interesting as they are the

next stable isotopes to the α -chain elements ^{52}Fe and ^{56}Ni . Further, ^{57}Ni can be measured from observations ([Graur et al. 2016](#)) via its decay to ^{57}Co allowing the determination of $^{57}\text{Ni}/^{56}\text{Ni}$.

An increase of the abundances originating from the He detonation with metallicity, however not as strong as for ^{55}Mn and ^{55}Co , can also be observed for ^{54}Fe and ^{58}Ni . In general, a higher metallicity leads to an increased production of stable IGE nuclides. This can also be observed in the core detonation (see Tables 1 to 12). The abundances of ^{54}Fe and ^{58}Ni at $3 Z_{\odot}$ increase to four times the value found at $0.01 Z_{\odot}$. The change in the nucleosynthetic yields is due to the presence of additional neutrons which stem from ^{22}Ne via $^{22}\text{Ne}(\alpha,n)^{25}\text{Mg}$ in the α -rich freeze-out regime ([Shigeyama et al. 1992](#)). The reaction produces the neutron-rich ^{25}Mg . In subsequent (α,n) and (n,γ) reactions other neutron-rich isotopes are formed up to IGEs, such as ^{54}Fe and ^{58}Ni which have two extra neutrons compared to the α -chain elements ^{52}Fe and ^{56}Ni . Additionally, the neutron, that is freed in the reaction of ^{22}Ne to ^{25}Mg , allows the production of C isotopes in reactions with ^{20}Ne . In this context free p are captured in exchange for α -particles ([Chamulak et al. 2007](#)). Contrary to this effect, the abundances of Fe and Ni which are produced in the He detonation are changed as ^{22}Ne and other isotopes alter the leading reactions. These isotopes compose the metallicity in the simulations and serve as seed nuclei for the reactions. As such $^{14}\text{N}(\alpha,p)^{17}\text{O}$ can lead to a speed up of the burning. The material undergoing explosive burning quickly reaches nuclear statistical quasi-equilibrium (QSE), which comprises two equilibrium clusters, around the Si and Fe groups (see also [Lach et al. 2020](#)). The clusters are separated by a bottleneck at $A \approx 45$ (Ca/Ti/Sc). This boundary of the QSE clusters depends on Y_e and the main nuclear reactions that connect the Si QSE cluster with the Fe-group cluster shift as a function of the neutron excess. At $Y_e \approx 0.5$ the bottleneck is by-passed with reactions such as the most important bridging flow through $^{45}\text{Sc}(p,\gamma)^{46}\text{Ti}$, but also $^{42}\text{Ca}(\alpha,\gamma)^{46}\text{Ti}$ and $^{45}\text{Ti}(n,\gamma)^{46}\text{Ti}$ ([Woosley et al. 1973](#)) and $^{44}\text{Ti}(\alpha,p)^{47}\text{V}$ ([Bodansky et al. 1968](#)). Instead, (α,n) and (α,γ) reactions on argon isotopes and (p,n) reactions on potassium isotopes, such as $^{40}\text{Ar}(\alpha,n)^{43}\text{Ca}$, $^{38}\text{Ar}(\alpha,\gamma)^{42}\text{Ca}$ or $^{42}\text{K}(p,n)^{42}\text{Ca}$, dominate the fluxes upwards out of the Si-group at $Y_e \approx 0.46$. $^{43}\text{Ca}(n,\gamma)^{44}\text{Ca}$ followed by a series of (n,γ) reactions along the Ca-isotopic chain up to ^{48}Ca then dominate the flux into the Fe-group QSE cluster ([Hix & Thielemann 1996](#)). A consequence of this shift is the increased production of neutron rich Fe-group isotopes, like ^{54}Fe and ^{58}Ni , in incomplete Si burning.

The production of ^{56}Ni and ^{58}Ni is illustrated in Figure 4 in the same way as in Figure 2 for Model M10_03_001 (left) and Model M10_03_3 (right). A comparison shows that the production of ^{56}Ni at lower densities in the incomplete Si burning regime decreases with higher metallicity, though the differences are only weakly pronounced. The same applies to ^{56}Ni produced in the He detonation. Changes in the ^{58}Ni abundances are more visible in Figure 4. The differences in the ^{58}Ni yields are most prominent in the density regime below $3 \times 10^6 \text{ g cm}^{-3}$ while a small increase is visible in the α -rich freeze-out regime as well.

[Timmes et al. \(2003\)](#) point out that the metallicity of the WD influences the electron fraction Y_e (an increase in metallicity decreases Y_e). A decrease in Y_e in turn increases the nucleosynthetic yields of $^{54-58}\text{Fe}$ and $^{57-60}\text{Ni}$. This is in agreement with [Curtis et al. \(2018\)](#) who state that a lower Y_e supports the production of ^{57}Ni over ^{56}Ni , thus changing the $^{57}\text{Ni}/^{56}\text{Ni}$ ratio. This is confirmed in our simulations (see Figure 5). Shown is the total ^{57}Ni mass over ^{56}Ni mass for all models. Models with the same mass configuration (e.g., all M08_03 models) have the same color and are connected by solid lines. The metallicity in-

creases to the top left and the total mass of the models increases to the top right. Two models (Models M08_10 and M10_03) have higher ^{56}Ni values than the model with the next highest total mass which is due to the different configurations of the models. For example, the shell mass of Model M08_10, along with the densities present in the shell, allows a production of ^{56}Ni in the He detonation which is of the order of $10^{-2} M_{\odot}$. This is significantly higher than for Model M09_03 and more than balances the small difference of the ^{56}Ni production in the core detonation. It is visible that the ^{56}Ni decreases and the ^{57}Ni increases with increasing metallicity. The yields at $0.01 Z_{\odot}$ and $0.1 Z_{\odot}$ show only small differences which are marginally visible for Models M11_05_001 and M11_05_01, but overlap for all other models. A comparison to SN 2011fe (case 1 of Dimitriadis et al. 2017) shows that it lies in the range covered by our models. It suggests that Model M09_10_3 can be a good fit and that a WD with this total mass (and possibly mass configuration of core and shell) can be its progenitor. Furthermore, SN 2012cg (Graur et al. 2016) could be explained by a progenitor similar to Model M10_10.

3.5. Nucleosynthetic yields relative to solar values

The variation of the nucleosynthetic abundances is apparent in Figures 6 and 7. Both figures give the elemental ratio relative to iron with respect to solar ratios (Asplund et al. 2009). For this, radioactive nuclides are decayed to 2 Gyr. Figure 6 shows the elemental ratios for Models M08_03 (top) and M10_03 (bottom) at four different metallicities, while Figure 7 illustrates the elemental ratios of all models sorted by metallicity. The models with the lowest metallicity of $0.01 Z_{\odot}$ at the top and at $3 Z_{\odot}$ at the bottom.

The influence of the metallicity on the elemental ratios is visible in Figure 6. The two panels show similar trends for both models. Among those is the previously discussed increase in Mn with increasing metallicity. It can further be seen that the Ti production decreases (a little) with increasing metallicity along with Cr. Generally, this decrease indicates a better match to observables as Ti and Cr often cause discrepancies in early observations (Höflich et al. 1996; Kromer et al. 2010). However, the decreasing values here are caused by changes in the nucleosynthetic yields coming from the core detonation and not the He detonation. An improved reproduction of observations is therefore not expected. One further trend is the odd-even effect in the production of intermediate mass elements (IMEs) (see Peterson 1981, and references therein). Elements with an even atomic number are mostly produced in the α -chain. The pairing effect results in a stable structure due to the high nuclear binding energy. Contrary to that, the nuclear binding energy of elements with an odd atomic number is low. The production of these elements further depends on the neutron excess of the white dwarf (Wheeler et al. 1989) which is visible in Figures 6 and 7. This is in most part due to the fact that stabilities shift toward neutron-rich isotopes for heavier elements.

A drop-off in the elemental ratios is noticeable for copper and zinc while cobalt is produced at sub-solar values as well. However, the effect decreases with increasing metallicity. Models with a more massive He shell further tend to reach higher values of Co, Cu, and Zn than the respective comparison models with lower shell masses at the same metallicity (see Figure 7). This confirms that Cu and Zn are mostly produced in the He detonation. The sub-solar production of the three elements Co, Cu, and Zn is typical for pure detonation models as pointed out by Lach et al. (2020). Generally some of these features are present

in all models as shown in Figure 7 and the relations between the models mostly stay the same with changing metallicity. A comparison of models with the same core mass at the various metallicities further allows to detect the influence of the He detonation on the elemental ratios which is already discussed in Lach et al. (2020) and confirmed here.

The super-solar production of Ti, V, and Cr is caused by the He detonation. However, the values are almost solar for Models M08_03, M09_03, and M10_03. Especially Model M10_03 is a good fit at all metallicities. The other models match Ti and V better than Cr and also show larger deviations toward higher metallicity. The Mn production is almost solar with an increasing trend at higher metallicity. At all metallicities it is visible that the Mn to Fe ratio is lower with increasing core mass as a high [Mn/Fe] stems from the Mn production in the shell. The relative contribution of Mn coming from the He detonation decreases with increasing core mass. Additionally, more Fe is produced at the higher densities in WDs with higher-mass cores because burning extends to higher-mass elements in these cases. Therefore, at solar metallicity only few models with sufficient mass to produce normal SNe Ia reach solar [Mn/Fe] (Models M09_05_1, M09_10_1, and M10_05_1). However, all models have super-solar values at a metallicity of $3 Z_{\odot}$.

3.6. Impact on observables

We have carried out radiative transfer simulations for a representative sub-set of models (Models M10_03) to investigate the influence of metallicity on the predicted observables. These will be presented in detail in a follow-up paper. However, we discuss the results qualitatively here.

Low metallicities ($\leq Z_{\odot}$) do not have a significant impact on the predicted photospheric-phase light curves and spectra. At early times, double detonation simulations tend to show colors too red compared to observations of normal SNe Ia, predominantly due to the production of heavy elements in the shell detonation (Cr, Ti, and IGEs, e.g., Kromer et al. 2010; Gronow et al. 2020). As discussed above, increasing the metallicity does not significantly impact the production of these elements in the shell detonation. Therefore, it is not unexpected that the metallicity of the model does not substantially alter the agreement with observations for low to moderate values. At high metallicity ($3 Z_{\odot}$), there is a noticeable impact on the predicted observables, such that the models are fainter and redder. This can be attributed to the lower masses of ^{56}Ni that are produced at this high metallicity, leading to lower ejecta temperatures and redder colors.

Although the impact on the early observables is relatively modest, metallicity can become more important when considering late times. This is because the metallicity affects the ratio of stable to radioactive isotopes produced in the model. In the nebular phase, the relatively rapid decay of ^{56}Ni means that ^{58}Ni becomes the dominant Ni isotope. Therefore, the abundance of this stable isotope can be directly probed in nebular spectra (Ruiz-Lapuente & Lucy 1992). Increasing metallicity provides a mechanism by which sub- M_{Ch} models can produce increasing amounts of stable Ni, although it remains unclear whether conditions in sub- M_{Ch} models can yield [Ni II] emission to the degree required by data (Shingles et al. 2020; Wilk et al. 2020).

4. Comparison to previous work

Other models involving a non-zero metallicity of the zero-age main sequence progenitor were investigated by Shigeyama et al.

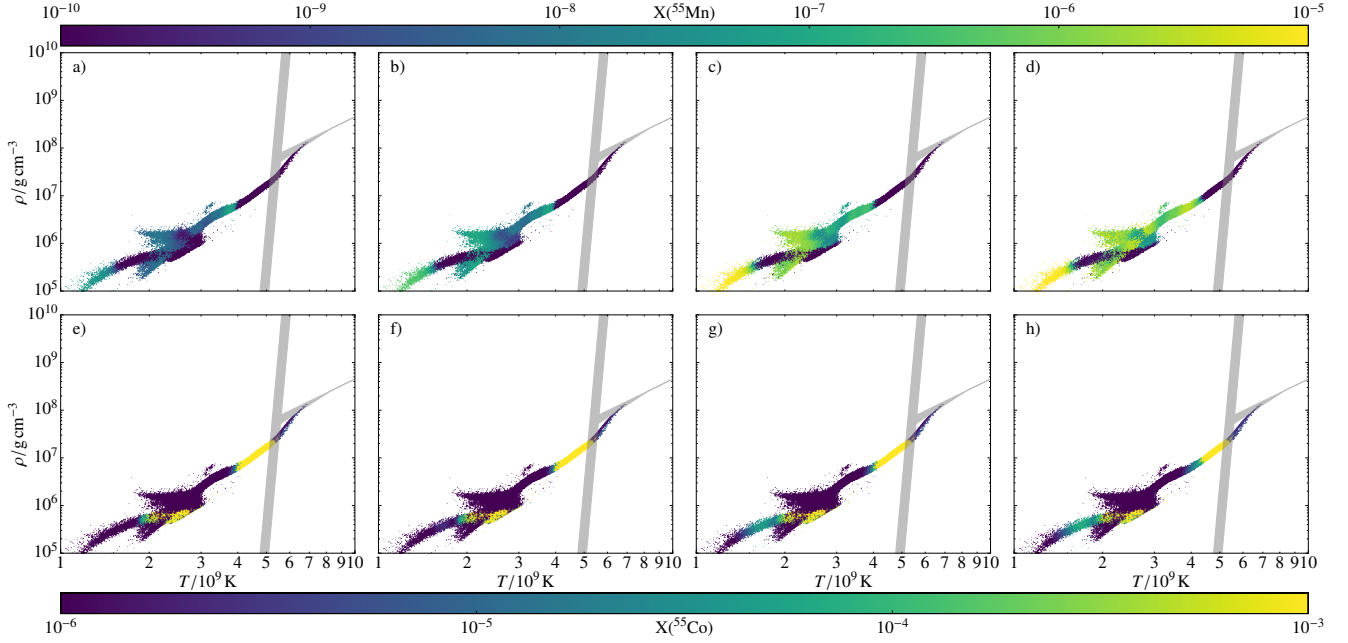


Fig. 2: Tracer particle distribution in the $T_{\text{peak}} - \rho_{\text{peak}}$ -plane for Models M10_03 at 0.01, 0.1, 1, and $3 Z_{\odot}$, mass fractions of ^{55}Mn (top, a) to d)) and ^{55}Co (bottom, e) to h)) at $t = 100$ s are color coded. The shaded areas split the domain into normal freeze-out from NSE, α -rich freeze-out and incomplete Si-burning (clockwise starting in the top right) following Woosley et al. (1973) (see also Lach et al. 2020).

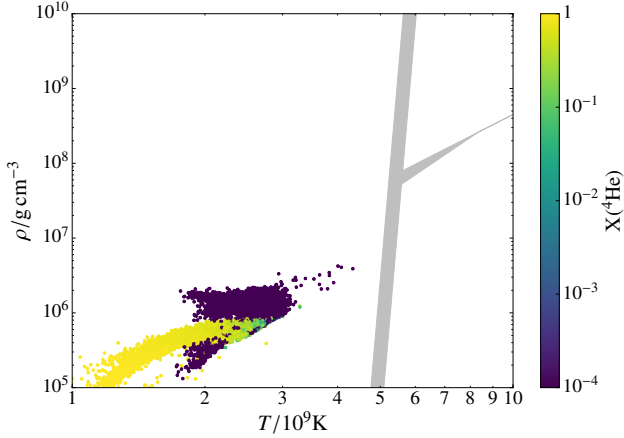


Fig. 3: Tracer particle distribution in the $T_{\text{peak}} - \rho_{\text{peak}}$ -plane of the He detonation for Model M10_03_001 at $t = 100$ s. The ^4He mass fraction is color coded. The shaded areas are the same as in Figure 2.

(1992); Timmes et al. (2003); Sim et al. (2010); Shen et al. (2018), and Leung & Nomoto (2020). In the following we compare our models to theirs where possible. We point out that only Leung & Nomoto (2020) examine a sub- M_{Ch} WD with a He shell with all others studying detonations in bar sub- M_{Ch} CO WD. A discussion of the models at solar metallicity was already carried out in Gronow et al. (2021).

Lach et al. (2020) discuss the nucleosynthesis results of Model M10_05_1 (Model M2a $_{\odot}$ in their paper) in connection with other explosion scenarios, such as delayed detonations or pure deflagrations, also analyzing their impact on GCE. A specific focus is given on Mn, Zn, and Cu. Similar to other work

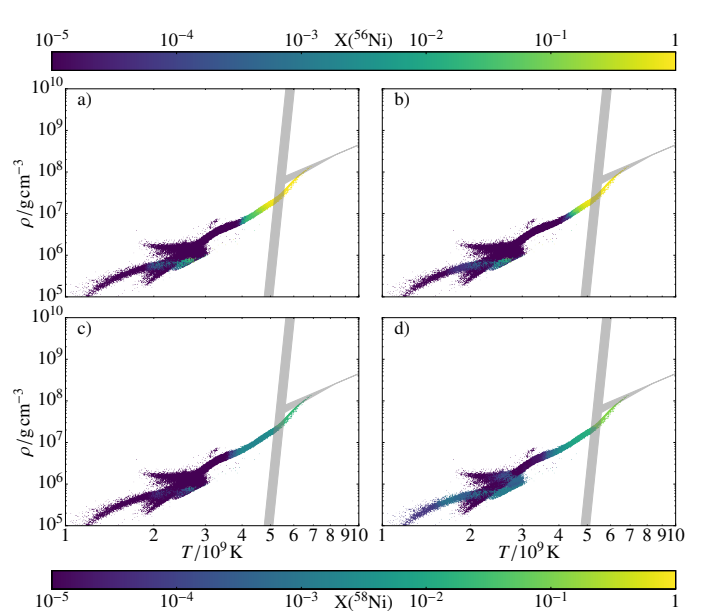


Fig. 4: Tracer particle distribution in the $T_{\text{peak}} - \rho_{\text{peak}}$ -plane for Models M10_03_001 (left) and M10_03_3, mass fractions of ^{56}Ni (top) and ^{58}Ni (bottom) at $t = 100$ s are color coded with shaded areas as in Figure 2.

(e.g., Seitenzahl et al. 2013a), they confirm metallicity as an important parameter for the production of Mn which we also find in the more detailed metallicity study presented here. We further confirm that the Cu production increases with metallicity though it is still underproduced compared to solar values also in our highest metallicity models.

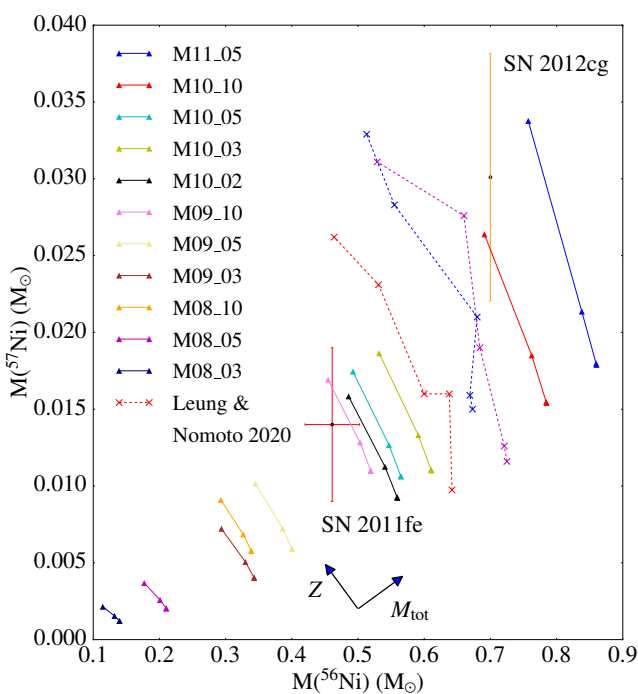


Fig. 5: Mass of ^{57}Ni over ^{56}Ni mass for all models (solid lines). Models of Leung & Nomoto (2020) are added for comparison (dashed lines). The data for SN 2011fe is taken from Dimitriadis et al. (2017) (case 1) and for SN 2012cg from Graur et al. (2016).

Flörs et al. (2019) use super-solar values of Mn and Ni to differentiate between M_{Ch} and sub- M_{Ch} WDs as progenitors in nebula spectra. As pointed out by Lach et al. (2020) the distinction between both models is not that straightforward. At high metallicity ($1 Z_{\odot}$) our models with a core mass of at least $1.0 M_{\odot}$ reach at least solar values for both elements.

Sim et al. (2010) explore detonations in a variety of sub- M_{Ch} CO WDs at different masses. Only one of the models is calculated at about $3 Z_{\odot}$. This model has a total mass of $1.06 M_{\odot}$ which is similar to our Models M10_05. However, their model does not have a He shell. They find that more stable IGEs are produced compared to the same model at zero metallicity. Figure 3 of Sim et al. (2010) also shows that less ^{56}Ni is synthesized in the inner and less IMEs in the outer regions. These changes are attributed to the presence of ^{22}Ne which is used to represent metallicity in the WD. While it is not possible to compare the respective detailed nucleosynthetic yields, our models agree with the trends found by Sim et al. (2010).

A similar model (WD without He shell) is calculated by Shen et al. (2018). However, they carry out a parameter study involving different WD masses and metallicities. Similar to us, they examine four different metallicities of the main sequence progenitor star, namely $0, 0.5, 1$, and $2 Z_{\odot}$. They use ^{22}Ne and ^{56}Fe as proxies for the metallicity in the hydrodynamic simulation. Similar to us they find that the production of ^{56}Ni decreases with increasing metallicity while other, stable IGEs are produced. A rough comparison of the Shen et al. (2018) models can be carried out to the yields originating from the core detonation in our models with the least massive He shells. Generally, the same behavior is found in all models. The yields of some isotopes, such as ^{32}S and ^{40}Ca , are within a few percent of each other at $0.01 Z_{\odot}$ (compared to zero metallicity of Shen et al. (2018)) and Z_{\odot} . Shen

et al. (2018) compare their solar metallicity models to the ones of Blondin et al. (2017) and argue that the discrepancy in the ^{56}Ni abundance is caused by the smaller nuclear reaction network used by Blondin et al. (2017). We point out that the differences in the ^{56}Ni abundance reach up to two-thirds of the values by Shen et al. (2018) depending on the WD mass. The models by Shen et al. (2018), however, match the models by Shigeyama et al. (1992) relatively well at $2 Z_{\odot}$.

The models by Shigeyama et al. (1992) are calculated in 1D and involve sub- M_{Ch} CO WDs without a He shell. Similar to us they find an increase in the production of neutron-rich IGEs due to the presence of ^{22}Ne which they use to approximate metallicity in the same way as done in our study. A more detailed comparison is not feasible due to the different setups of the models.

Timmes et al. (2003) predict a relation between the amount of produced ^{56}Ni and the metallicity of the white dwarf. Their 1D models of M_{Ch} WDs show a decrease of ^{56}Ni by 25% going from $0.3 Z_{\odot}$ to $3 Z_{\odot}$. Shen et al. (2018) find a similar trend when the metallicity is changed from 0 to $2 Z_{\odot}$ but the amount of the reduction varies with WD mass in their case. Models with a mass of $0.8 M_{\odot}$ show a decrease of 50% in ^{56}Ni and models of a $1.0 M_{\odot}$ WD only of 10%. Bravo (2019) carry out a parameter study involving sub- M_{Ch} CO WDs with masses between $0.88 M_{\odot}$ and $1.15 M_{\odot}$ at varying metallicities. Their ^{56}Ni abundances show a similar decrease by about 17%. Our models agree with the trend found in these previous studies. The decrease, however, is lower with values from 12% to 21%. While the difference of the ^{56}Ni abundance at $0.01 Z_{\odot}$ and $3 Z_{\odot}$ is of the same order for most models, our model with the smallest total mass shows the highest value of 21%. The derived linear relation of Timmes et al. (2003) assumes a fixed ^{56}Ni mass of $0.6 M_{\odot}$ produced in a normal SN Ia. However, this mass is in large part influenced by the total mass of the white dwarf. Lower-mass stars produce significantly less ^{56}Ni as can be seen in Tables 1 to 12. The relative change of this mass with increasing metallicity is therefore larger at lower total masses.

Seitenzahl et al. (2013b) and Leung & Nomoto (2018) carry out studies involving different metallicities for near- M_{Ch} WDs. A comparison of the models is therefore only possible analog to the comparison with the studies of Sim et al. (2010) and Shen et al. (2018). Instead we focus on a study by Leung & Nomoto (2020) who investigate double detonations of sub- M_{Ch} WDs. They look into similar core and shell masses as presented in our paper. However, our models reach down to lower core and shell masses. In contrast to our models, Leung & Nomoto (2020) do not consider any mixing between core and shell. This has an influence on the nucleosynthetic yields produced in the He detonation as shown by Gronow et al. (2020). The metallicities they include in their study reach from $0 Z_{\odot}$ to $5 Z_{\odot}$ which is approximated by ^{22}Ne similar to our hydrodynamic models. The metallicity is treated more accurately in the postprocessing step of our models as ^{14}N is included as a proxy for the metallicity in the He shell of the hydrodynamic simulation while Leung & Nomoto (2020) do not include this in the hydrodynamic and postprocessing calculations (Leung, priv. comm.). In addition, the solar abundances of Asplund et al. (2009) are scaled to the respective metallicity as described in Section 2. Lach et al. (2020) compare an approach that only includes ^{22}Ne in the post-processing calculation as proxy for the metallicity, such as used by Leung & Nomoto (2020) and other authors before, with the one presented here as well as in their study. The simulations by Leung & Nomoto (2020) are only carried out in 2D and cover one quarter of the star. Furthermore, their hydrodynamic simulations only include seven isotopes in the nuclear reaction network.

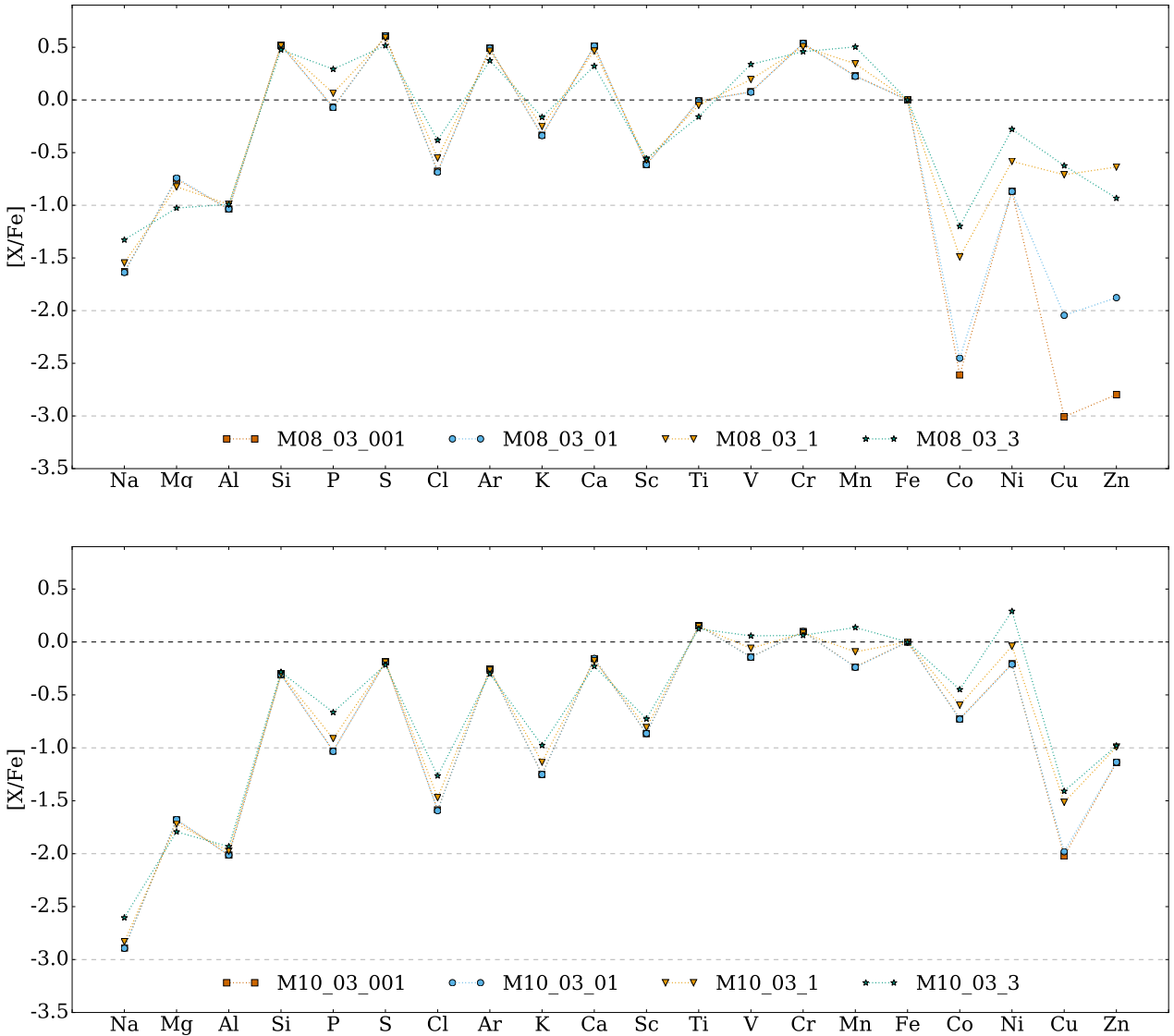


Fig. 6: Elemental ratios relative to Fe compared to solar ratios for Models M08_03 (top) and M10_03 (bottom) at four different metallicities.

This is not best suited to cover the energetics of the shell detonation as pointed out by [Shen et al. \(2018\)](#) and [Townsley et al. \(2019\)](#). The nuclear network used in the hydrodynamic models of [Gronow et al. \(2021\)](#) comprises 55 isotopes to match the one of [Townsley et al. \(2019\)](#). This allows to cover the He and Si burning more accurately than with a small nuclear network. Additionally, the level-set method used in [Leung & Nomoto \(2020\)](#) is not optimal to follow the detonation front at low densities present in the shell and in low-mass WDs in general ([Gronow et al. 2020, 2021](#)). The energy release and nuclear burning are not calculated self-consistently using this method ([Gronow et al. 2020](#)). Instead the energy release in the burning is treated in a parametric way which requires a calibration for the simulation ([Fink et al. 2010](#)). The AREPO code instead enables a coupling of the nuclear network to the hydrodynamics ([Pakmor et al. 2013](#)). The groups H, I, and J of [Leung & Nomoto \(2020\)](#) focus on the effect of the metallicity on the explosion characteristics and nucleosynthetic yields. Out of these models, Group I is most similar to Model M10_10 as it has a total mass of $1.1 M_{\odot}$ with a

$0.1 M_{\odot}$ shell. [Leung & Nomoto \(2020\)](#) find that the production of ^{56}Ni decreases with increasing metallicity. Similar to [Timmes et al. \(2003\)](#) they find a decrease of about 20%. They conclude that the metallicity has only little to no impact on the explosion energy, final energy, detonation channel, detonation position and time of core ignition. This supports our computational approach in which we do not calculate the hydrodynamic simulation for each of our 44 models, but use the hydrodynamic simulation of eleven and follow-up on those with detailed nucleosynthesis calculations at different metallicities in a postprocessing step. A detailed analysis of the models of Group I in [Leung & Nomoto \(2020\)](#) shows an increase in the production of stable isotopes (both IMEs and IGEs) while the final yields of the α -chain elements are not affected by the metallicity. The difference of the neutron-rich isotopes can be as high as four orders of magnitude as stated by [Leung & Nomoto \(2020\)](#). We find a similar increase, most significantly in the yields of ^{55}Mn as discussed in Section 3.3. Tables 6 and 7 of [Leung & Nomoto \(2020\)](#) list nucleosynthetic yields of stable and some radioactive

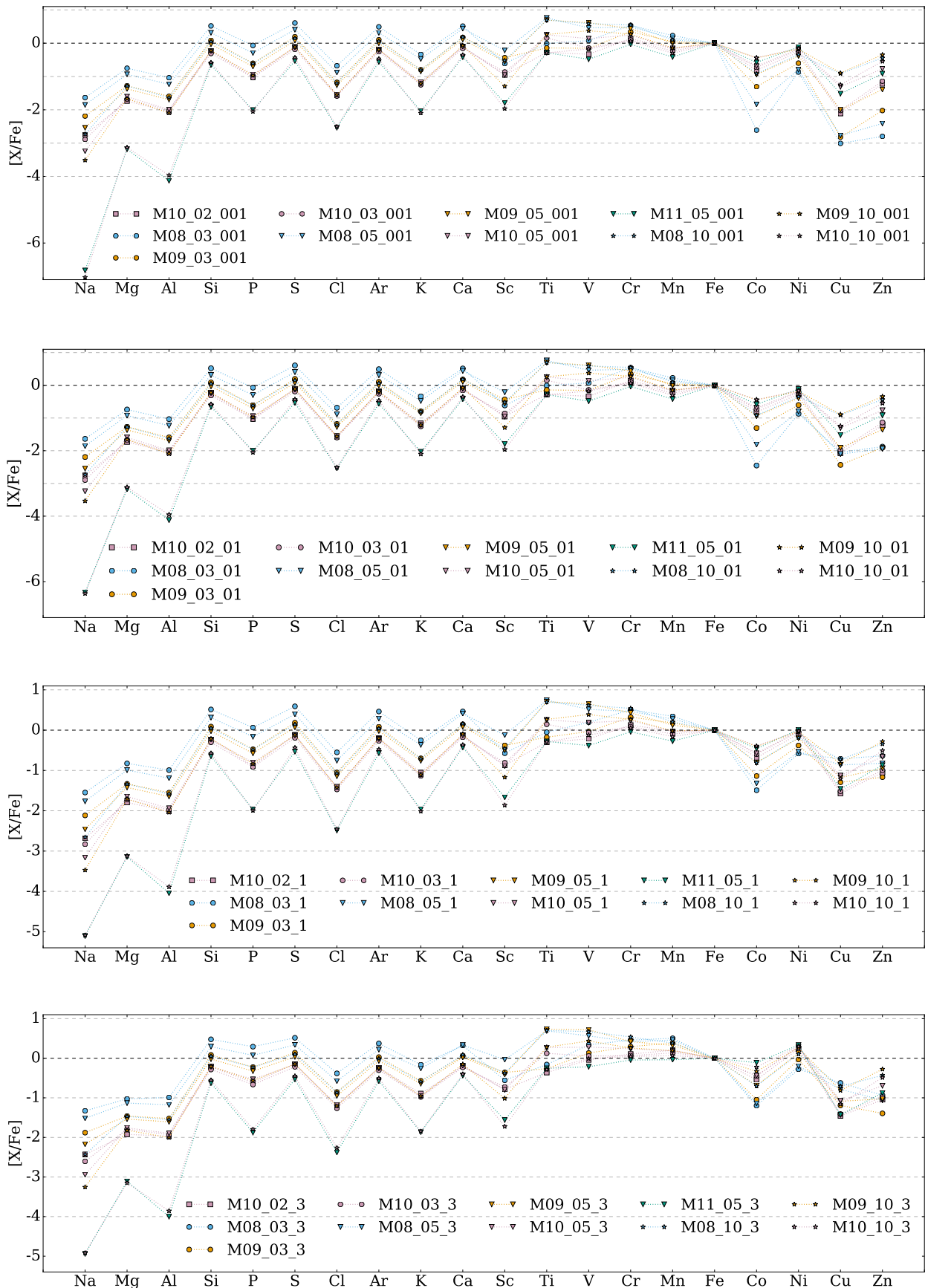


Fig. 7: Elemental ratios relative to Fe compared to solar ratios for all models sorted by metallicity, from top to bottom: $0.01 Z_{\odot}$, $0.1 Z_{\odot}$, $1 Z_{\odot}$, and $3 Z_{\odot}$.

isotopes of the benchmark model in Group I. Here seven different metallicities are included out of which three are part of our study. Comparable yields of Model M10_10 are given in the appendix and the appendix of Gronow et al. (2021). A comparison of the abundances shows that the ^{56}Ni production is higher in our models though the decreasing trend with metallicity is similar. Other isotopes confirm that our models and the models by Leung & Nomoto (2020) agree in the dependency of the respective isotope production on metallicity. However, a discrepancy is visible in the yields of selected isotopes. ^{30}Si and ^{34}S are produced less in our simulations, showing differences of one order of magnitude in some cases. Smaller differences are apparent for ^{44}Ti (yields by Leung & Nomoto (2020) are higher), ^{55}Mn (yields by Leung & Nomoto (2020) are lower) and ^{64}Zn (yields by Leung & Nomoto (2020) are lower). In all three cases our models give better matches relative to solar values since about solar values of Mn are reached and the under-/overproduction of Zn/Ti is decreased. Figure 5 illustrates the abundances of ^{57}Ni over ^{56}Ni as discussed in Section 3.4. For comparison three models of Leung & Nomoto (2020) are included (at zero, 0.1, 1, and 5 Z_\odot , dashed lines). They represent models with a total mass of 1.0 M_\odot and 1.1 M_\odot and follow the same trend as our models, both regarding metallicity and ^{56}Ni mass. However, the models of Leung & Nomoto (2020) show higher values of ^{57}Ni . The differences in the nucleosynthesis yields of our models compared to Leung & Nomoto (2020) are attributed to the different numerical treatments. The details of the approach used for the hydrodynamic simulations of our models are given in Gronow et al. (2020, 2021) and are more accurate for the multi-dimensional structure of the double detonation. The size of the nuclear reaction network is critical to capture the energetics accurately as pointed out earlier.

5. Influence on Galactic Chemical Evolution

In this section, we incorporate the metallicity-dependent sub- M_{Ch} WD explosion yields presented in Section 3 in the GCE code OMEGA+ (Côté et al. 2018) in order to explore their impact on the predicted evolution of Mn in the solar neighbourhood (see also Lach et al. 2020). OMEGA+ is a two-zone model that consists of a central galaxy surrounded by a large gas reservoir that fills the host dark matter halo. In addition to the star formation and chemical enrichment processes, the code includes parametrized large-scale gas circulation processes such as galactic inflows and outflows. For this work, the GCE code is calibrated to broadly reproduce general properties of the Milky Way, such as the current star formation rate, gas inflow rate, stellar-to-gas mass ratio, and CC and Type Ia SN rates².

Although OMEGA+ can account for a wide range of astrophysical sites, we only include in this work the contribution of CC SNe, low- and intermediate-mass (LIMS) stars, and SNe Ia. The nucleosynthesis ejecta are assumed to mix homogeneously within the galactic gas, but the lifetime of stars and the delay-time distribution (DTD) of SNe Ia are taken into account in the enrichment process (see Ritter et al. 2018 for more details). Given the exploratory nature of our GCE calculations, we assume that all SNe Ia are sub- M_{Ch} explosions, with the goal to explore how such a SN Ia channel can contribute to the production of Mn in our Galaxy. As a test case, we adopt the metallicity-dependent yields for the model with an initial core of 1 M_\odot and a shell mass of 0.03 M_\odot , Model M10_03. Although the yields are

metallicity-dependent, we adopt the same DTD for all metallicities, which comes from the double detonation SN Ia prescription with a He shell found in Ruter et al. (2014). This DTD is normalized such that about 10^{-3} SNe Ia occur in total per unit of stellar mass formed, which is sufficient to account for the overall SN Ia rate observed in nearby galaxies (see Table 5 in Côté et al. 2016).

In all of our GCE calculations, the mass- and metallicity-dependent yields for LIMS stars are taken from Cristallo et al. (2015). For massive stars, we consider both the mass- and metallicity-dependent yields of LC18 and N13. For LC18, we adopt the mixture of rotation velocities introduced and described in Prantzos et al. (2018), which depends on metallicity. These yields are applied to all massive stars from 8 to 100 M_\odot . For N13, we assume that 50 % of the stars above an initial mass of 20 M_\odot end up as hypernovae, and apply the yields to all massive stars from 8 to 50 M_\odot . This lower maximum threshold mass relative to the LC18 case was chosen in order to avoid overproducing the amount of metals synthesized by massive stars.

Figure 8 shows the predicted evolution of [Mn/Fe] as a function of [Fe/H] in the solar neighbourhood, assuming different CC SN yields and different SN Ia treatments. The required contribution of SNe Ia in order to reproduce the upward Mn trend depends on the adopted CC SN yields (see also Lach et al. 2020). As can be seen from the grey solid line, the massive star yields of LC18 contribute to the rise of Mn at $[\text{Fe}/\text{H}] > -0.5$ (upper panel), as opposed to the yields of N13 (lower panel). In fact, when using our metallicity-dependent SN Ia yields (orange line) along with the massive star yields of LC18, our prediction agrees relatively well with the spectroscopic data (Battistini & Bensby 2015). We point out that the CC SN yields used in Seitenzahl et al. (2013a) are similar to N13. Accordingly the chemical evolution of Mn presented in Figure 1 of Seitenzahl et al. (2013a) (thick blue line) is similar to the one in the bottom panel of Figure 8 (orange line).

To visualize the impact of using metallicity-dependent SN Ia yields, we ran three additional GCE calculations in which we assumed that all SNe Ia eject the yields of a specific metallicity (0.01 Z_\odot , Z_\odot , and 3 Z_\odot , see blue lines in Figure 8). As expected, using higher-metallicity yields lead to higher [Mn/Fe] ratios. Although our metallicity-dependent predictions are similar to the ones with a constant metallicity of 0.01 Z_\odot and Z_\odot , the effect of metallicity is still important for extending and maintaining the upward [Mn/Fe] trend at $[\text{Fe}/\text{H}] > 0$.

In Figure 9, we show our predicted solar elemental abundances when using our metallicity-dependent SN Ia yields along with the LC18 yields (top) and N13 yields (bottom). As described above, using the LC18 yields suggests that Mn could be significantly produced by massive stars, which would reduce the need for SNe Ia originating from explosions of M_{Ch} WDs. In fact, when assuming that sub- M_{Ch} double detonations are the dominant SN Ia channel, our GCE model can account for more than 80 % of the solar Mn abundance. This prediction, however, is affected by several uncertainties including the exact number of SNe Ia that occurred in the Milky Way prior to the formation of the Solar System. Furthermore, the use of other CC SNe yields still requires some contribution of M_{Ch} WD explosions. The bottom panel in Figure 9 illustrates this as the Mn production is much lower using N13 yields compared with LC18 yields.

Given the nucleosynthesis signature of our sub- M_{Ch} models, the maximum contribution of these SNe Ia to the evolution of Mn is limited by other elements. In particular, Ti and Cr are produced in a substantial amount in the ejecta of the adopted SN Ia models, and as shown in Figure 9, our GCE prediction

² https://github.com/becot85/JINAPyCEE/blob/master/DOC/OMEGA%2B_Milky_Way_model.ipynb

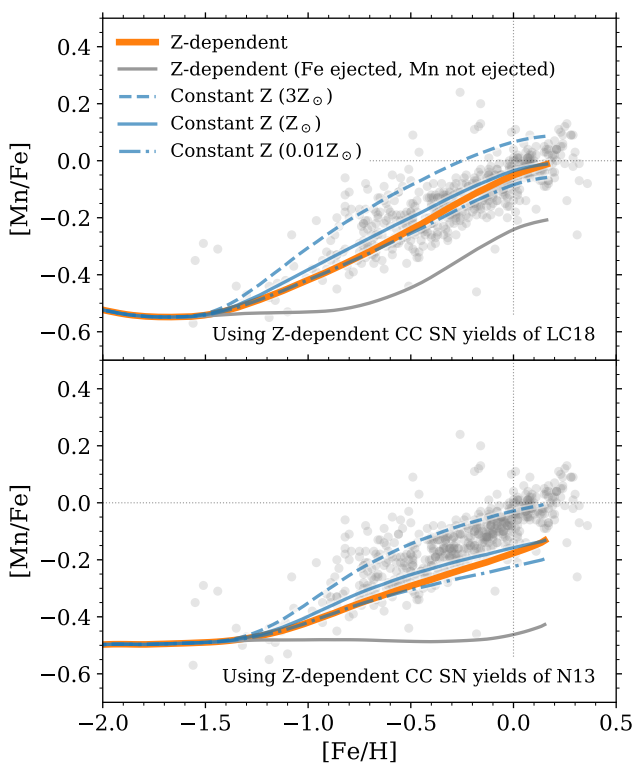


Fig. 8: Chemical evolution of Mn in the solar neighbourhood, as predicted by OMEGA+ (lines, Section 5) and derived from stellar spectroscopy (dots, Battistini & Bensby 2015). All predictions include the contribution of Type Ia and CC SNe, using the massive star yields of Limongi & Chieffi (2018, LC18) and Nomoto et al. (2013, N13) for the top and bottom panels, respectively. In each panel, the three blue lines show our predictions when we assume that all SNe Ia eject the yields of a given metallicity. The orange line shows our prediction when adopting our metallicity-dependent SN Ia yields. The grey line shows the metallicity-dependent case, but when SNe Ia are assumed to only eject Fe, without Mn, while CC SNe still eject both Fe and Mn.

already fills the solar composition for these elements. Adjusting the contribution of SNe Ia to reproduce 100% of the solar Mn abundance would lead to an overproduction of Ti and Cr. Ca and Ni are overestimated in our GCE calculations when using the massive star yields of LC18, but it is not the case when using the N13 yields.

6. Conclusions

Our parameter study followed up on previous work by Gronow et al. (2021). Explosions of sub- M_{Ch} WDs with varying core and shell masses were simulated at different metallicities. The core mass lay between $0.8 M_{\odot}$ and $1.1 M_{\odot}$ and the initial shell mass was in the range $0.02 M_{\odot}$ to $0.1 M_{\odot}$. Models at solar metallicity of the zero-age main sequence progenitor have been presented by Gronow et al. (2021). We now included metallicities of 0.01, 0.1, and $3 Z_{\odot}$ and showed that the results of the postprocessing step at these metallicities are in good agreement with a full recalculation of the hydrodynamic model allowing to decrease the computational costs of our study.

We found that the influence of the metallicity varies with the model. The impact is larger on the nucleosynthetic yields of the core detonation than on those of the He detonation. In accor-

dance with this, the nucleosynthetic yields produced in the He detonation do not show significant changes with varying metallicity up to elements as heavy as ^{44}Ti . However, the amount of ^{55}Mn produced in the He detonation increases by one order of magnitude with each metallicity increase (from $0.01 Z_{\odot}$ to $0.1 Z_{\odot}$ to $1 Z_{\odot}$ to $3 Z_{\odot}$) since the presence of ^{14}N and ^{22}Ne (mixed into the shell during the relaxation) supports its production (see Section 3.3). The production of ^{54}Fe and ^{58}Ni increases with metallicity as well. This is caused by a shift in the leading reactions toward neutron-rich isotopes.

This neutron-excess also results in a change of the nucleosynthetic yields produced in the core detonation. For $Z = 3 Z_{\odot}$, ^{54}Fe and ^{58}Ni increase to four times the value obtained at $0.01 Z_{\odot}$. The effect is particularly strong on ^{55}Mn (Seitenzahl et al. 2013a) causing a significant increase with metallicity.

The models are further analysed regarding changes in the elemental ratios relative to Fe compared to solar values. All models show similar features. Most prominent, an odd-even effect is visible in the production of IMEs. This is due to the higher stability of elements with an even atomic number. In addition, the production of elements with an odd atomic number depends on the metallicity of the white dwarf (increasing with metallicity). The models also confirm that Cu and Zn are in large part produced in He detonations. Nevertheless, double detonations have sub-solar Cu and Zn to Fe ratios due to the sub-solar production of Co, Cu, and Zn in the core detonation. This is a feature of a pure detonation (Lach et al. 2020) and suppresses a rise of the ratio to solar values. The contribution of the core detonation to the ratio of the double detonation is proportionally larger than the one of the He detonation. The super-solar production of ^{44}Ti is caused by the He detonation. However, we do point out that some models reproduce solar values. While the ratios of Cu and Zn to Fe are higher for models with larger He shells, models with lower He shell masses show a better match with observations. Both factors need to be taken into account when a model of a sub- M_{Ch} WD is verified as progenitor of a SN Ia.

Only few parameter studies involving different metallicities of a sub- M_{Ch} WD were carried out (Shigeyama et al. 1992; Sim et al. 2010; Shen et al. 2018; Leung & Nomoto 2020). Among them only Leung & Nomoto (2020) analyze explosions of WDs with a He shell. We nevertheless see the same relative change in the nucleosynthetic yields produced in the core detonation and the pure detonations of sub- M_{Ch} WDs by Shigeyama et al. (1992), Sim et al. (2010), and Shen et al. (2018). The relation between metallicity and ^{56}Ni production found by Timmes et al. (2003) and Shen et al. (2018) is confirmed. The dependence is not as strong in our models as the increase of the metallicity only leads to a decrease of about 13% on average. It is, however, in agreement with a change of 15% found by Ohkubo et al. (2006) who consider metallicities between $0.001 Z_{\odot}$ and $0.05 Z_{\odot}$.

The initial mass configurations of some models in Leung & Nomoto (2020) are in good agreement with our M10_10 models. The nucleosynthetic yields of some isotopes show differences. For example, the ^{56}Ni production is higher in our models and the ^{30}Si and ^{34}S production lower. However, the trends in the production of the isotopes are the same depending on metallicity. The differences in the detailed nucleosynthetic yields are presumably caused by the different numerical treatments and initial setup.

Our parameter study shows that super-solar values of Mn can be reached in double detonations of sub- M_{Ch} WDs (see also Lach et al. 2020). If such a channel is assumed to be the dominant source of SNe Ia, explosions of sub- M_{Ch} WDs could contribute significantly to the increasing $[\text{Mn}/\text{Fe}]$ trend at $[\text{Fe}/\text{H}] > -1$ observed in the solar neighborhood. Seitenzahl et al.

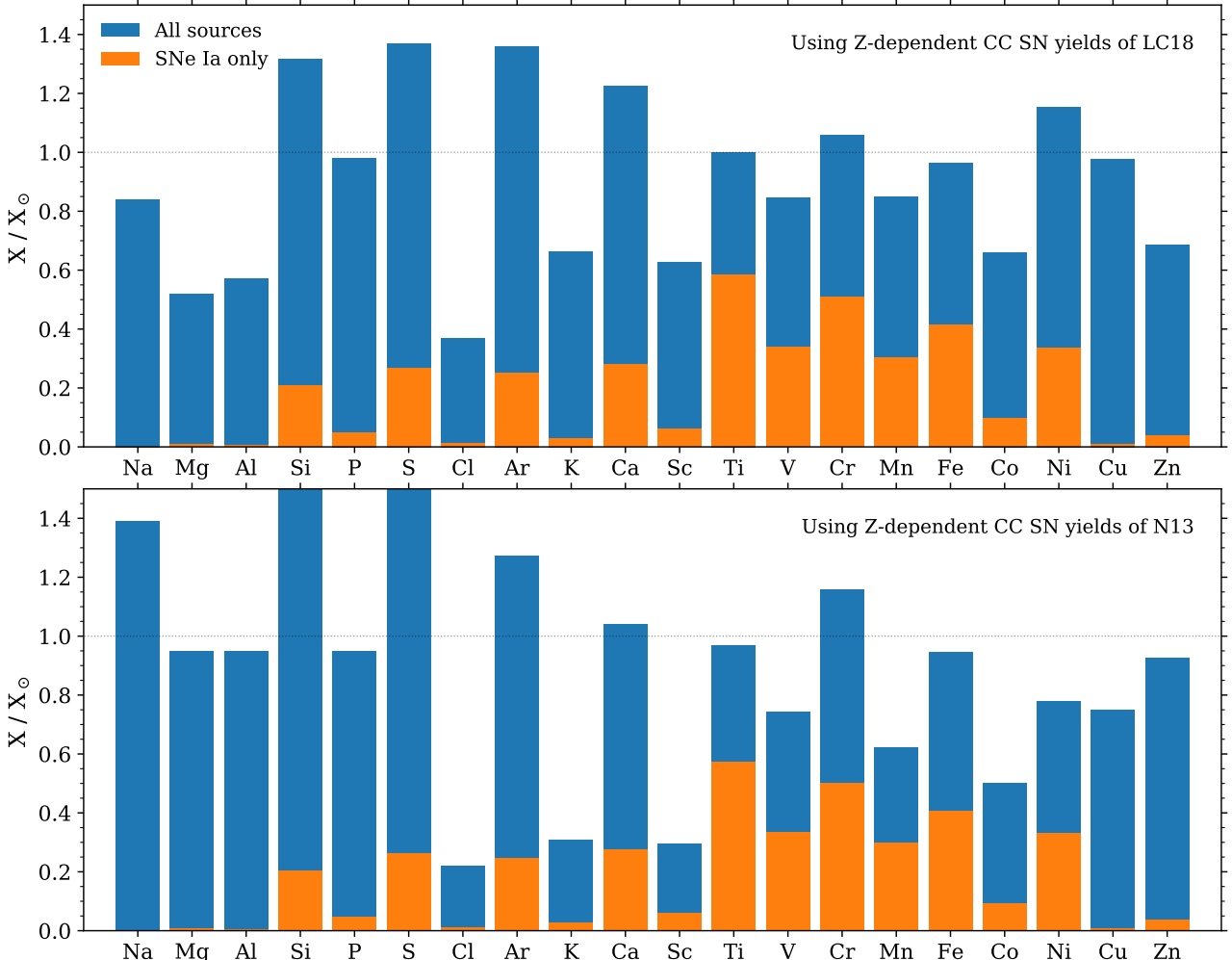


Fig. 9: Predicted solar elemental distribution normalized to the solar abundances of Asplund et al. (2009). The blue bars show our chemical evolution prediction when combining the contribution of CC SNe (top: Limongi & Chieffi 2018, bottom: Nomoto et al. 2013), low- and intermediate-mass stars (Cristallo et al. 2015), and SNe Ia (using the metallicity-dependent yields from this work). The orange bands show the specific contribution of SNe Ia within the combined predicted abundances.

(2013a) find that a contribution of at least 50 % by M_{Ch} WD to SNe Ia is necessary to reach solar values of [Mn/Fe] (see also Eitner et al. 2020; Kobayashi et al. 2020). This requirement is weakened by our analysis indicating that a larger fraction of SNe Ia originates from sub- M_{Ch} WDs if CC SN yields of LC18 are considered. When adopting the massive-star yields of LC18, along with our metallicity-dependent SN Ia yields, our GCE predictions can account for more than 80% of the solar Mn, without the contribution of M_{Ch} WD explosions. It is important that the contribution of the He shell detonation is included in the models. The Mn production during this detonation significantly raises the total Mn over Fe ratio. Our GCE results are obtained from a rather simplified galaxy model, and should therefore be taken as exploratory.

Acknowledgements. We thank Shing-Chi Leung for providing details on the treatment of metallicity effects in his simulations. This work was supported by the Deutsche Forschungsgemeinschaft (DFG, German Research Foundation) – Project-ID 138713538 – SFB 881 (“The Milky Way System”, subproject A10). SG, FL, and FKR acknowledge support by the Klaus Tschira Foundation. BC was supported by the ERC Consolidator Grant (Hungary) funding scheme (Project RADIOSTAR, G.A. n. 724560) and by the Lendület grant (LP17- 2014) of the Hungarian Academy of Sciences. IRS was supported by the Australian Research Council through grant number FT160100028. This article is based upon

work from the “ChETEC” COST Action (CA16117), supported by COST (European Cooperation in Science and Technology). CEC acknowledges support by the European Research Council (ERC) under the European Union’s Horizon 2020 research and innovation programme under grant agreement No. 759253. NumPy and SciPy (Oliphant 2007), IPython (Pérez & Granger 2007), and Matplotlib (Hunter 2007) were used for data processing and plotting. The authors gratefully acknowledge the Gauss Centre for Supercomputing e.V. (www.gauss-centre.eu) for funding this project by providing computing time on the GCS Supercomputer JUWELS (Jülich Supercomputing Centre 2019) at Jülich Supercomputing Centre (JSC). This work was performed using the Cambridge Service for Data Driven Discovery (CSD3), part of which is operated by the University of Cambridge Research Computing on behalf of the STFC DiRAC HPC Facility (www.dirac.ac.uk). The DiRAC component of CSD3 was funded by BEIS capital funding via STFC capital grants ST/P002307/1 and ST/R002452/1 and STFC operations grant ST/R00689X/1. DiRAC is part of the National e-Infrastructure. This research was undertaken with the assistance of resources from the National Computational Infrastructure (NCI Australia), an NCRIS enabled capability supported by the Australian Government.

References

- Asplund, M., Grevesse, N., Sauval, A. J., & Scott, P. 2009, ARA&A, 47, 481
- Battistini, C. & Bensby, T. 2015, A&A, 577, A9
- Bildsten, L. & Hall, D. M. 2001, ApJ, 549, L219

- Blondin, S., Dessart, L., Hillier, D. J., & Khokhlov, A. M. 2017, MNRAS, 470, 157
- Bodansky, D., Clayton, D. D., & Fowler, W. A. 1968, ApJS, 16, 299
- Brachwitz, F., Dean, D. J., Hix, W. R., et al. 2000, ApJ, 536, 934
- Bravo, E. 2019, A&A, 624, A139
- Bravo, E., Badenes, C., & Martínez-Rodríguez, H. 2019, MNRAS, 482, 4346
- Bravo, E., Domínguez, I., Badenes, C., Piersanti, L., & Straniero, O. 2010, ApJ, 711, L66
- Bravo, E. & Martínez-Pinedo, G. 2012, Phys. Rev. C, 85, 055805
- Cescutti, G. & Kobayashi, C. 2017, Astronomy & Astrophysics, 607, A23
- Cescutti, G., Matteucci, F., Lanfranchi, G. A., & McWilliam, A. 2008, A&A, 491, 401
- Chamulak, D. A., Brown, E. F., & Timmes, F. X. 2007, ApJ, 655, L93
- Côté, B., Ritter, C., O’Shea, B. W., et al. 2016, ApJ, 824, 82
- Côté, B., Silvia, D. W., O’Shea, B. W., Smith, B., & Wise, J. H. 2018, ApJ, 859, 67
- Cristallo, S., Straniero, O., Piersanti, L., & Gobrecht, D. 2015, ApJS, 219, 40
- Curtis, S., Ebinger, K., Fröhlich, C., et al. 2018, The Astrophysical Journal, 870, 2
- de los Reyes, M. A., Kirby, E. N., Seitenzahl, I. R., & Shen, K. J. 2020, The Astrophysical Journal, 891, 85
- Deloye, C. J. & Bildsten, L. 2002, ApJ, 580, 1077
- Dimitriadis, G., Sullivan, M., Kerzendorf, W., et al. 2017, MNRAS, 468, 3798
- Etner, P., Bergemann, M., Hansen, C. J., et al. 2020, Astronomy & Astrophysics, 635, A38
- Fink, M., Röpke, F. K., Hillebrandt, W., et al. 2010, A&A, 514, A53
- Flörs, A., Spyromilio, J., Taubenberger, S., et al. 2019, Monthly Notices of the Royal Astronomical Society, 491, 2902
- García-Berro, E., Althaus, L. G., Córscico, A. H., & Isern, J. 2008, ApJ, 677, 473
- Gratton, R. G. & Sneden, C. 1988, A&A, 204, 193
- Gratton, R. G. & Sneden, C. 1991, A&A, 241, 501
- Graur, O., Zurek, D., Shara, M. M., et al. 2016, ApJ, 819, 31
- Greggio, L. & Renzini, A. 1983, A&A, 118, 217
- Gronow, S., Collins, C., Ohlmann, S. T., et al. 2020, A&A, 635, A169
- Gronow, S., Collins, C. E., Sim, S. A., & Röpke, F. K. 2021, arXiv e-prints, arXiv:2102.06719, accepted by A&A
- Hashimoto, M. A., Hanawa, T., & Sugimoto, D. 1983, PASJ, 35, 1
- Hix, W. R. & Thielemann, F. 1996, ApJ, 460, 869
- Hix, W. R. & Thielemann, F. 1999, ApJ, 511, 862
- Höflich, P., Khokhlov, A., Wheeler, J. C., et al. 1996, ApJ, 472, L81
- Höflich, P., Wheeler, J. C., & Thielemann, F. K. 1998, ApJ, 495, 617
- Howard, W. M., Goriely, S., Rayet, M., & Arnould, M. 1993, in Nuclei in the Cosmos 2, 607–612
- Hunter, J. D. 2007, Computing in Science & Engineering, 9, 90
- Iwamoto, K., Brachwitz, F., Nomoto, K., et al. 1999, ApJS, 125, 439
- Jülich Supercomputing Centre. 2019, Journal of large-scale research facilities, 5
- Khokhlov, A. M. 1984, Soviet Astronomy Letters, 10, 123
- Khokhlov, A. M. & Érgma, É. V. 1985, Astrofizika, 23, 605
- Kobayashi, C., Leung, S.-C., & Nomoto, K. 2020, ApJ, 895, 138
- Kobayashi, C., Tsujimoto, T., Nomoto, K., Hachisu, I., & Kato, M. 1998, ApJ, 503, L155
- Kromer, M., Ohlmann, S., & Röpke, F. K. 2017, Mem. Soc. Astron. Italiana, 88, 312
- Kromer, M., Sim, S. A., Fink, M., et al. 2010, ApJ, 719, 1067
- Lach, F., Roepeke, F. K., Seitenzahl, I. R., et al. 2020, A&A, 644, A118
- Langanke, K. & Martínez-Pinedo, G. 2001, Atomic Data and Nuclear Data Tables, 79, 1
- Lentz, E. J., Baron, E., Branch, D., Hauschildt, P. H., & Nugent, P. E. 2000, ApJ, 530, 966
- Leung, S.-C. & Nomoto, K. 2018, ApJ, 861, 143
- Leung, S.-C. & Nomoto, K. 2020, The Astrophysical Journal, 888, 80
- Limongi, M. & Chieffi, A. 2018, The Astrophysical Journal Supplement Series, 237, 13
- Matteucci, F. & Greggio, L. 1986, A&A, 154, 279
- Mazzali, P. A. & Podsiadlowski, P. 2006, MNRAS, 369, L19
- McWilliam, A. 1997, ARA&A, 35, 503
- Meakin, C. A., Seitenzahl, I., Townsley, D., et al. 2009, ApJ, 693, 1188
- Nomoto, K., Kobayashi, C., & Tominaga, N. 2013, ARA&A, 51, 457
- North, P., Cescutti, G., Jablonka, P., et al. 2012, A&A, 541, A45
- Nugent, P., Baron, E., Branch, D., Fisher, A., & Hauschildt, P. H. 1997, ApJ, 485, 812
- Ohkubo, T., Umeda, H., Nomoto, K., & Yoshida, T. 2006, in American Institute of Physics Conference Series, Vol. 847, Origin of Matter and Evolution of Galaxies, ed. S. Kubono, W. Aoki, T. Kajino, T. Motobayashi, & K. Nomoto, 458–460
- Oliphant, T. E. 2007, Computing in Science & Engineering, 9, 10
- Pakmor, R., Edelmann, P., Röpke, F. K., & Hillebrandt, W. 2012, MNRAS, 424, 2222
- Pakmor, R., Kromer, M., Taubenberger, S., & Springel, V. 2013, ApJ, 770, L8
- Pérez, F. & Granger, B. E. 2007, Computing in Science & Engineering, 9, 21
- Peterson, R. C. 1981, ApJ, 244, 989
- Prantzos, N., Abia, C., Limongi, M., Chieffi, A., & Cristallo, S. 2018, Monthly Notices of the Royal Astronomical Society, 476, 3432
- Rauscher, T. & Thielemann, F.-K. 2000, Atomic Data and Nuclear Data Tables, 75, 1
- Ritter, C., Côté, B., Herwig, F., Navarro, J. F., & Fryer, C. L. 2018, ApJS, 237, 42
- Ruiter, A. J., Belczynski, K., Sim, S. A., Seitenzahl, I. R., & Kwiatkowski, D. 2014, MNRAS, 440, L101
- Ruiz-Lapuente, P. & Lucy, L. B. 1992, ApJ, 400, 127
- Seitenzahl, I. R., Cescutti, G., Röpke, F. K., Ruiter, A. J., & Pakmor, R. 2013a, A&A, 559, L5
- Seitenzahl, I. R., Ciaraldi-Schoolmann, F., Röpke, F. K., et al. 2013b, MNRAS, 429, 1156
- Shen, K. J., Kasen, D., Miles, B. J., & Townsley, D. M. 2018, ApJ, 854, 52
- Shen, K. J. & Moore, K. 2014, ApJ, 797, 46
- Shigeyama, T., Nomoto, K., Yamaoka, H., & Thielemann, F. 1992, ApJ, 386, L13
- Shingles, L. J., Sim, S. A., Kromer, M., et al. 2020, MNRAS, 492, 2029
- Sim, S. A., Röpke, F. K., Hillebrandt, W., et al. 2010, ApJ, 714, L52
- Springel, V. 2010, MNRAS, 401, 791
- Taubenberger, S., Hachinger, S., Pignata, G., et al. 2008, MNRAS, 385, 75
- Thielemann, F.-K., Nomoto, K., & Yokoi, K. 1986, A&A, 158, 17
- Timmes, F. X., Brown, E. F., & Truran, J. W. 2003, ApJ, 590, L83
- Timmes, F. X., Woosley, S. E., & Weaver, T. A. 1995, ApJS, 98, 617
- Townsley, D. M., Miles, B. J., Shen, K. J., & Kasen, D. 2019, ApJ, 878, L38
- Travaglio, C., Hillebrandt, W., Reinecke, M., & Thielemann, F.-K. 2004, A&A, 425, 1029
- Truran, J. W., Arnett, W. D., & Cameron, A. G. W. 1967, Can. J. Phys., 45, 2315
- Umeda, H., Nomoto, K., Yamaoka, H., & Wanajo, S. 1999, ApJ, 513, 861
- Wheeler, J. C., Sneden, C., & Truran, James W. J. 1989, ARA&A, 27, 279
- Wilk, K. D., Hillier, D. J., & Dessart, L. 2020, MNRAS, 494, 2221
- Woosley, S. E., Arnett, W. D., & Clayton, D. D. 1973, ApJS, 26, 231
- Woosley, S. E. & Weaver, T. A. 1995, ApJS, 101, 181
- Yoon, S., Langer, N., & Scheithauer, S. 2004, A&A, 425, 217

Appendix A: Abundances tables

We list the nucleosynthesis yields of our models in Tables A.1 to A.22. They are created in the same way as in Gronow et al. (2021). The yields for the solar metallicity model are already included in Gronow et al. (2021). The stable nuclides, radioactive nuclides with lifetimes lower than 2 Gyr decayed to stability and radioactive nuclides with longer lifetimes at time $t = 100$ s are listed in Table A.1 to A.11. Nucleosynthesis yields of selected radioactive nuclides at $t = 100$ s are given in Table A.12 to A.22.

Table A.1: Asymptotic nucleosynthesis yields (in solar masses) for Model M08_03 with 0.01, 0.1, and $3 Z_{\odot}$.

	M08_03_001		M08_03_01		M08_03_3	
	He det [M_{\odot}]	core det [M_{\odot}]	He det [M_{\odot}]	core det [M_{\odot}]	He det [M_{\odot}]	core det [M_{\odot}]
^{12}C	3.43e-03	1.26e-02	3.43e-03	1.26e-02	3.33e-03	1.21e-02
^{13}C	1.81e-09	2.42e-07	1.80e-09	2.32e-07	1.19e-09	9.05e-07
^{14}N	6.43e-07	9.97e-06	1.73e-06	9.67e-06	3.67e-05	1.29e-05
^{15}N	2.33e-07	2.11e-08	2.47e-07	2.06e-08	6.49e-07	2.62e-08
^{16}O	2.51e-03	1.44e-01	2.52e-03	1.44e-01	2.83e-03	1.46e-01
^{17}O	5.55e-08	3.48e-06	5.73e-08	3.40e-06	9.40e-08	4.32e-06
^{18}O	2.69e-07	4.71e-08	2.93e-07	4.54e-08	1.04e-06	6.96e-08
^{19}F	2.68e-07	6.87e-10	2.83e-07	7.22e-10	7.35e-07	4.97e-09
^{20}Ne	1.58e-03	6.42e-03	1.58e-03	6.42e-03	1.70e-03	5.70e-03
^{21}Ne	8.07e-07	2.38e-06	8.34e-07	2.29e-06	1.67e-06	7.77e-06
^{22}Ne	9.42e-07	1.47e-04	1.00e-06	1.43e-04	2.60e-06	8.18e-04
^{23}Na	1.03e-05	7.12e-05	1.03e-05	7.01e-05	1.06e-05	1.73e-04
^{24}Mg	2.04e-03	1.26e-02	2.04e-03	1.30e-02	2.16e-03	5.77e-03
^{25}Mg	3.46e-05	1.07e-04	3.49e-05	1.05e-04	4.90e-05	3.82e-04
^{26}Mg	3.56e-05	1.34e-04	3.56e-05	1.31e-04	3.71e-05	5.19e-04
^{27}Al	8.23e-05	5.28e-04	8.22e-05	5.31e-04	8.48e-05	6.76e-04
^{28}Si	4.15e-03	2.57e-01	4.16e-03	2.57e-01	4.38e-03	2.54e-01
^{29}Si	5.74e-05	7.62e-04	5.71e-05	7.54e-04	5.47e-05	2.56e-03
^{30}Si	7.15e-05	1.06e-03	7.14e-05	1.05e-03	7.29e-05	5.61e-03
^{31}P	6.62e-05	5.29e-04	6.62e-05	5.22e-04	6.89e-05	1.46e-03
^{32}S	2.34e-03	1.45e-01	2.35e-03	1.45e-01	2.59e-03	1.23e-01
^{33}S	1.33e-05	4.07e-04	1.33e-05	4.01e-04	1.58e-05	7.46e-04
^{34}S	1.14e-05	2.10e-03	1.14e-05	2.05e-03	1.32e-05	9.81e-03
^{36}S	6.46e-10	6.35e-08	3.18e-09	6.99e-08	3.24e-08	6.19e-06
^{35}Cl	4.61e-05	1.31e-04	4.63e-05	1.28e-04	5.50e-05	3.45e-04
^{37}Cl	6.60e-07	2.79e-05	6.76e-07	2.73e-05	1.22e-06	5.40e-05
^{36}Ar	1.06e-03	2.53e-02	1.07e-03	2.52e-02	1.23e-03	1.81e-02
^{38}Ar	2.00e-06	8.73e-04	2.05e-06	8.44e-04	3.66e-06	3.96e-03
^{40}Ar	4.72e-10	6.21e-09	4.13e-09	1.03e-08	3.25e-08	5.95e-07
^{39}K	9.16e-05	6.68e-05	9.23e-05	6.53e-05	1.20e-04	1.48e-04
^{41}K	5.60e-06	4.64e-06	5.56e-06	4.54e-06	4.82e-06	8.14e-06
^{40}Ca	3.13e-03	2.15e-02	3.13e-03	2.15e-02	3.03e-03	1.46e-02
^{42}Ca	6.36e-06	2.25e-05	6.42e-06	2.16e-05	8.27e-06	9.31e-05
^{43}Ca	1.78e-05	7.20e-08	1.79e-05	7.15e-08	2.00e-05	5.33e-07
^{44}Ca	2.26e-04	1.30e-05	2.25e-04	1.30e-05	1.91e-04	1.01e-05
^{46}Ca	1.56e-10	2.64e-10	1.50e-09	2.35e-09	1.23e-08	2.82e-07
^{48}Ca	2.86e-11	3.09e-11	2.73e-10	3.00e-10	5.21e-09	2.60e-08
^{45}Sc	1.13e-06	2.23e-07	1.13e-06	2.23e-07	9.56e-07	7.69e-07
^{46}Ti	9.30e-07	8.28e-06	9.34e-07	7.99e-06	1.07e-06	3.04e-05
^{47}Ti	7.18e-06	3.23e-07	7.14e-06	3.17e-07	5.88e-06	1.80e-06
^{48}Ti	8.33e-06	3.21e-04	8.23e-06	3.22e-04	6.14e-06	2.17e-04
^{49}Ti	2.86e-07	1.87e-05	2.83e-07	1.86e-05	2.20e-07	2.56e-05
^{50}Ti	1.25e-10	7.16e-10	1.28e-09	4.64e-09	4.33e-08	7.48e-07
^{50}V	1.28e-10	4.15e-09	1.77e-10	5.15e-09	3.84e-09	1.98e-07
^{51}V	2.57e-07	4.51e-05	2.56e-07	4.46e-05	2.47e-07	9.21e-05

Table A.1 continued.

	M08_03_001		M08_03_01		M08_03_3	
	He det [M_{\odot}]	core det [M_{\odot}]	He det [M_{\odot}]	core det [M_{\odot}]	He det [M_{\odot}]	core det [M_{\odot}]
^{50}Cr	1.30e-07	1.39e-04	1.30e-07	1.37e-04	1.29e-07	6.93e-04
^{52}Cr	8.65e-07	6.20e-03	8.78e-07	6.21e-03	1.35e-06	4.87e-03
^{53}Cr	2.90e-08	4.66e-04	3.19e-08	4.62e-04	1.55e-07	8.24e-04
^{54}Cr	2.74e-10	2.17e-08	2.82e-09	3.62e-08	1.19e-07	1.42e-06
^{55}Mn	1.09e-07	2.19e-03	1.28e-07	2.17e-03	8.88e-07	4.61e-03
^{54}Fe	2.20e-08	1.34e-02	7.53e-08	1.31e-02	1.87e-06	5.41e-02
^{56}Fe	8.98e-07	1.40e-01	1.75e-06	1.40e-01	3.40e-05	1.17e-01
^{57}Fe	9.69e-08	1.22e-03	2.00e-07	1.22e-03	6.39e-06	2.21e-03
^{58}Fe	8.95e-09	3.13e-08	9.77e-08	2.65e-07	7.06e-06	9.47e-06
^{59}Co	3.05e-08	1.21e-06	2.12e-07	1.57e-06	8.03e-06	2.77e-05
^{58}Ni	4.26e-08	1.15e-03	1.89e-07	1.13e-03	9.23e-06	4.60e-03
^{60}Ni	1.17e-07	8.42e-06	5.49e-07	1.37e-05	6.29e-06	2.15e-04
^{61}Ni	3.38e-08	2.36e-07	2.13e-07	7.28e-07	2.13e-06	2.60e-05
^{62}Ni	4.93e-08	1.36e-06	3.73e-07	4.28e-06	2.71e-06	1.43e-04
^{64}Ni	1.13e-09	1.29e-08	1.16e-08	1.25e-07	2.08e-07	1.17e-05
^{63}Cu	7.17e-09	4.58e-08	4.31e-08	4.49e-07	5.17e-07	1.06e-05
^{64}Zn	1.08e-08	9.90e-08	2.24e-08	7.80e-07	1.27e-07	2.13e-06
^{66}Zn	4.87e-09	2.01e-07	3.44e-08	1.78e-06	1.91e-07	1.94e-05
^{67}Zn	8.20e-10	2.89e-09	6.37e-09	2.79e-08	2.46e-08	1.70e-06
^{68}Zn	7.00e-10	1.00e-08	5.59e-09	9.69e-08	3.67e-08	3.47e-06
^{70}Zn	6.84e-12	9.76e-11	7.75e-11	9.44e-10	7.45e-09	7.57e-08
^{69}Ga	7.03e-11	5.99e-09	6.65e-10	5.83e-08	1.43e-08	5.47e-07
^{71}Ga	3.99e-11	7.92e-10	4.02e-10	7.54e-09	9.63e-09	2.25e-07

Table A.2: Asymptotic nucleosynthesis yields (in solar masses) for Model M08_05 with 0.01, 0.1, and $3 Z_{\odot}$.

	M08_05_001		M08_05_01		M08_05_3	
	He det [M_{\odot}]	core det [M_{\odot}]	He det [M_{\odot}]	core det [M_{\odot}]	He det [M_{\odot}]	core det [M_{\odot}]
^{12}C	2.34e-03	7.55e-03	2.33e-03	7.55e-03	2.27e-03	7.25e-03
^{13}C	5.16e-10	7.76e-08	5.15e-10	7.40e-08	3.61e-10	4.36e-07
^{14}N	3.44e-07	6.82e-06	1.42e-06	6.57e-06	3.62e-05	1.08e-05
^{15}N	3.46e-08	1.49e-08	3.62e-08	1.45e-08	9.03e-08	1.95e-08
^{16}O	6.07e-03	1.16e-01	6.10e-03	1.16e-01	6.61e-03	1.18e-01
^{17}O	2.19e-08	1.67e-06	2.35e-08	1.62e-06	6.59e-08	2.37e-06
^{18}O	3.67e-08	2.99e-08	4.63e-08	2.88e-08	3.53e-07	4.39e-08
^{19}F	2.08e-08	4.93e-10	2.19e-08	4.75e-10	5.84e-08	1.52e-09
^{20}Ne	3.05e-03	5.39e-03	3.05e-03	5.39e-03	3.07e-03	4.75e-03
^{21}Ne	2.30e-07	2.02e-06	2.32e-07	1.93e-06	3.14e-07	7.43e-06
^{22}Ne	1.66e-07	3.39e-05	1.89e-07	3.26e-05	8.76e-07	3.07e-04
^{23}Na	1.65e-05	5.54e-05	1.65e-05	5.44e-05	1.63e-05	1.49e-04
^{24}Mg	4.17e-03	1.00e-02	4.18e-03	1.03e-02	4.27e-03	4.54e-03
^{25}Mg	2.25e-05	8.73e-05	2.25e-05	8.56e-05	2.67e-05	3.33e-04
^{26}Mg	3.82e-05	1.21e-04	3.81e-05	1.18e-04	3.76e-05	4.75e-04
^{27}Al	1.47e-04	4.19e-04	1.47e-04	4.21e-04	1.51e-04	5.37e-04
^{28}Si	9.24e-03	2.28e-01	9.24e-03	2.28e-01	9.41e-03	2.26e-01
^{29}Si	1.15e-04	6.29e-04	1.14e-04	6.23e-04	1.13e-04	2.07e-03
^{30}Si	1.05e-04	8.54e-04	1.05e-04	8.45e-04	1.10e-04	4.51e-03
^{31}P	8.62e-05	4.32e-04	8.63e-05	4.26e-04	9.14e-05	1.19e-03
^{32}S	4.69e-03	1.31e-01	4.69e-03	1.31e-01	4.81e-03	1.11e-01
^{33}S	5.55e-05	3.34e-04	5.53e-05	3.30e-04	5.46e-05	6.19e-04
^{34}S	2.75e-05	1.78e-03	2.73e-05	1.73e-03	2.76e-05	8.29e-03
^{36}S	1.98e-09	5.30e-08	3.22e-09	5.93e-08	1.93e-08	5.06e-06
^{35}Cl	4.36e-05	1.11e-04	4.38e-05	1.08e-04	5.49e-05	2.89e-04
^{37}Cl	1.03e-05	2.40e-05	1.03e-05	2.35e-05	1.04e-05	4.66e-05
^{36}Ar	2.09e-03	2.34e-02	2.10e-03	2.34e-02	2.16e-03	1.69e-02
^{38}Ar	1.29e-05	7.54e-04	1.30e-05	7.30e-04	1.71e-05	3.43e-03
^{40}Ar	5.12e-10	5.24e-09	2.08e-09	9.26e-09	1.60e-08	5.27e-07
^{39}K	1.07e-04	5.86e-05	1.09e-04	5.73e-05	1.66e-04	1.30e-04
^{41}K	9.15e-06	4.08e-06	9.15e-06	3.99e-06	1.06e-05	7.17e-06
^{40}Ca	7.85e-03	2.04e-02	7.86e-03	2.04e-02	8.47e-03	1.41e-02
^{42}Ca	4.36e-06	1.95e-05	4.44e-06	1.87e-05	8.01e-06	8.10e-05
^{43}Ca	1.93e-05	6.43e-08	1.93e-05	6.41e-08	2.31e-05	4.50e-07
^{44}Ca	2.57e-03	1.33e-05	2.58e-03	1.33e-05	2.87e-03	1.02e-05
^{46}Ca	6.73e-11	2.55e-10	6.49e-10	2.29e-09	6.20e-09	2.48e-07
^{48}Ca	1.40e-11	1.95e-11	1.35e-10	1.85e-10	2.87e-09	2.16e-08
^{45}Sc	4.73e-06	2.01e-07	4.78e-06	2.00e-07	7.28e-06	6.66e-07
^{46}Ti	2.65e-06	7.26e-06	2.69e-06	7.01e-06	4.32e-06	2.68e-05
^{47}Ti	6.88e-05	3.01e-07	6.94e-05	2.96e-07	9.45e-05	1.56e-06
^{48}Ti	2.67e-03	3.48e-04	2.66e-03	3.49e-04	2.43e-03	2.40e-04
^{49}Ti	2.03e-05	1.98e-05	2.05e-05	1.97e-05	2.83e-05	2.79e-05
^{50}Ti	5.56e-11	6.15e-10	5.66e-10	2.79e-09	2.04e-08	5.87e-07
^{50}V	4.16e-11	3.44e-09	1.77e-10	4.28e-09	3.41e-09	1.55e-07
^{51}V	1.12e-04	4.83e-05	1.12e-04	4.78e-05	1.17e-04	9.96e-05

Table A.2 continued.

	M08_05_001		M08_05_01		M08_05_3	
	He det [M_{\odot}]	core det [M_{\odot}]	He det [M_{\odot}]	core det [M_{\odot}]	He det [M_{\odot}]	core det [M_{\odot}]
⁵⁰ Cr	7.60e-06	1.33e-04	7.69e-06	1.31e-04	1.12e-05	6.63e-04
⁵² Cr	8.92e-04	7.37e-03	8.84e-04	7.39e-03	6.40e-04	5.77e-03
⁵³ Cr	2.00e-05	5.39e-04	2.01e-05	5.35e-04	2.20e-05	9.48e-04
⁵⁴ Cr	2.18e-10	1.96e-08	1.52e-09	2.51e-08	6.56e-08	1.19e-06
⁵⁵ Mn	3.04e-05	2.65e-03	3.04e-05	2.63e-03	2.76e-05	5.77e-03
⁵⁴ Fe	8.74e-06	1.37e-02	8.81e-06	1.35e-02	1.07e-05	5.72e-02
⁵⁶ Fe	7.54e-05	2.10e-01	7.51e-05	2.10e-01	7.40e-05	1.79e-01
⁵⁷ Fe	6.53e-06	2.04e-03	6.71e-06	2.02e-03	1.57e-05	3.73e-03
⁵⁸ Fe	6.06e-09	2.48e-08	6.49e-08	1.95e-07	5.09e-06	7.55e-06
⁵⁹ Co	8.19e-07	9.85e-06	1.33e-06	1.01e-05	2.39e-05	3.28e-05
⁵⁸ Ni	2.64e-06	1.81e-03	3.03e-06	1.78e-03	3.25e-05	7.82e-03
⁶⁰ Ni	1.39e-06	1.49e-04	2.41e-06	1.54e-04	2.17e-05	2.39e-04
⁶¹ Ni	5.72e-07	4.44e-06	9.83e-07	4.84e-06	8.73e-06	2.41e-05
⁶² Ni	6.61e-07	2.57e-05	1.58e-06	2.77e-05	1.57e-05	1.67e-04
⁶⁴ Ni	1.44e-09	1.09e-08	1.43e-08	1.06e-07	2.57e-07	9.25e-06
⁶³ Cu	5.06e-08	4.72e-08	2.14e-07	3.82e-07	2.53e-06	8.72e-06
⁶⁴ Zn	1.31e-07	3.96e-07	2.48e-07	9.31e-07	2.35e-06	1.80e-06
⁶⁶ Zn	8.59e-08	4.94e-07	2.42e-07	1.76e-06	1.97e-06	1.63e-05
⁶⁷ Zn	2.72e-08	2.72e-09	8.30e-08	2.46e-08	7.25e-07	1.37e-06
⁶⁸ Zn	3.58e-08	8.24e-09	1.20e-07	7.91e-08	6.68e-07	2.77e-06
⁷⁰ Zn	7.38e-12	8.42e-11	7.73e-11	8.14e-10	5.30e-09	6.08e-08
⁶⁹ Ga	2.87e-09	5.06e-09	1.05e-08	4.93e-08	6.18e-08	4.48e-07
⁷¹ Ga	5.64e-10	6.97e-10	2.62e-09	6.65e-09	2.24e-08	1.82e-07

Table A.3: Asymptotic nucleosynthesis yields (in solar masses) for Model M08_10 with 0.01, 0.1, and $3 Z_{\odot}$.

	M08_10_001		M08_10_01		M08_10_3	
	He det [M_{\odot}]	core det [M_{\odot}]	He det [M_{\odot}]	core det [M_{\odot}]	He det [M_{\odot}]	core det [M_{\odot}]
^{12}C	1.18e-04	1.07e-03	1.17e-04	1.07e-03	1.17e-04	1.04e-03
^{13}C	7.87e-11	6.23e-11	7.69e-11	5.96e-11	4.72e-11	7.91e-10
^{14}N	1.62e-07	1.02e-08	1.22e-06	8.98e-09	3.53e-05	1.02e-07
^{15}N	1.00e-08	1.14e-09	1.05e-08	1.36e-09	2.70e-08	4.79e-10
^{16}O	9.09e-03	8.03e-02	9.10e-03	8.02e-02	9.60e-03	8.17e-02
^{17}O	1.86e-10	2.94e-09	1.58e-09	2.79e-09	4.65e-08	2.67e-08
^{18}O	8.37e-09	1.50e-10	1.62e-08	1.44e-10	2.67e-07	1.02e-09
^{19}F	4.11e-09	1.21e-11	4.42e-09	1.20e-11	1.41e-08	7.68e-11
^{20}Ne	1.56e-04	2.93e-03	1.55e-04	2.93e-03	1.60e-04	2.67e-03
^{21}Ne	1.51e-08	7.23e-08	1.65e-08	6.98e-08	6.13e-08	6.82e-07
^{22}Ne	1.21e-08	2.04e-08	3.11e-08	1.97e-08	6.44e-07	6.34e-07
^{23}Na	1.45e-06	1.36e-05	1.45e-06	1.36e-05	1.62e-06	2.86e-05
^{24}Mg	3.05e-03	7.07e-03	3.09e-03	7.26e-03	3.20e-03	3.22e-03
^{25}Mg	2.23e-06	1.99e-05	2.29e-06	1.94e-05	3.38e-06	9.07e-05
^{26}Mg	2.20e-06	3.30e-05	2.22e-06	3.22e-05	3.31e-06	1.41e-04
^{27}Al	7.63e-05	2.83e-04	7.71e-05	2.84e-04	7.98e-05	3.55e-04
^{28}Si	1.28e-02	1.91e-01	1.28e-02	1.91e-01	1.30e-02	1.90e-01
^{29}Si	8.93e-05	4.17e-04	8.96e-05	4.13e-04	9.29e-05	1.42e-03
^{30}Si	1.02e-04	6.09e-04	1.03e-04	6.02e-04	1.10e-04	3.28e-03
^{31}P	7.62e-05	3.17e-04	7.61e-05	3.13e-04	7.81e-05	8.81e-04
^{32}S	5.58e-03	1.13e-01	5.56e-03	1.13e-01	5.59e-03	9.62e-02
^{33}S	7.76e-05	2.51e-04	7.71e-05	2.48e-04	7.67e-05	4.72e-04
^{34}S	1.31e-04	1.33e-03	1.31e-04	1.30e-03	1.35e-04	6.24e-03
^{36}S	3.73e-09	3.36e-08	3.78e-09	3.25e-08	5.07e-09	3.29e-06
^{35}Cl	3.14e-05	8.59e-05	3.13e-05	8.35e-05	3.61e-05	2.29e-04
^{37}Cl	7.89e-06	1.88e-05	7.84e-06	1.84e-05	8.15e-06	3.65e-05
^{36}Ar	1.82e-03	2.10e-02	1.82e-03	2.10e-02	1.84e-03	1.55e-02
^{38}Ar	3.92e-05	5.76e-04	3.90e-05	5.57e-04	4.52e-05	2.64e-03
^{40}Ar	5.79e-10	3.76e-09	5.79e-10	3.78e-09	9.88e-10	2.07e-07
^{39}K	7.96e-05	4.67e-05	8.02e-05	4.56e-05	1.04e-04	1.04e-04
^{41}K	3.21e-06	3.27e-06	3.21e-06	3.21e-06	4.16e-06	5.72e-06
^{40}Ca	6.22e-03	1.91e-02	6.22e-03	1.91e-02	6.34e-03	1.36e-02
^{42}Ca	6.48e-06	1.50e-05	6.52e-06	1.44e-05	9.41e-06	6.28e-05
^{43}Ca	2.98e-05	1.39e-07	2.98e-05	1.38e-07	3.01e-05	3.13e-07
^{44}Ca	1.78e-03	1.52e-05	1.78e-03	1.52e-05	1.83e-03	1.10e-05
^{46}Ca	1.08e-12	5.56e-11	3.99e-12	3.29e-10	5.82e-11	9.89e-08
^{48}Ca	6.43e-12	1.58e-12	6.44e-11	1.12e-11	1.94e-09	4.61e-09
^{45}Sc	3.73e-06	1.73e-07	3.75e-06	1.70e-07	4.99e-06	4.48e-07
^{46}Ti	7.92e-06	5.71e-06	7.88e-06	5.51e-06	7.62e-06	2.14e-05
^{47}Ti	6.90e-05	4.01e-07	6.90e-05	3.95e-07	7.23e-05	1.28e-06
^{48}Ti	3.78e-03	3.68e-04	3.79e-03	3.69e-04	3.92e-03	2.58e-04
^{49}Ti	3.06e-05	2.01e-05	3.09e-05	2.00e-05	4.20e-05	2.92e-05
^{50}Ti	2.10e-11	8.20e-09	1.03e-10	1.51e-07	2.48e-09	4.25e-07
^{50}V	2.60e-10	2.91e-09	2.80e-10	3.23e-09	1.26e-09	1.14e-07
^{51}V	2.92e-04	4.96e-05	2.92e-04	4.91e-05	3.11e-04	1.03e-04

Table A.3 continued.

	M08_10_001		M08_10_01		M08_10_3	
	He det [M_{\odot}]	core det [M_{\odot}]	He det [M_{\odot}]	core det [M_{\odot}]	He det [M_{\odot}]	core det [M_{\odot}]
⁵⁰ Cr	4.27e-05	1.21e-04	4.23e-05	1.19e-04	3.49e-05	6.06e-04
⁵² Cr	7.36e-03	7.93e-03	7.37e-03	7.94e-03	7.90e-03	6.23e-03
⁵³ Cr	9.66e-05	5.68e-04	9.77e-05	5.65e-04	1.36e-04	9.99e-04
⁵⁴ Cr	3.27e-10	3.32e-08	6.48e-10	1.94e-07	9.85e-09	8.86e-07
⁵⁵ Mn	9.20e-04	2.83e-03	9.22e-04	2.81e-03	9.72e-04	6.29e-03
⁵⁴ Fe	6.25e-05	1.30e-02	6.32e-05	1.28e-02	8.74e-05	5.57e-02
⁵⁶ Fe	1.49e-02	3.24e-01	1.49e-02	3.24e-01	1.49e-02	2.79e-01
⁵⁷ Fe	1.29e-03	4.50e-03	1.29e-03	4.47e-03	1.31e-03	7.84e-03
⁵⁸ Fe	1.03e-09	1.76e-08	8.95e-09	1.18e-07	2.79e-07	2.70e-06
⁵⁹ Co	4.16e-05	1.00e-04	4.18e-05	9.93e-05	5.33e-05	1.80e-04
⁵⁸ Ni	1.74e-04	4.15e-03	1.76e-04	4.07e-03	2.47e-04	2.04e-02
⁶⁰ Ni	1.59e-03	2.17e-03	1.59e-03	2.18e-03	1.57e-03	1.35e-03
⁶¹ Ni	2.97e-04	6.96e-05	2.97e-04	6.96e-05	2.86e-04	8.84e-05
⁶² Ni	1.24e-04	3.90e-04	1.26e-04	3.86e-04	1.80e-04	1.20e-03
⁶⁴ Ni	3.95e-10	7.29e-09	3.78e-09	7.00e-08	8.19e-08	6.80e-06
⁶³ Cu	5.67e-06	1.74e-07	5.72e-06	3.85e-07	6.82e-06	6.42e-06
⁶⁴ Zn	1.43e-04	6.61e-06	1.42e-04	7.06e-06	1.13e-04	3.78e-06
⁶⁶ Zn	1.56e-05	7.05e-06	1.61e-05	7.90e-06	2.39e-05	2.68e-05
⁶⁷ Zn	1.34e-06	5.95e-09	1.50e-06	2.27e-08	4.03e-06	1.06e-06
⁶⁸ Zn	8.78e-07	7.59e-09	1.37e-06	6.14e-08	4.36e-06	2.11e-06
⁷⁰ Zn	1.60e-12	5.33e-11	1.55e-11	5.05e-10	3.57e-10	4.68e-08
⁶⁹ Ga	5.31e-08	4.05e-09	1.03e-07	3.96e-08	3.10e-07	3.37e-07
⁷¹ Ga	3.32e-09	6.53e-10	8.27e-09	6.24e-09	2.68e-08	1.45e-07

Table A.4: Asymptotic nucleosynthesis yields (in solar masses) for Model M09_03 with 0.01, 0.1, and $3 Z_{\odot}$.

	M09_03_001		M09_03_01		M09_03_3	
	He det [M_{\odot}]	core det [M_{\odot}]	He det [M_{\odot}]	core det [M_{\odot}]	He det [M_{\odot}]	core det [M_{\odot}]
^{12}C	3.52e-03	4.94e-03	3.51e-03	4.94e-03	3.42e-03	4.74e-03
^{13}C	1.07e-09	6.50e-08	1.07e-09	6.18e-08	7.16e-10	3.37e-07
^{14}N	3.59e-07	3.81e-06	1.42e-06	3.67e-06	3.57e-05	5.32e-06
^{15}N	5.76e-08	8.09e-09	6.03e-08	7.90e-09	1.50e-07	1.03e-08
^{16}O	3.78e-03	9.17e-02	3.79e-03	9.15e-02	4.17e-03	9.31e-02
^{17}O	3.34e-08	1.01e-06	3.49e-08	9.85e-07	7.45e-08	1.30e-06
^{18}O	5.35e-08	1.55e-08	6.39e-08	1.49e-08	3.99e-07	2.23e-08
^{19}F	4.24e-08	3.01e-10	4.46e-08	2.90e-10	1.17e-07	1.05e-09
^{20}Ne	2.81e-03	3.43e-03	2.81e-03	3.43e-03	2.91e-03	3.02e-03
^{21}Ne	3.60e-07	1.25e-06	3.64e-07	1.19e-06	4.97e-07	4.64e-06
^{22}Ne	3.02e-07	2.56e-05	3.28e-07	2.47e-05	1.09e-06	2.05e-04
^{23}Na	1.92e-05	3.40e-05	1.92e-05	3.34e-05	1.90e-05	9.11e-05
^{24}Mg	3.12e-03	7.17e-03	3.12e-03	7.37e-03	3.23e-03	3.19e-03
^{25}Mg	3.09e-05	5.32e-05	3.10e-05	5.22e-05	3.80e-05	2.06e-04
^{26}Mg	4.71e-05	7.52e-05	4.70e-05	7.34e-05	4.58e-05	3.05e-04
^{27}Al	1.14e-04	2.84e-04	1.14e-04	2.85e-04	1.15e-04	3.62e-04
^{28}Si	5.76e-03	2.20e-01	5.77e-03	2.20e-01	5.88e-03	2.19e-01
^{29}Si	8.69e-05	4.69e-04	8.65e-05	4.65e-04	8.20e-05	1.47e-03
^{30}Si	8.52e-05	6.45e-04	8.51e-05	6.38e-04	8.51e-05	3.41e-03
^{31}P	7.16e-05	3.37e-04	7.16e-05	3.32e-04	7.29e-05	9.23e-04
^{32}S	2.74e-03	1.31e-01	2.74e-03	1.31e-01	2.88e-03	1.11e-01
^{33}S	2.41e-05	2.67e-04	2.40e-05	2.64e-04	2.39e-05	5.13e-04
^{34}S	1.29e-05	1.54e-03	1.29e-05	1.50e-03	1.36e-05	7.20e-03
^{36}S	1.15e-09	3.94e-08	3.30e-09	4.32e-08	2.87e-08	3.40e-06
^{35}Cl	3.86e-05	9.08e-05	3.88e-05	8.84e-05	4.64e-05	2.36e-04
^{37}Cl	3.00e-06	2.14e-05	3.00e-06	2.10e-05	3.15e-06	4.22e-05
^{36}Ar	1.10e-03	2.44e-02	1.11e-03	2.44e-02	1.21e-03	1.80e-02
^{38}Ar	3.39e-06	6.85e-04	3.43e-06	6.64e-04	5.14e-06	3.17e-03
^{40}Ar	4.34e-10	3.89e-09	3.34e-09	6.44e-09	2.66e-08	3.48e-07
^{39}K	6.89e-05	5.42e-05	6.96e-05	5.30e-05	9.54e-05	1.22e-04
^{41}K	1.04e-05	3.82e-06	1.03e-05	3.75e-06	1.10e-05	6.80e-06
^{40}Ca	3.95e-03	2.23e-02	3.95e-03	2.23e-02	4.07e-03	1.59e-02
^{42}Ca	3.92e-06	1.75e-05	4.00e-06	1.68e-05	7.15e-06	7.50e-05
^{43}Ca	8.68e-06	6.57e-08	8.78e-06	6.51e-08	1.39e-05	3.38e-07
^{44}Ca	7.50e-04	1.58e-05	7.47e-04	1.58e-05	6.50e-04	1.19e-05
^{46}Ca	1.20e-10	1.74e-10	1.15e-09	1.54e-09	1.01e-08	1.64e-07
^{48}Ca	2.09e-11	1.32e-11	1.99e-10	1.25e-10	3.60e-09	1.48e-08
^{45}Sc	4.60e-06	1.92e-07	4.63e-06	1.91e-07	5.30e-06	5.30e-07
^{46}Ti	2.23e-06	6.73e-06	2.25e-06	6.51e-06	3.17e-06	2.53e-05
^{47}Ti	4.07e-05	3.13e-07	4.07e-05	3.08e-07	4.13e-05	1.38e-06
^{48}Ti	1.26e-04	4.29e-04	1.24e-04	4.30e-04	7.52e-05	3.02e-04
^{49}Ti	3.70e-06	2.34e-05	3.69e-06	2.32e-05	3.17e-06	3.39e-05
^{50}Ti	1.07e-10	7.98e-10	1.09e-09	1.98e-09	3.77e-08	3.97e-07
^{50}V	3.04e-10	2.57e-09	3.74e-10	3.13e-09	4.33e-09	1.08e-07
^{51}V	5.48e-06	5.72e-05	5.42e-06	5.67e-05	3.74e-06	1.19e-04

Table A.4 continued.

	M09_03_001		M09_03_01		M09_03_3	
	He det [M_{\odot}]	core det [M_{\odot}]	He det [M_{\odot}]	core det [M_{\odot}]	He det [M_{\odot}]	core det [M_{\odot}]
⁵⁰ Cr	1.37e-06	1.41e-04	1.37e-06	1.38e-04	1.34e-06	7.01e-04
⁵² Cr	5.26e-06	9.50e-03	5.17e-06	9.51e-03	3.14e-06	7.45e-03
⁵³ Cr	4.67e-07	6.72e-04	4.65e-07	6.67e-04	4.37e-07	1.18e-03
⁵⁴ Cr	3.18e-10	2.14e-08	2.99e-09	2.24e-08	1.25e-07	1.01e-06
⁵⁵ Mn	2.61e-07	3.37e-03	2.76e-07	3.34e-03	9.72e-07	7.50e-03
⁵⁴ Fe	1.53e-07	1.55e-02	1.88e-07	1.52e-02	1.45e-06	6.63e-02
⁵⁶ Fe	8.12e-07	3.43e-01	1.38e-06	3.43e-01	2.62e-05	2.95e-01
⁵⁷ Fe	1.09e-07	4.05e-03	2.14e-07	4.02e-03	7.64e-06	7.28e-03
⁵⁸ Fe	1.13e-08	2.32e-08	1.23e-07	1.19e-07	8.69e-06	4.88e-06
⁵⁹ Co	4.38e-08	5.84e-05	3.01e-07	5.81e-05	1.19e-05	9.69e-05
⁵⁸ Ni	4.99e-08	3.78e-03	2.37e-07	3.71e-03	1.28e-05	1.77e-02
⁶⁰ Ni	1.35e-07	1.04e-03	7.78e-07	1.05e-03	9.88e-06	5.98e-04
⁶¹ Ni	3.92e-08	3.14e-05	2.69e-07	3.16e-05	2.54e-06	4.02e-05
⁶² Ni	5.63e-08	1.84e-04	4.65e-07	1.83e-04	3.87e-06	4.98e-04
⁶⁴ Ni	1.54e-09	7.28e-09	1.57e-08	7.06e-08	2.79e-07	6.07e-06
⁶³ Cu	8.89e-09	8.71e-08	7.59e-08	3.12e-07	8.26e-07	5.90e-06
⁶⁴ Zn	1.85e-08	2.15e-06	4.00e-08	2.54e-06	2.35e-07	1.79e-06
⁶⁶ Zn	6.70e-09	2.45e-06	4.80e-08	3.34e-06	2.77e-07	1.49e-05
⁶⁷ Zn	1.15e-09	2.93e-09	9.15e-09	1.83e-08	4.25e-08	8.87e-07
⁶⁸ Zn	1.10e-09	5.97e-09	8.89e-09	5.40e-08	5.31e-08	1.88e-06
⁷⁰ Zn	8.56e-12	5.68e-11	9.59e-11	5.51e-10	9.23e-09	3.93e-08
⁶⁹ Ga	1.03e-10	3.47e-09	9.17e-10	3.39e-08	1.85e-08	3.09e-07
⁷¹ Ga	6.12e-11	4.95e-10	6.04e-10	4.74e-09	1.09e-08	1.23e-07

Table A.5: Asymptotic nucleosynthesis yields (in solar masses) for Model M09_05 with 0.01, 0.1, and $3 Z_{\odot}$.

	M09_05_001		M09_05_01		M09_05_3	
	He det [M_{\odot}]	core det [M_{\odot}]	He det [M_{\odot}]	core det [M_{\odot}]	He det [M_{\odot}]	core det [M_{\odot}]
^{12}C	4.37e-04	2.67e-03	4.36e-04	2.66e-03	4.29e-04	2.58e-03
^{13}C	2.49e-11	3.02e-09	2.40e-11	2.83e-09	1.87e-11	3.17e-08
^{14}N	1.66e-07	4.48e-07	1.23e-06	4.26e-07	3.54e-05	1.70e-06
^{15}N	1.00e-08	2.92e-09	1.06e-08	2.93e-09	2.67e-08	4.12e-09
^{16}O	7.12e-03	7.73e-02	7.14e-03	7.71e-02	7.61e-03	7.86e-02
^{17}O	6.28e-10	9.49e-08	2.03e-09	9.06e-08	4.70e-08	2.48e-07
^{18}O	7.88e-09	2.76e-09	1.57e-08	2.65e-09	2.67e-07	9.41e-09
^{19}F	5.20e-09	7.40e-11	5.58e-09	7.09e-11	1.71e-08	3.94e-10
^{20}Ne	1.05e-03	3.65e-03	1.04e-03	3.65e-03	1.03e-03	3.26e-03
^{21}Ne	2.89e-08	3.53e-07	3.03e-08	3.33e-07	7.42e-08	2.49e-06
^{22}Ne	1.88e-08	9.32e-07	3.82e-08	8.74e-07	6.58e-07	2.48e-05
^{23}Na	5.44e-06	2.20e-05	5.41e-06	2.17e-05	5.55e-06	5.77e-05
^{24}Mg	3.19e-03	6.48e-03	3.20e-03	6.66e-03	3.28e-03	2.89e-03
^{25}Mg	6.19e-06	3.29e-05	6.24e-06	3.21e-05	7.53e-06	1.58e-04
^{26}Mg	1.00e-05	5.66e-05	1.00e-05	5.51e-05	1.10e-05	2.68e-04
^{27}Al	1.08e-04	2.58e-04	1.08e-04	2.59e-04	1.12e-04	3.32e-04
^{28}Si	9.96e-03	1.91e-01	9.97e-03	1.91e-01	1.01e-02	1.90e-01
^{29}Si	9.01e-05	4.23e-04	9.00e-05	4.19e-04	9.22e-05	1.38e-03
^{30}Si	9.47e-05	5.68e-04	9.49e-05	5.62e-04	1.00e-04	2.96e-03
^{31}P	8.31e-05	2.93e-04	8.31e-05	2.89e-04	8.59e-05	8.01e-04
^{32}S	4.46e-03	1.14e-01	4.46e-03	1.14e-01	4.49e-03	9.72e-02
^{33}S	6.94e-05	2.28e-04	6.92e-05	2.24e-04	6.91e-05	4.37e-04
^{34}S	5.41e-05	1.30e-03	5.41e-05	1.27e-03	5.88e-05	6.11e-03
^{36}S	2.52e-09	3.43e-08	2.55e-09	3.49e-08	4.77e-09	3.12e-06
^{35}Cl	3.74e-05	8.04e-05	3.74e-05	7.83e-05	4.21e-05	2.09e-04
^{37}Cl	9.44e-06	1.82e-05	9.41e-06	1.78e-05	9.55e-06	3.61e-05
^{36}Ar	1.53e-03	2.15e-02	1.53e-03	2.15e-02	1.56e-03	1.60e-02
^{38}Ar	2.13e-05	5.80e-04	2.14e-05	5.62e-04	2.67e-05	2.69e-03
^{40}Ar	6.19e-10	3.38e-09	7.13e-10	4.48e-09	2.21e-09	2.99e-07
^{39}K	8.48e-05	4.65e-05	8.54e-05	4.55e-05	1.07e-04	1.05e-04
^{41}K	6.35e-06	3.26e-06	6.35e-06	3.20e-06	7.10e-06	5.83e-06
^{40}Ca	5.08e-03	1.99e-02	5.08e-03	1.99e-02	5.22e-03	1.44e-02
^{42}Ca	7.13e-06	1.48e-05	7.19e-06	1.42e-05	1.01e-05	6.38e-05
^{43}Ca	2.44e-05	1.50e-07	2.43e-05	1.49e-07	2.49e-05	3.22e-07
^{44}Ca	1.99e-03	1.65e-05	2.00e-03	1.66e-05	2.13e-03	1.18e-05
^{46}Ca	6.66e-12	1.08e-10	5.97e-11	9.20e-10	6.68e-10	1.58e-07
^{48}Ca	6.87e-12	4.52e-12	6.85e-11	4.15e-11	2.00e-09	1.20e-08
^{45}Sc	4.00e-06	1.68e-07	4.02e-06	1.67e-07	5.34e-06	4.76e-07
^{46}Ti	3.56e-06	5.70e-06	3.60e-06	5.51e-06	5.23e-06	2.16e-05
^{47}Ti	5.47e-05	4.25e-07	5.50e-05	4.21e-07	6.80e-05	1.30e-06
^{48}Ti	4.48e-03	4.03e-04	4.49e-03	4.04e-04	4.97e-03	2.86e-04
^{49}Ti	4.11e-05	2.16e-05	4.14e-05	2.15e-05	5.48e-05	3.19e-05
^{50}Ti	1.92e-11	3.30e-10	1.53e-10	1.32e-09	4.80e-09	3.44e-07
^{50}V	1.25e-10	2.16e-09	2.15e-10	2.76e-09	2.43e-09	9.38e-08
^{51}V	3.73e-04	5.30e-05	3.74e-04	5.25e-05	4.23e-04	1.11e-04

Table A.5 continued.

	M09_05_001		M09_05_01		M09_05_3	
	He det [M_{\odot}]	core det [M_{\odot}]	He det [M_{\odot}]	core det [M_{\odot}]	He det [M_{\odot}]	core det [M_{\odot}]
⁵⁰ Cr	1.83e-05	1.25e-04	1.85e-05	1.22e-04	2.49e-05	6.20e-04
⁵² Cr	5.09e-03	8.80e-03	5.10e-03	8.81e-03	5.27e-03	6.91e-03
⁵³ Cr	1.36e-04	6.21e-04	1.37e-04	6.17e-04	1.72e-04	1.09e-03
⁵⁴ Cr	2.85e-10	1.61e-08	7.55e-10	1.86e-08	1.84e-08	8.47e-07
⁵⁵ Mn	4.12e-04	3.10e-03	4.12e-04	3.07e-03	3.95e-04	6.94e-03
⁵⁴ Fe	8.26e-05	1.38e-02	8.31e-05	1.35e-02	9.72e-05	5.93e-02
⁵⁶ Fe	2.13e-03	3.98e-01	2.12e-03	3.98e-01	1.72e-03	3.45e-01
⁵⁷ Fe	1.38e-04	5.79e-03	1.38e-04	5.76e-03	1.31e-04	1.01e-02
⁵⁸ Fe	1.67e-09	1.16e-08	1.52e-08	7.01e-08	1.05e-06	3.01e-06
⁵⁹ Co	1.22e-05	1.45e-04	1.25e-05	1.44e-04	2.37e-05	2.55e-04
⁵⁸ Ni	7.34e-05	5.47e-03	7.42e-05	5.36e-03	1.12e-04	2.72e-02
⁶⁰ Ni	7.56e-05	3.21e-03	7.56e-05	3.22e-03	6.70e-05	1.89e-03
⁶¹ Ni	1.00e-05	1.01e-04	1.01e-05	1.01e-04	1.27e-05	1.19e-04
⁶² Ni	1.30e-05	5.82e-04	1.37e-05	5.75e-04	3.05e-05	1.70e-03
⁶⁴ Ni	1.17e-09	7.32e-09	1.12e-08	7.10e-08	2.05e-07	5.24e-06
⁶³ Cu	5.36e-07	2.40e-07	6.37e-07	4.51e-07	3.07e-06	6.80e-06
⁶⁴ Zn	1.48e-06	9.50e-06	1.66e-06	9.89e-06	4.52e-06	4.26e-06
⁶⁶ Zn	9.24e-07	1.04e-05	1.21e-06	1.10e-05	6.33e-06	3.04e-05
⁶⁷ Zn	2.57e-07	7.43e-09	3.69e-07	2.34e-08	2.21e-06	8.20e-07
⁶⁸ Zn	3.75e-07	6.68e-09	6.45e-07	4.70e-08	2.59e-06	1.54e-06
⁷⁰ Zn	6.03e-12	6.02e-11	5.60e-11	5.82e-10	1.73e-09	3.47e-08
⁶⁹ Ga	3.35e-08	2.96e-09	6.63e-08	2.90e-08	2.23e-07	2.67e-07
⁷¹ Ga	2.83e-09	4.88e-10	7.19e-09	4.69e-09	3.17e-08	1.02e-07

Table A.6: Asymptotic nucleosynthesis yields (in solar masses) for Model M09_10 with 0.01, 0.1, and $3 Z_{\odot}$.

	M09_10_001		M09_10_01		M09_10_3	
	He det [M_{\odot}]	core det [M_{\odot}]	He det [M_{\odot}]	core det [M_{\odot}]	He det [M_{\odot}]	core det [M_{\odot}]
^{12}C	3.82e-05	1.36e-04	3.82e-05	1.35e-04	3.80e-05	1.32e-04
^{13}C	1.89e-09	5.87e-12	1.88e-09	5.74e-12	1.55e-09	2.21e-11
^{14}N	2.49e-07	1.93e-10	1.31e-06	1.93e-10	3.55e-05	4.65e-10
^{15}N	1.39e-08	3.94e-10	1.47e-08	4.25e-10	3.74e-08	2.34e-10
^{16}O	8.36e-03	5.46e-02	8.37e-03	5.45e-02	8.82e-03	5.55e-02
^{17}O	2.08e-10	2.45e-11	1.61e-09	2.37e-11	4.67e-08	1.29e-10
^{18}O	1.69e-08	1.80e-12	2.53e-08	1.31e-12	2.93e-07	4.78e-12
^{19}F	4.86e-09	5.08e-13	5.22e-09	4.89e-13	1.62e-08	3.78e-12
^{20}Ne	8.63e-06	6.41e-04	8.84e-06	6.38e-04	1.82e-05	5.90e-04
^{21}Ne	1.95e-08	1.31e-08	2.13e-08	1.27e-08	7.74e-08	7.73e-08
^{22}Ne	1.11e-08	6.66e-09	3.03e-08	6.32e-09	6.47e-07	8.89e-09
^{23}Na	1.93e-07	3.57e-06	1.98e-07	3.39e-06	3.95e-07	6.21e-06
^{24}Mg	2.37e-03	4.04e-03	2.40e-03	4.16e-03	2.51e-03	1.80e-03
^{25}Mg	5.95e-07	5.91e-06	6.37e-07	5.81e-06	1.72e-06	2.01e-05
^{26}Mg	4.63e-07	7.57e-06	5.03e-07	7.32e-06	1.60e-06	2.48e-05
^{27}Al	3.59e-05	1.52e-04	3.65e-05	1.53e-04	3.82e-05	1.86e-04
^{28}Si	1.26e-02	1.54e-01	1.26e-02	1.55e-01	1.28e-02	1.54e-01
^{29}Si	6.67e-05	2.44e-04	6.71e-05	2.42e-04	7.00e-05	7.32e-04
^{30}Si	8.74e-05	3.80e-04	8.87e-05	3.76e-04	9.40e-05	2.09e-03
^{31}P	4.43e-05	2.17e-04	4.44e-05	2.14e-04	4.56e-05	5.96e-04
^{32}S	4.37e-03	9.47e-02	4.35e-03	9.46e-02	4.31e-03	8.07e-02
^{33}S	4.66e-05	1.78e-04	4.63e-05	1.76e-04	4.58e-05	3.44e-04
^{34}S	2.28e-04	9.94e-04	2.26e-04	9.70e-04	2.21e-04	4.67e-03
^{36}S	3.24e-09	2.00e-08	3.32e-09	1.97e-08	4.56e-09	1.42e-06
^{35}Cl	1.90e-05	5.96e-05	1.90e-05	5.79e-05	2.06e-05	1.54e-04
^{37}Cl	3.61e-06	1.44e-05	3.58e-06	1.41e-05	3.77e-06	2.80e-05
^{36}Ar	1.24e-03	1.83e-02	1.24e-03	1.82e-02	1.25e-03	1.37e-02
^{38}Ar	6.03e-05	4.42e-04	5.98e-05	4.28e-04	6.11e-05	2.04e-03
^{40}Ar	1.73e-10	2.39e-09	1.79e-10	2.38e-09	5.15e-10	7.22e-08
^{39}K	3.80e-05	3.69e-05	3.82e-05	3.60e-05	4.97e-05	8.22e-05
^{41}K	1.14e-06	2.59e-06	1.15e-06	2.54e-06	1.74e-06	4.58e-06
^{40}Ca	4.70e-03	1.72e-02	4.70e-03	1.72e-02	4.81e-03	1.26e-02
^{42}Ca	3.54e-06	1.16e-05	3.54e-06	1.11e-05	4.91e-06	4.90e-05
^{43}Ca	1.36e-05	3.10e-07	1.36e-05	3.10e-07	1.34e-05	2.68e-07
^{44}Ca	8.70e-04	1.81e-05	8.71e-04	1.81e-05	9.07e-04	1.18e-05
^{46}Ca	6.34e-13	4.57e-11	2.14e-12	1.43e-10	4.49e-11	1.99e-08
^{48}Ca	6.43e-12	4.24e-12	6.43e-11	6.42e-12	1.94e-09	4.36e-08
^{45}Sc	8.47e-07	1.44e-07	8.58e-07	1.41e-07	1.53e-06	3.01e-07
^{46}Ti	4.17e-05	4.43e-06	4.13e-05	4.28e-06	3.06e-05	1.69e-05
^{47}Ti	5.70e-05	6.54e-07	5.68e-05	6.48e-07	5.25e-05	1.09e-06
^{48}Ti	1.88e-03	3.74e-04	1.88e-03	3.74e-04	1.99e-03	2.63e-04
^{49}Ti	2.04e-05	1.96e-05	2.07e-05	1.95e-05	2.80e-05	2.91e-05
^{50}Ti	2.12e-11	4.05e-10	8.87e-11	1.64e-09	2.25e-09	1.10e-06
^{50}V	2.00e-10	1.88e-09	1.99e-10	1.94e-09	5.53e-10	6.62e-08
^{51}V	2.67e-04	4.88e-05	2.66e-04	4.83e-05	2.50e-04	1.02e-04

Table A.6 continued.

	M09_10_001		M09_10_01		M09_10_3	
	He det [M_{\odot}]	core det [M_{\odot}]	He det [M_{\odot}]	core det [M_{\odot}]	He det [M_{\odot}]	core det [M_{\odot}]
⁵⁰ Cr	2.26e-04	1.07e-04	2.25e-04	1.05e-04	1.86e-04	5.33e-04
⁵² Cr	3.98e-03	8.10e-03	3.98e-03	8.12e-03	4.08e-03	6.35e-03
⁵³ Cr	6.05e-05	5.69e-04	6.11e-05	5.66e-04	8.41e-05	9.98e-04
⁵⁴ Cr	2.57e-10	1.63e-08	4.38e-10	2.02e-08	7.17e-09	1.03e-06
⁵⁵ Mn	3.68e-04	2.89e-03	3.69e-04	2.86e-03	3.83e-04	6.49e-03
⁵⁴ Fe	4.00e-05	1.20e-02	4.05e-05	1.18e-02	6.01e-05	5.23e-02
⁵⁶ Fe	2.60e-02	4.93e-01	2.60e-02	4.93e-01	2.65e-02	4.29e-01
⁵⁷ Fe	2.40e-03	8.62e-03	2.40e-03	8.57e-03	2.42e-03	1.45e-02
⁵⁸ Fe	4.63e-10	1.17e-08	3.79e-09	4.41e-08	1.12e-07	1.66e-06
⁵⁹ Co	3.57e-04	2.81e-04	3.56e-04	2.79e-04	3.01e-04	4.97e-04
⁵⁸ Ni	6.69e-04	8.16e-03	6.68e-04	7.99e-03	6.42e-04	4.14e-02
⁶⁰ Ni	2.70e-03	6.39e-03	2.70e-03	6.41e-03	2.68e-03	3.82e-03
⁶¹ Ni	3.93e-04	2.11e-04	3.92e-04	2.10e-04	3.75e-04	2.39e-04
⁶² Ni	1.65e-04	1.19e-03	1.65e-04	1.18e-03	1.68e-04	3.50e-03
⁶⁴ Ni	5.11e-11	2.43e-09	5.06e-10	2.14e-08	1.29e-08	3.72e-06
⁶³ Cu	1.36e-05	4.85e-07	1.36e-05	5.66e-07	1.35e-05	4.08e-06
⁶⁴ Zn	2.59e-04	2.11e-05	2.59e-04	2.15e-05	2.71e-04	8.70e-06
⁶⁶ Zn	2.44e-05	2.32e-05	2.46e-05	2.35e-05	3.08e-05	5.69e-05
⁶⁷ Zn	9.43e-07	1.43e-08	1.00e-06	1.91e-08	2.02e-06	5.60e-07
⁶⁸ Zn	5.22e-07	8.47e-09	7.67e-07	3.93e-08	2.09e-06	1.53e-06
⁷⁰ Zn	4.77e-13	1.48e-11	4.59e-12	1.35e-10	1.11e-10	2.51e-08
⁶⁹ Ga	3.26e-08	2.50e-09	5.93e-08	2.43e-08	1.37e-07	2.72e-07
⁷¹ Ga	2.18e-09	2.99e-10	4.92e-09	2.84e-09	9.66e-09	1.11e-07

Table A.7: Asymptotic nucleosynthesis yields (in solar masses) for Model M10_02 with 0.01, 0.1, and $3 Z_{\odot}$.

	M10_02_001		M10_02_01		M10_02_3	
	He det [M_{\odot}]	core det [M_{\odot}]	He det [M_{\odot}]	core det [M_{\odot}]	He det [M_{\odot}]	core det [M_{\odot}]
^{12}C	1.69e-03	1.97e-03	1.69e-03	1.97e-03	1.65e-03	1.90e-03
^{13}C	3.51e-10	1.77e-08	3.50e-10	1.67e-08	2.44e-10	9.78e-08
^{14}N	2.02e-07	9.45e-07	1.25e-06	9.07e-07	3.50e-05	1.55e-06
^{15}N	2.72e-08	2.50e-09	2.85e-08	2.46e-09	6.99e-08	3.17e-09
^{16}O	1.77e-03	5.67e-02	1.78e-03	5.66e-02	2.02e-03	5.76e-02
^{17}O	8.79e-09	2.32e-07	1.02e-08	2.26e-07	5.32e-08	3.20e-07
^{18}O	2.43e-08	3.93e-09	3.29e-08	3.77e-09	3.11e-07	6.90e-09
^{19}F	1.96e-08	8.79e-11	2.07e-08	8.47e-11	5.59e-08	3.43e-10
^{20}Ne	1.30e-03	1.96e-03	1.30e-03	1.96e-03	1.35e-03	1.75e-03
^{21}Ne	1.16e-07	3.91e-07	1.19e-07	3.73e-07	2.00e-07	1.84e-06
^{22}Ne	9.70e-08	5.45e-06	1.19e-07	5.24e-06	7.90e-07	5.14e-05
^{23}Na	8.84e-06	1.44e-05	8.83e-06	1.42e-05	8.92e-06	3.84e-05
^{24}Mg	1.50e-03	4.27e-03	1.50e-03	4.38e-03	1.56e-03	1.86e-03
^{25}Mg	1.32e-05	2.23e-05	1.32e-05	2.18e-05	1.68e-05	9.46e-05
^{26}Mg	2.03e-05	3.49e-05	2.03e-05	3.40e-05	2.11e-05	1.51e-04
^{27}Al	5.56e-05	1.62e-04	5.56e-05	1.63e-04	5.68e-05	2.03e-04
^{28}Si	2.92e-03	1.70e-01	2.92e-03	1.70e-01	3.00e-03	1.70e-01
^{29}Si	4.44e-05	2.86e-04	4.42e-05	2.83e-04	4.23e-05	8.85e-04
^{30}Si	4.46e-05	3.99e-04	4.46e-05	3.94e-04	4.46e-05	2.05e-03
^{31}P	3.79e-05	2.12e-04	3.79e-05	2.09e-04	3.89e-05	5.81e-04
^{32}S	1.58e-03	1.05e-01	1.58e-03	1.05e-01	1.67e-03	8.95e-02
^{33}S	1.37e-05	1.67e-04	1.36e-05	1.65e-04	1.38e-05	3.35e-04
^{34}S	1.14e-05	1.02e-03	1.13e-05	9.91e-04	1.05e-05	4.80e-03
^{36}S	6.19e-10	2.33e-08	1.46e-09	2.41e-08	1.22e-08	1.98e-06
^{35}Cl	2.35e-05	6.10e-05	2.36e-05	5.95e-05	2.92e-05	1.62e-04
^{37}Cl	1.96e-06	1.47e-05	1.96e-06	1.44e-05	2.22e-06	3.03e-05
^{36}Ar	7.64e-04	2.06e-02	7.66e-04	2.06e-02	8.49e-04	1.55e-02
^{38}Ar	2.12e-06	4.68e-04	2.14e-06	4.54e-04	3.20e-06	2.23e-03
^{40}Ar	1.89e-10	2.40e-09	1.38e-09	3.27e-09	1.15e-08	1.79e-07
^{39}K	4.79e-05	3.91e-05	4.85e-05	3.83e-05	7.02e-05	9.01e-05
^{41}K	4.61e-06	2.77e-06	4.61e-06	2.72e-06	5.18e-06	5.09e-06
^{40}Ca	2.32e-03	1.96e-02	2.33e-03	1.97e-02	2.52e-03	1.44e-02
^{42}Ca	1.74e-06	1.19e-05	1.78e-06	1.14e-05	3.18e-06	5.33e-05
^{43}Ca	4.35e-06	2.86e-07	4.39e-06	2.86e-07	6.67e-06	2.78e-07
^{44}Ca	5.72e-04	1.99e-05	5.72e-04	1.99e-05	5.54e-04	1.31e-05
^{46}Ca	5.62e-11	7.27e-11	5.40e-10	6.29e-10	4.78e-09	9.12e-08
^{48}Ca	1.25e-11	4.35e-12	1.21e-10	4.08e-11	2.68e-09	7.35e-09
^{45}Sc	2.18e-06	1.50e-07	2.20e-06	1.49e-07	2.95e-06	3.62e-07
^{46}Ti	1.08e-06	4.71e-06	1.09e-06	4.56e-06	1.58e-06	1.85e-05
^{47}Ti	2.73e-05	6.31e-07	2.75e-05	6.28e-07	3.15e-05	1.18e-06
^{48}Ti	2.53e-04	4.32e-04	2.51e-04	4.33e-04	1.95e-04	3.06e-04
^{49}Ti	3.65e-06	2.25e-05	3.67e-06	2.24e-05	4.30e-06	3.35e-05
^{50}Ti	5.78e-11	2.10e-10	5.92e-10	8.31e-10	1.99e-08	2.21e-07
^{50}V	8.61e-11	1.41e-09	1.26e-10	1.80e-09	2.34e-09	6.25e-08
^{51}V	1.10e-05	5.55e-05	1.10e-05	5.50e-05	9.88e-06	1.16e-04

Table A.7 continued.

	M10_02_001		M10_02_01		M10_02_3	
	He det [M_{\odot}]	core det [M_{\odot}]	He det [M_{\odot}]	core det [M_{\odot}]	He det [M_{\odot}]	core det [M_{\odot}]
⁵⁰ Cr	1.36e-06	1.20e-04	1.37e-06	1.18e-04	1.64e-06	6.02e-04
⁵² Cr	2.92e-05	9.50e-03	2.89e-05	9.51e-03	1.98e-05	7.44e-03
⁵³ Cr	1.29e-06	6.62e-04	1.29e-06	6.57e-04	1.35e-06	1.16e-03
⁵⁴ Cr	1.73e-10	1.38e-08	1.59e-09	1.55e-08	6.43e-08	7.00e-07
⁵⁵ Mn	1.28e-06	3.34e-03	1.29e-06	3.30e-03	1.62e-06	7.51e-03
⁵⁴ Fe	5.00e-07	1.38e-02	5.30e-07	1.35e-02	1.55e-06	6.04e-02
⁵⁶ Fe	1.87e-06	5.59e-01	2.33e-06	5.59e-01	2.03e-05	4.87e-01
⁵⁷ Fe	3.03e-07	9.28e-03	3.85e-07	9.23e-03	5.05e-06	1.59e-02
⁵⁸ Fe	5.78e-09	8.59e-09	6.29e-08	4.47e-08	4.29e-06	2.23e-06
⁵⁹ Co	7.96e-08	2.94e-04	2.56e-07	2.91e-04	7.37e-06	5.20e-04
⁵⁸ Ni	9.22e-08	8.91e-03	2.53e-07	8.73e-03	9.67e-06	4.55e-02
⁶⁰ Ni	1.35e-07	6.90e-03	4.66e-07	6.92e-03	5.31e-06	4.05e-03
⁶¹ Ni	5.07e-08	2.20e-04	1.76e-07	2.19e-04	1.65e-06	2.49e-04
⁶² Ni	5.97e-08	1.27e-03	2.99e-07	1.26e-03	2.41e-06	3.73e-03
⁶⁴ Ni	7.97e-10	4.46e-09	8.13e-09	4.33e-08	1.40e-07	3.16e-06
⁶³ Cu	8.85e-09	5.00e-07	4.80e-08	6.27e-07	4.93e-07	5.56e-06
⁶⁴ Zn	1.29e-08	2.24e-05	2.74e-08	2.28e-05	1.78e-07	8.56e-06
⁶⁶ Zn	6.43e-09	2.46e-05	3.23e-08	2.48e-05	1.63e-07	5.70e-05
⁶⁷ Zn	1.59e-09	1.47e-08	8.25e-09	2.44e-08	3.43e-08	5.27e-07
⁶⁸ Zn	1.62e-09	7.74e-09	9.24e-09	3.17e-08	3.89e-08	9.38e-07
⁷⁰ Zn	4.88e-12	3.38e-11	5.42e-11	3.26e-10	4.69e-09	2.05e-08
⁶⁹ Ga	1.26e-10	1.82e-09	8.43e-10	1.78e-08	1.03e-08	1.60e-07
⁷¹ Ga	4.64e-11	3.03e-10	3.95e-10	2.90e-09	6.05e-09	6.13e-08

Table A.8: Asymptotic nucleosynthesis yields (in solar masses) for Model M10_03 with 0.01, 0.1, and $3 Z_{\odot}$.

	M10_03_001		M10_03_01		M10_03_3	
	He det [M_{\odot}]	core det [M_{\odot}]	He det [M_{\odot}]	core det [M_{\odot}]	He det [M_{\odot}]	core det [M_{\odot}]
^{12}C	7.71e-04	1.24e-03	7.68e-04	1.24e-03	7.55e-04	1.20e-03
^{13}C	4.95e-11	1.12e-09	4.92e-11	1.04e-09	3.96e-11	1.19e-08
^{14}N	1.71e-07	1.37e-07	1.22e-06	1.29e-07	3.51e-05	5.12e-07
^{15}N	1.27e-08	1.12e-09	1.33e-08	1.12e-09	3.35e-08	1.27e-09
^{16}O	6.60e-03	4.85e-02	6.62e-03	4.84e-02	7.09e-03	4.93e-02
^{17}O	1.55e-09	3.01e-08	2.94e-09	2.87e-08	4.73e-08	8.03e-08
^{18}O	1.11e-08	8.35e-10	1.91e-08	7.95e-10	2.74e-07	2.83e-09
^{19}F	6.87e-09	2.58e-11	7.33e-09	2.47e-11	2.16e-08	1.52e-10
^{20}Ne	1.70e-03	1.83e-03	1.69e-03	1.83e-03	1.68e-03	1.64e-03
^{21}Ne	4.93e-08	1.34e-07	5.10e-08	1.27e-07	1.02e-07	1.03e-06
^{22}Ne	2.89e-08	3.28e-07	4.84e-08	3.08e-07	6.70e-07	8.38e-06
^{23}Na	8.08e-06	1.04e-05	8.05e-06	1.03e-05	8.14e-06	2.59e-05
^{24}Mg	3.44e-03	3.71e-03	3.45e-03	3.80e-03	3.51e-03	1.61e-03
^{25}Mg	9.30e-06	1.52e-05	9.34e-06	1.48e-05	1.09e-05	7.31e-05
^{26}Mg	1.65e-05	2.64e-05	1.64e-05	2.57e-05	1.73e-05	1.25e-04
^{27}Al	1.25e-04	1.40e-04	1.25e-04	1.40e-04	1.29e-04	1.76e-04
^{28}Si	8.88e-03	1.51e-01	8.88e-03	1.51e-01	8.96e-03	1.50e-01
^{29}Si	9.37e-05	2.48e-04	9.36e-05	2.46e-04	9.48e-05	7.82e-04
^{30}Si	9.79e-05	3.42e-04	9.80e-05	3.38e-04	1.02e-04	1.76e-03
^{31}P	8.39e-05	1.83e-04	8.39e-05	1.81e-04	8.71e-05	5.04e-04
^{32}S	3.70e-03	9.38e-02	3.70e-03	9.38e-02	3.74e-03	7.98e-02
^{33}S	5.85e-05	1.45e-04	5.83e-05	1.43e-04	5.79e-05	2.93e-04
^{34}S	2.87e-05	8.86e-04	2.87e-05	8.66e-04	3.07e-05	4.20e-03
^{36}S	2.22e-09	1.92e-08	2.39e-09	1.91e-08	6.01e-09	1.65e-06
^{35}Cl	2.93e-05	5.36e-05	2.94e-05	5.23e-05	3.32e-05	1.42e-04
^{37}Cl	7.94e-06	1.32e-05	7.92e-06	1.29e-05	7.96e-06	2.70e-05
^{36}Ar	1.20e-03	1.84e-02	1.20e-03	1.84e-02	1.25e-03	1.39e-02
^{38}Ar	1.20e-05	4.18e-04	1.20e-05	4.06e-04	1.49e-05	1.99e-03
^{40}Ar	5.42e-10	1.97e-09	7.76e-10	2.38e-09	3.60e-09	1.47e-07
^{39}K	4.00e-05	3.56e-05	4.04e-05	3.49e-05	5.93e-05	8.11e-05
^{41}K	6.33e-06	2.52e-06	6.32e-06	2.48e-06	6.70e-06	4.60e-06
^{40}Ca	3.19e-03	1.77e-02	3.20e-03	1.77e-02	3.46e-03	1.30e-02
^{42}Ca	2.59e-06	1.07e-05	2.63e-06	1.03e-05	4.11e-06	4.77e-05
^{43}Ca	5.19e-06	3.56e-07	5.20e-06	3.57e-07	6.40e-06	2.65e-07
^{44}Ca	1.05e-03	2.01e-05	1.05e-03	2.02e-05	1.17e-03	1.27e-05
^{46}Ca	1.51e-11	4.74e-11	1.43e-10	3.95e-10	1.49e-09	7.98e-08
^{48}Ca	7.45e-12	1.82e-12	7.39e-11	1.66e-11	2.06e-09	5.89e-09
^{45}Sc	2.97e-06	1.37e-07	2.98e-06	1.36e-07	3.77e-06	3.22e-07
^{46}Ti	1.94e-06	4.27e-06	1.96e-06	4.14e-06	2.76e-06	1.67e-05
^{47}Ti	3.38e-05	7.36e-07	3.41e-05	7.33e-07	4.74e-05	1.12e-06
^{48}Ti	1.71e-03	4.03e-04	1.71e-03	4.04e-04	1.55e-03	2.86e-04
^{49}Ti	1.14e-05	2.07e-05	1.14e-05	2.06e-05	1.39e-05	3.12e-05
^{50}Ti	2.46e-11	1.73e-10	2.31e-10	6.26e-10	7.80e-09	1.83e-07
^{50}V	7.62e-11	1.19e-09	1.93e-10	1.52e-09	2.91e-09	5.25e-08
^{51}V	6.08e-05	5.14e-05	6.09e-05	5.09e-05	6.20e-05	1.08e-04

Table A.8 continued.

	M10_03_001		M10_03_01		M10_03_3	
	He det [M_{\odot}]	core det [M_{\odot}]	He det [M_{\odot}]	core det [M_{\odot}]	He det [M_{\odot}]	core det [M_{\odot}]
⁵⁰ Cr	3.87e-06	1.08e-04	3.90e-06	1.06e-04	5.06e-06	5.40e-04
⁵² Cr	7.32e-04	8.74e-03	7.25e-04	8.76e-03	5.14e-04	6.87e-03
⁵³ Cr	1.27e-05	6.09e-04	1.27e-05	6.05e-04	1.22e-05	1.07e-03
⁵⁴ Cr	1.23e-10	1.27e-08	7.42e-10	1.42e-08	2.83e-08	6.21e-07
⁵⁵ Mn	1.74e-05	3.07e-03	1.73e-05	3.04e-03	1.44e-05	6.94e-03
⁵⁴ Fe	4.67e-06	1.24e-02	4.69e-06	1.22e-02	5.33e-06	5.44e-02
⁵⁶ Fe	6.96e-05	6.10e-01	6.90e-05	6.11e-01	5.93e-05	5.33e-01
⁵⁷ Fe	3.40e-06	1.11e-02	3.45e-06	1.10e-02	7.22e-06	1.87e-02
⁵⁸ Fe	2.26e-09	7.07e-09	2.40e-08	3.25e-08	2.06e-06	1.59e-06
⁵⁹ Co	3.87e-07	3.88e-04	6.65e-07	3.85e-04	1.39e-05	6.88e-04
⁵⁸ Ni	2.33e-06	1.08e-02	2.56e-06	1.06e-02	2.22e-05	5.49e-02
⁶⁰ Ni	8.46e-07	8.97e-03	1.67e-06	9.00e-03	1.82e-05	5.24e-03
⁶¹ Ni	2.10e-07	2.91e-04	4.06e-07	2.90e-04	4.42e-06	3.25e-04
⁶² Ni	2.62e-07	1.69e-03	7.12e-07	1.67e-03	6.75e-06	4.85e-03
⁶⁴ Ni	1.36e-09	3.80e-09	1.34e-08	3.69e-08	2.30e-07	2.61e-06
⁶³ Cu	3.34e-08	6.63e-07	1.57e-07	7.67e-07	1.76e-06	5.94e-06
⁶⁴ Zn	8.45e-08	2.91e-05	2.39e-07	2.95e-05	2.16e-06	1.06e-05
⁶⁶ Zn	3.27e-08	3.25e-05	1.12e-07	3.25e-05	8.35e-07	6.99e-05
⁶⁷ Zn	8.82e-09	1.92e-08	2.68e-08	2.73e-08	1.76e-07	4.57e-07
⁶⁸ Zn	1.18e-08	9.11e-09	4.01e-08	2.89e-08	1.78e-07	7.86e-07
⁷⁰ Zn	6.94e-12	3.01e-11	6.98e-11	2.91e-10	2.80e-09	1.69e-08
⁶⁹ Ga	1.17e-09	1.49e-09	5.73e-09	1.45e-08	4.70e-08	1.35e-07
⁷¹ Ga	2.42e-10	2.50e-10	1.33e-09	2.40e-09	1.42e-08	4.95e-08

Table A.9: Asymptotic nucleosynthesis yields (in solar masses) for Model M10_05 with 0.01, 0.1, and $3 Z_{\odot}$.

	M10_05_001		M10_05_01		M10_05_3	
	He det [M_{\odot}]	core det [M_{\odot}]	He det [M_{\odot}]	core det [M_{\odot}]	He det [M_{\odot}]	core det [M_{\odot}]
^{12}C	3.96e-05	4.45e-04	3.95e-05	4.43e-04	3.97e-05	4.30e-04
^{13}C	1.91e-10	1.25e-10	1.88e-10	1.20e-10	9.33e-11	7.98e-10
^{14}N	1.49e-07	2.49e-08	1.21e-06	2.40e-08	3.55e-05	7.19e-08
^{15}N	4.65e-09	5.90e-10	4.93e-09	1.08e-09	1.25e-08	7.36e-10
^{16}O	9.17e-03	6.04e-02	9.18e-03	6.03e-02	9.67e-03	6.15e-02
^{17}O	1.81e-10	6.15e-09	1.58e-09	5.94e-09	4.67e-08	1.72e-08
^{18}O	6.40e-09	1.93e-10	1.42e-08	1.83e-10	2.63e-07	5.29e-10
^{19}F	1.60e-09	5.51e-12	1.80e-09	5.44e-12	7.77e-09	2.81e-11
^{20}Ne	1.42e-05	1.54e-03	1.44e-05	1.53e-03	2.26e-05	1.41e-03
^{21}Ne	7.07e-09	3.61e-08	8.12e-09	3.58e-08	3.97e-08	2.66e-07
^{22}Ne	6.14e-09	1.18e-07	2.51e-08	1.15e-07	6.34e-07	9.70e-07
^{23}Na	3.58e-07	7.28e-06	3.62e-07	7.30e-06	5.55e-07	1.41e-05
^{24}Mg	2.82e-03	5.14e-03	2.86e-03	5.27e-03	2.98e-03	2.31e-03
^{25}Mg	8.31e-07	1.15e-05	8.73e-07	1.13e-05	1.87e-06	4.73e-05
^{26}Mg	6.27e-07	1.71e-05	6.66e-07	1.67e-05	1.73e-06	6.51e-05
^{27}Al	4.93e-05	2.08e-04	5.01e-05	2.09e-04	5.23e-05	2.56e-04
^{28}Si	1.31e-02	1.61e-01	1.31e-02	1.62e-01	1.32e-02	1.60e-01
^{29}Si	7.85e-05	2.98e-04	7.90e-05	2.95e-04	8.22e-05	9.91e-04
^{30}Si	9.60e-05	4.52e-04	9.74e-05	4.47e-04	1.04e-04	2.43e-03
^{31}P	5.55e-05	2.50e-04	5.55e-05	2.47e-04	5.67e-05	6.91e-04
^{32}S	4.98e-03	9.88e-02	4.95e-03	9.87e-02	4.94e-03	8.43e-02
^{33}S	6.19e-05	1.96e-04	6.14e-05	1.93e-04	6.09e-05	3.73e-04
^{34}S	1.71e-04	1.02e-03	1.70e-04	9.94e-04	1.73e-04	4.85e-03
^{36}S	3.94e-09	2.43e-08	4.02e-09	2.35e-08	5.29e-09	2.18e-06
^{35}Cl	1.58e-05	7.05e-05	1.57e-05	6.86e-05	1.82e-05	1.86e-04
^{37}Cl	5.46e-06	1.52e-05	5.41e-06	1.49e-05	5.67e-06	2.98e-05
^{36}Ar	1.39e-03	1.90e-02	1.38e-03	1.90e-02	1.40e-03	1.43e-02
^{38}Ar	4.51e-05	4.56e-04	4.47e-05	4.43e-04	4.97e-05	2.12e-03
^{40}Ar	2.52e-10	3.04e-09	2.56e-10	2.97e-09	5.93e-10	1.26e-07
^{39}K	4.03e-05	4.09e-05	4.06e-05	4.00e-05	5.21e-05	8.75e-05
^{41}K	1.84e-06	2.74e-06	1.84e-06	2.69e-06	2.43e-06	4.82e-06
^{40}Ca	4.26e-03	1.79e-02	4.26e-03	1.79e-02	4.31e-03	1.31e-02
^{42}Ca	4.59e-06	1.24e-05	4.58e-06	1.20e-05	6.16e-06	5.11e-05
^{43}Ca	1.38e-05	7.77e-07	1.38e-05	7.77e-07	1.35e-05	4.92e-07
^{44}Ca	7.79e-04	2.42e-05	7.80e-04	2.43e-05	8.10e-04	1.41e-05
^{46}Ca	7.74e-13	2.41e-11	2.15e-12	1.09e-10	4.35e-11	4.89e-08
^{48}Ca	6.33e-12	1.31e-12	6.33e-11	4.67e-12	1.90e-09	1.74e-09
^{45}Sc	2.19e-06	1.56e-07	2.19e-06	1.53e-07	2.87e-06	3.59e-07
^{46}Ti	5.21e-06	4.64e-06	5.20e-06	4.49e-06	5.46e-06	1.76e-05
^{47}Ti	3.15e-05	9.28e-07	3.15e-05	9.23e-07	3.33e-05	1.29e-06
^{48}Ti	2.06e-03	3.95e-04	2.06e-03	3.96e-04	2.15e-03	2.77e-04
^{49}Ti	2.05e-05	2.03e-05	2.07e-05	2.02e-05	2.64e-05	3.03e-05
^{50}Ti	2.22e-11	2.29e-10	8.62e-11	6.06e-10	2.17e-09	2.66e-07
^{50}V	2.45e-10	2.02e-09	2.41e-10	2.22e-09	6.34e-10	8.63e-08
^{51}V	1.48e-04	5.05e-05	1.48e-04	5.00e-05	1.59e-04	1.06e-04

Table A.9 continued.

	M10_05_001		M10_05_01		M10_05_3	
	He det [M_{\odot}]	core det [M_{\odot}]	He det [M_{\odot}]	core det [M_{\odot}]	He det [M_{\odot}]	core det [M_{\odot}]
⁵⁰ Cr	2.56e-05	1.11e-04	2.54e-05	1.08e-04	2.13e-05	5.51e-04
⁵² Cr	4.02e-03	8.43e-03	4.03e-03	8.44e-03	4.37e-03	6.61e-03
⁵³ Cr	5.77e-05	5.91e-04	5.83e-05	5.87e-04	7.91e-05	1.04e-03
⁵⁴ Cr	2.97e-10	1.39e-08	4.68e-10	1.69e-08	6.75e-09	7.03e-07
⁵⁵ Mn	4.78e-04	2.98e-03	4.79e-04	2.95e-03	4.94e-04	6.71e-03
⁵⁴ Fe	3.50e-05	1.24e-02	3.54e-05	1.22e-02	4.98e-05	5.43e-02
⁵⁶ Fe	8.32e-03	5.56e-01	8.31e-03	5.57e-01	8.10e-03	4.85e-01
⁵⁷ Fe	5.75e-04	1.01e-02	5.76e-04	1.00e-02	5.73e-04	1.69e-02
⁵⁸ Fe	3.88e-10	7.81e-09	3.23e-09	3.34e-08	1.31e-07	2.03e-06
⁵⁹ Co	2.75e-05	3.67e-04	2.75e-05	3.63e-04	3.03e-05	6.40e-04
⁵⁸ Ni	1.02e-04	9.59e-03	1.03e-04	9.40e-03	1.44e-04	4.89e-02
⁶⁰ Ni	7.48e-04	9.15e-03	7.48e-04	9.17e-03	7.29e-04	5.44e-03
⁶¹ Ni	1.20e-04	2.92e-04	1.20e-04	2.92e-04	1.12e-04	3.28e-04
⁶² Ni	5.98e-05	1.57e-03	6.07e-05	1.55e-03	8.78e-05	4.54e-03
⁶⁴ Ni	7.39e-11	3.84e-09	7.39e-10	3.63e-08	1.77e-08	4.93e-06
⁶³ Cu	5.17e-06	8.00e-07	5.17e-06	9.36e-07	4.87e-06	6.29e-06
⁶⁴ Zn	6.41e-05	3.05e-05	6.37e-05	3.11e-05	4.88e-05	1.19e-05
⁶⁶ Zn	7.08e-06	3.22e-05	7.35e-06	3.25e-05	1.21e-05	7.46e-05
⁶⁷ Zn	5.48e-07	2.13e-08	6.18e-07	2.98e-08	1.73e-06	8.28e-07
⁶⁸ Zn	3.67e-07	1.05e-08	5.71e-07	4.54e-08	1.86e-06	1.66e-06
⁷⁰ Zn	4.68e-13	2.51e-11	4.60e-12	2.29e-10	1.18e-10	3.56e-08
⁶⁹ Ga	2.39e-08	3.16e-09	4.57e-08	3.08e-08	1.43e-07	3.10e-07
⁷¹ Ga	1.47e-09	4.21e-10	3.43e-09	4.00e-09	9.10e-09	1.37e-07

Table A.10: Asymptotic nucleosynthesis yields (in solar masses) for Model M10_10 with 0.01, 0.1, and 3 Z_{\odot} .

	M10_10_001		M10_10_01		M10_10_3	
	He det [M_{\odot}]	core det [M_{\odot}]	He det [M_{\odot}]	core det [M_{\odot}]	He det [M_{\odot}]	core det [M_{\odot}]
^{12}C	7.39e-06	2.46e-06	7.25e-06	2.47e-06	7.52e-06	1.12e-06
^{13}C	4.23e-09	2.49e-12	4.21e-09	2.57e-12	3.65e-09	1.12e-12
^{14}N	1.25e-07	3.04e-12	1.16e-06	3.13e-12	3.46e-05	1.88e-11
^{15}N	3.15e-10	2.12e-12	3.27e-10	2.13e-12	8.11e-10	4.36e-11
^{16}O	3.02e-03	2.70e-03	3.02e-03	2.70e-03	3.24e-03	2.75e-03
^{17}O	1.98e-10	4.28e-16	1.57e-09	4.26e-16	4.56e-08	6.50e-16
^{18}O	1.61e-09	1.60e-17	8.88e-09	1.59e-17	2.43e-07	1.62e-11
^{19}F	2.39e-10	1.53e-19	3.53e-10	1.54e-19	4.14e-09	9.82e-15
^{20}Ne	1.74e-06	1.05e-07	1.98e-06	1.03e-07	9.96e-06	1.16e-07
^{21}Ne	1.17e-08	5.33e-13	1.23e-08	5.27e-13	2.91e-08	9.70e-13
^{22}Ne	1.53e-08	5.44e-13	3.33e-08	5.57e-13	6.18e-07	1.84e-10
^{23}Na	1.61e-09	1.12e-10	7.83e-09	1.10e-10	2.09e-07	3.51e-10
^{24}Mg	2.27e-04	1.02e-04	2.32e-04	1.06e-04	2.53e-04	4.12e-05
^{25}Mg	7.32e-07	1.50e-08	7.62e-07	1.57e-08	1.68e-06	1.00e-08
^{26}Mg	8.44e-07	1.08e-08	8.66e-07	1.12e-08	1.59e-06	2.23e-08
^{27}Al	2.11e-06	1.68e-06	2.16e-06	1.73e-06	2.67e-06	1.94e-06
^{28}Si	3.68e-02	7.28e-02	3.68e-02	7.28e-02	3.75e-02	7.29e-02
^{29}Si	3.33e-05	1.07e-05	3.36e-05	1.08e-05	3.61e-05	2.40e-05
^{30}Si	5.15e-05	1.10e-05	5.22e-05	1.10e-05	5.60e-05	6.55e-05
^{31}P	2.31e-05	9.49e-06	2.31e-05	9.43e-06	2.45e-05	3.10e-05
^{32}S	1.59e-02	5.55e-02	1.59e-02	5.56e-02	1.61e-02	4.85e-02
^{33}S	1.58e-05	1.02e-05	1.58e-05	1.00e-05	1.67e-05	2.77e-05
^{34}S	1.50e-04	6.91e-05	1.50e-04	6.76e-05	1.51e-04	3.53e-04
^{36}S	3.34e-10	3.68e-10	4.01e-10	3.63e-10	1.35e-09	4.22e-09
^{35}Cl	8.94e-06	3.81e-06	8.89e-06	3.74e-06	8.95e-06	1.19e-05
^{37}Cl	1.63e-06	1.67e-06	1.62e-06	1.64e-06	1.68e-06	4.14e-06
^{36}Ar	2.79e-03	1.28e-02	2.79e-03	1.28e-02	2.82e-03	1.05e-02
^{38}Ar	4.40e-05	3.90e-05	4.37e-05	3.77e-05	4.51e-05	1.96e-04
^{40}Ar	3.76e-11	5.19e-11	4.70e-11	5.00e-11	3.35e-10	2.82e-10
^{39}K	9.96e-06	4.57e-06	1.00e-05	4.49e-06	1.29e-05	1.17e-05
^{41}K	3.19e-07	4.10e-07	3.21e-07	4.03e-07	4.79e-07	8.57e-07
^{40}Ca	3.43e-03	1.42e-02	3.43e-03	1.42e-02	3.48e-03	1.14e-02
^{42}Ca	8.96e-07	1.15e-06	8.95e-07	1.11e-06	1.26e-06	4.89e-06
^{43}Ca	4.65e-06	4.09e-07	4.62e-06	4.11e-07	4.55e-06	1.09e-07
^{44}Ca	2.68e-04	2.04e-05	2.68e-04	2.04e-05	2.78e-04	1.25e-05
^{46}Ca	1.38e-13	3.20e-14	1.57e-12	2.73e-14	3.94e-11	5.58e-12
^{48}Ca	6.10e-12	3.16e-15	6.11e-11	3.86e-19	1.83e-09	9.46e-15
^{45}Sc	2.59e-07	5.86e-08	2.60e-07	5.80e-08	4.16e-07	1.06e-07
^{46}Ti	9.78e-06	5.98e-07	9.66e-06	5.80e-07	6.51e-06	3.16e-06
^{47}Ti	1.72e-05	7.81e-07	1.71e-05	7.80e-07	1.66e-05	5.36e-07
^{48}Ti	5.30e-04	4.14e-04	5.32e-04	4.14e-04	5.97e-04	3.00e-04
^{49}Ti	9.15e-06	2.01e-05	9.20e-06	1.99e-05	1.12e-05	3.18e-05
^{50}Ti	1.23e-11	2.15e-10	1.10e-10	8.78e-11	2.11e-09	1.79e-08
^{50}V	3.23e-11	3.83e-11	3.89e-11	4.36e-11	3.28e-10	8.07e-10
^{51}V	8.52e-05	4.91e-05	8.50e-05	4.86e-05	7.96e-05	1.05e-04

Table A.10 continued.

	M10_10_001		M10_10_01		M10_10_3	
	He det [M_{\odot}]	core det [M_{\odot}]	He det [M_{\odot}]	core det [M_{\odot}]	He det [M_{\odot}]	core det [M_{\odot}]
⁵⁰ Cr	1.03e-04	7.59e-05	1.03e-04	7.44e-05	8.37e-05	3.89e-04
⁵² Cr	1.97e-03	9.27e-03	1.97e-03	9.28e-03	2.06e-03	7.22e-03
⁵³ Cr	5.50e-05	6.23e-04	5.53e-05	6.19e-04	6.65e-05	1.07e-03
⁵⁴ Cr	1.74e-09	1.14e-08	1.95e-09	1.72e-09	1.44e-08	2.51e-07
⁵⁵ Mn	2.52e-04	3.16e-03	2.53e-04	3.13e-03	2.78e-04	7.24e-03
⁵⁴ Fe	9.41e-04	1.05e-02	9.48e-04	1.03e-02	1.17e-03	4.89e-02
⁵⁶ Fe	3.95e-02	7.45e-01	3.95e-02	7.45e-01	3.90e-02	6.52e-01
⁵⁷ Fe	1.37e-03	1.41e-02	1.37e-03	1.40e-02	1.50e-03	2.49e-02
⁵⁸ Fe	4.72e-10	1.44e-07	1.60e-09	7.18e-10	3.52e-08	6.49e-07
⁵⁹ Co	4.51e-04	5.19e-04	4.47e-04	5.14e-04	3.19e-04	1.18e-03
⁵⁸ Ni	5.86e-04	1.39e-02	5.86e-04	1.36e-02	5.58e-04	6.84e-02
⁶⁰ Ni	2.07e-03	1.16e-02	2.07e-03	1.16e-02	2.02e-03	6.70e-03
⁶¹ Ni	1.41e-04	3.81e-04	1.41e-04	3.80e-04	1.44e-04	4.02e-04
⁶² Ni	9.91e-05	2.25e-03	9.90e-05	2.22e-03	9.61e-05	6.05e-03
⁶⁴ Ni	1.65e-11	2.03e-07	1.65e-10	1.07e-11	4.92e-09	8.11e-09
⁶³ Cu	1.39e-05	8.70e-07	1.39e-05	8.56e-07	1.60e-05	3.90e-06
⁶⁴ Zn	2.16e-04	3.69e-05	2.16e-04	3.72e-05	2.26e-04	1.27e-05
⁶⁶ Zn	1.44e-05	4.25e-05	1.45e-05	4.20e-05	1.63e-05	7.98e-05
⁶⁷ Zn	3.23e-07	2.45e-08	3.40e-07	2.37e-08	5.96e-07	7.59e-08
⁶⁸ Zn	1.38e-07	1.02e-08	2.05e-07	9.21e-09	4.85e-07	8.51e-08
⁷⁰ Zn	2.69e-13	4.07e-11	2.68e-12	9.93e-16	7.94e-11	2.10e-12
⁶⁹ Ga	6.90e-09	3.71e-12	1.34e-08	2.28e-11	2.27e-08	2.98e-10
⁷¹ Ga	3.88e-10	1.60e-12	9.89e-10	7.60e-13	1.84e-09	3.99e-11

Table A.11: Asymptotic nucleosynthesis yields (in solar masses) for Model M11_05 with 0.01, 0.1, and 3 Z_{\odot} .

	M11_05_001		M11_05_01		M11_05_3	
	He det [M_{\odot}]	core det [M_{\odot}]	He det [M_{\odot}]	core det [M_{\odot}]	He det [M_{\odot}]	core det [M_{\odot}]
^{12}C	5.24e-06	3.11e-06	5.27e-06	3.12e-06	5.65e-06	1.23e-06
^{13}C	1.01e-09	3.17e-12	1.00e-09	3.27e-12	8.18e-10	1.04e-12
^{14}N	1.38e-07	7.05e-13	1.20e-06	7.21e-13	3.54e-05	4.99e-11
^{15}N	2.43e-09	1.14e-12	2.56e-09	1.15e-12	6.49e-09	1.37e-10
^{16}O	3.74e-03	7.48e-04	3.74e-03	7.47e-04	4.02e-03	7.62e-04
^{17}O	1.96e-10	1.02e-16	1.60e-09	1.02e-16	4.67e-08	5.95e-16
^{18}O	4.18e-09	3.96e-18	1.18e-08	3.96e-18	2.56e-07	6.23e-11
^{19}F	8.08e-10	9.86e-20	9.57e-10	9.97e-20	5.73e-09	3.40e-14
^{20}Ne	7.67e-07	4.48e-08	1.02e-06	4.43e-08	9.37e-06	3.90e-08
^{21}Ne	7.03e-09	1.52e-13	7.80e-09	1.51e-13	3.29e-08	2.64e-13
^{22}Ne	1.11e-08	1.74e-13	2.98e-08	1.77e-13	6.33e-07	6.86e-10
^{23}Na	2.98e-09	3.96e-11	9.36e-09	3.91e-11	2.15e-07	3.04e-10
^{24}Mg	2.98e-04	2.07e-05	3.03e-04	2.15e-05	3.40e-04	9.17e-06
^{25}Mg	2.44e-07	2.90e-09	2.72e-07	3.04e-09	1.19e-06	1.83e-09
^{26}Mg	3.30e-07	1.89e-09	3.59e-07	1.97e-09	1.31e-06	3.77e-09
^{27}Al	2.51e-06	3.15e-07	2.57e-06	3.23e-07	3.20e-06	3.61e-07
^{28}Si	5.55e-02	4.54e-02	5.55e-02	4.54e-02	5.62e-02	4.43e-02
^{29}Si	4.59e-05	3.15e-06	4.62e-05	3.18e-06	5.07e-05	7.57e-06
^{30}Si	6.09e-05	2.80e-06	6.15e-05	2.88e-06	6.96e-05	1.62e-05
^{31}P	3.60e-05	3.34e-06	3.62e-05	3.33e-06	3.94e-05	1.03e-05
^{32}S	2.45e-02	3.76e-02	2.45e-02	3.76e-02	2.45e-02	3.35e-02
^{33}S	2.65e-05	3.98e-06	2.65e-05	3.94e-06	2.85e-05	1.06e-05
^{34}S	1.80e-04	2.18e-05	1.80e-04	2.15e-05	1.96e-04	1.15e-04
^{36}S	4.31e-10	8.10e-11	4.67e-10	8.51e-11	1.50e-09	7.47e-10
^{35}Cl	1.00e-05	1.85e-06	1.00e-05	1.83e-06	1.15e-05	4.61e-06
^{37}Cl	3.57e-06	8.73e-07	3.57e-06	8.62e-07	3.95e-06	1.94e-06
^{36}Ar	4.34e-03	9.35e-03	4.34e-03	9.36e-03	4.35e-03	7.97e-03
^{38}Ar	7.81e-05	1.57e-05	7.81e-05	1.52e-05	8.93e-05	7.88e-05
^{40}Ar	7.68e-11	1.97e-11	8.59e-11	1.92e-11	3.92e-10	9.32e-11
^{39}K	1.51e-05	2.95e-06	1.52e-05	2.92e-06	1.98e-05	5.22e-06
^{41}K	9.97e-07	2.58e-07	1.00e-06	2.55e-07	1.30e-06	4.85e-07
^{40}Ca	5.72e-03	1.09e-02	5.72e-03	1.09e-02	5.85e-03	9.10e-03
^{42}Ca	2.19e-06	6.32e-07	2.20e-06	6.16e-07	2.93e-06	2.14e-06
^{43}Ca	2.60e-06	5.40e-07	2.59e-06	5.43e-07	2.42e-06	1.29e-07
^{44}Ca	1.53e-04	2.05e-05	1.53e-04	2.05e-05	1.74e-04	1.15e-05
^{46}Ca	1.45e-13	2.14e-15	1.40e-12	6.86e-15	4.08e-11	4.18e-13
^{48}Ca	6.27e-12	3.32e-21	6.27e-11	1.37e-19	1.88e-09	7.17e-15
^{45}Sc	4.64e-07	4.56e-08	4.68e-07	4.52e-08	7.37e-07	8.50e-08
^{46}Ti	2.95e-06	3.22e-07	2.96e-06	3.14e-07	3.55e-06	1.59e-06
^{47}Ti	5.71e-06	9.79e-07	5.72e-06	9.79e-07	6.56e-06	5.31e-07
^{48}Ti	7.17e-04	3.52e-04	7.19e-04	3.53e-04	8.03e-04	2.57e-04
^{49}Ti	1.39e-05	1.63e-05	1.40e-05	1.62e-05	1.67e-05	2.68e-05
^{50}Ti	1.32e-11	1.44e-12	7.86e-11	2.04e-11	2.30e-09	1.32e-08
^{50}V	5.28e-11	1.14e-11	6.52e-11	1.50e-11	6.19e-10	2.61e-10
^{51}V	3.15e-05	4.01e-05	3.16e-05	3.97e-05	3.63e-05	8.80e-05

Table A.11 continued.

	M11_05_001		M11_05_01		M11_05_3	
	He det [M_{\odot}]	core det [M_{\odot}]	He det [M_{\odot}]	core det [M_{\odot}]	He det [M_{\odot}]	core det [M_{\odot}]
⁵⁰ Cr	4.09e-05	5.39e-05	4.10e-05	5.29e-05	4.57e-05	2.66e-04
⁵² Cr	2.04e-03	7.80e-03	2.05e-03	7.81e-03	2.24e-03	6.11e-03
⁵³ Cr	7.19e-05	5.16e-04	7.21e-05	5.13e-04	8.16e-05	8.97e-04
⁵⁴ Cr	4.45e-09	7.59e-10	4.77e-09	1.14e-09	2.32e-08	1.71e-07
⁵⁵ Mn	2.14e-04	2.63e-03	2.15e-04	2.61e-03	2.32e-04	6.14e-03
⁵⁴ Fe	1.48e-03	7.96e-03	1.49e-03	7.82e-03	1.77e-03	3.78e-02
⁵⁶ Fe	1.24e-02	8.47e-01	1.24e-02	8.48e-01	1.14e-02	7.46e-01
⁵⁷ Fe	3.04e-04	1.77e-02	3.04e-04	1.76e-02	3.00e-04	3.35e-02
⁵⁸ Fe	1.15e-09	2.69e-10	2.46e-09	4.32e-10	3.98e-08	4.95e-07
⁵⁹ Co	5.17e-05	7.12e-04	5.10e-05	7.06e-04	3.47e-05	2.05e-03
⁵⁸ Ni	1.91e-04	1.83e-02	1.91e-04	1.79e-02	2.11e-04	8.08e-02
⁶⁰ Ni	2.72e-04	1.54e-02	2.71e-04	1.54e-02	2.42e-04	8.87e-03
⁶¹ Ni	2.01e-05	5.15e-04	2.00e-05	5.14e-04	1.78e-05	5.10e-04
⁶² Ni	2.09e-05	3.08e-03	2.10e-05	3.04e-03	2.27e-05	7.57e-03
⁶⁴ Ni	1.73e-11	1.23e-13	1.72e-10	1.22e-12	5.06e-09	1.28e-09
⁶³ Cu	7.84e-06	1.22e-06	7.82e-06	1.20e-06	7.33e-06	5.23e-06
⁶⁴ Zn	3.52e-05	4.88e-05	3.49e-05	4.92e-05	2.72e-05	1.69e-05
⁶⁶ Zn	2.86e-06	5.82e-05	2.86e-06	5.75e-05	2.69e-06	1.01e-04
⁶⁷ Zn	1.76e-07	3.39e-08	1.80e-07	3.34e-08	1.95e-07	9.78e-08
⁶⁸ Zn	8.39e-08	1.34e-08	1.09e-07	1.31e-08	1.30e-07	1.00e-07
⁷⁰ Zn	2.98e-13	4.12e-19	2.94e-12	4.02e-18	8.27e-11	1.07e-15
⁶⁹ Ga	3.50e-09	5.02e-13	6.67e-09	3.00e-12	7.07e-09	2.14e-11
⁷¹ Ga	2.93e-10	3.84e-14	7.98e-10	1.26e-13	1.31e-09	1.23e-12

Table A.12: Nucleosynthesis yields (in solar masses) for select radioactive nuclides of Model M08_03 with 0.01, 0.1, and $3 Z_{\odot}$.

	M08_03_001		M08_03_01		M08_03_3	
	He det [M_{\odot}]	core det [M_{\odot}]	He det [M_{\odot}]	core det [M_{\odot}]	He det [M_{\odot}]	core det [M_{\odot}]
^{14}C	7.29e-08	4.85e-06	7.43e-08	4.62e-06	9.15e-08	8.76e-06
^{22}Na	5.45e-07	2.50e-08	5.75e-07	2.50e-08	1.44e-06	1.74e-08
^{26}Al	1.13e-05	1.37e-05	1.14e-05	1.37e-05	1.53e-05	5.47e-06
^{32}Si	8.10e-10	7.80e-10	1.39e-09	1.05e-09	2.34e-09	8.25e-08
^{32}P	7.78e-09	2.23e-07	8.35e-09	2.19e-07	1.27e-08	3.92e-06
^{33}P	1.94e-09	1.65e-07	2.43e-09	1.64e-07	1.25e-08	2.53e-06
^{35}S	1.95e-09	1.61e-07	2.68e-09	1.55e-07	1.51e-08	5.73e-06
^{36}Cl	4.68e-09	6.97e-07	4.80e-09	6.76e-07	8.63e-09	5.33e-06
^{37}Ar	6.59e-07	2.73e-05	6.69e-07	2.68e-05	1.07e-06	4.70e-05
^{39}Ar	3.73e-10	6.49e-09	3.50e-09	1.27e-08	6.29e-08	5.16e-07
^{40}K	4.30e-10	4.27e-08	8.18e-10	4.18e-08	9.09e-09	4.46e-07
^{41}Ca	5.60e-06	4.63e-06	5.56e-06	4.54e-06	4.80e-06	7.89e-06
^{44}Ti	2.26e-04	1.29e-05	2.25e-04	1.29e-05	1.91e-04	8.87e-06
^{48}V	1.00e-07	5.76e-08	1.00e-07	5.72e-08	8.65e-08	1.10e-07
^{49}V	2.03e-08	2.07e-07	2.09e-08	2.10e-07	4.18e-08	1.04e-06
^{48}Cr	8.23e-06	3.21e-04	8.13e-06	3.21e-04	5.97e-06	2.14e-04
^{49}Cr	2.66e-07	1.85e-05	2.62e-07	1.84e-05	1.59e-07	2.42e-05
^{51}Cr	5.82e-09	1.03e-06	6.12e-09	1.02e-06	1.33e-08	1.51e-05
^{51}Mn	2.51e-07	4.40e-05	2.49e-07	4.36e-05	2.07e-07	7.59e-05
^{52}Mn	7.45e-09	2.69e-06	7.56e-09	2.68e-06	1.02e-08	3.93e-06
^{53}Mn	2.85e-09	1.86e-05	4.03e-09	1.84e-05	5.36e-08	1.70e-04
^{54}Mn	2.56e-11	2.10e-08	2.24e-10	2.35e-08	9.49e-09	9.59e-07
^{52}Fe	8.56e-07	6.19e-03	8.59e-07	6.20e-03	9.58e-07	4.49e-03
^{53}Fe	2.61e-08	4.47e-04	2.65e-08	4.44e-04	4.07e-08	6.53e-04
^{55}Fe	6.43e-10	3.00e-05	4.00e-09	2.94e-05	1.73e-07	5.90e-04
^{59}Fe	7.18e-09	1.68e-08	7.71e-08	1.70e-07	3.24e-06	4.15e-06
^{60}Fe	2.88e-08	4.48e-08	2.86e-07	4.40e-07	2.96e-06	2.83e-05
^{55}Co	1.08e-07	2.16e-03	1.14e-07	2.14e-03	4.29e-07	4.02e-03
^{56}Co	6.58e-10	7.18e-06	1.76e-09	7.11e-06	4.64e-08	2.11e-05
^{57}Co	6.74e-09	3.83e-06	6.70e-08	3.77e-06	2.96e-06	6.27e-05
^{58}Co	4.52e-10	7.29e-09	4.72e-09	1.25e-08	3.25e-07	2.42e-07
^{60}Co	7.49e-09	1.64e-08	7.39e-08	1.64e-07	6.22e-07	3.34e-06
^{56}Ni	8.04e-07	1.40e-01	8.11e-07	1.40e-01	1.18e-06	1.14e-01
^{57}Ni	8.62e-08	1.22e-03	9.15e-08	1.21e-03	3.13e-07	2.14e-03
^{59}Ni	5.68e-09	9.79e-07	3.92e-08	1.05e-06	1.28e-06	1.30e-05
^{63}Ni	1.02e-09	1.04e-08	1.03e-08	1.00e-07	2.66e-07	4.72e-06
^{62}Zn	3.26e-08	1.03e-06	2.23e-07	1.02e-06	1.94e-06	3.43e-06
^{65}Zn	1.02e-10	9.59e-09	8.96e-10	9.77e-08	7.30e-09	2.67e-07
^{65}Ge	4.73e-10	8.68e-10	2.25e-09	8.64e-10	8.75e-09	1.03e-09

Table A.13: Nucleosynthesis yields (in solar masses) for select radioactive nuclides of Model M08_05 with 0.01, 0.1, and $3 Z_{\odot}$.

	M08_05_001		M08_05_01		M08_05_3	
	He det [M_{\odot}]	core det [M_{\odot}]	He det [M_{\odot}]	core det [M_{\odot}]	He det [M_{\odot}]	core det [M_{\odot}]
^{14}C	2.09e-08	3.37e-06	2.12e-08	3.19e-06	2.26e-08	7.51e-06
^{22}Na	5.09e-08	2.15e-08	5.29e-08	2.15e-08	1.16e-07	1.47e-08
^{26}Al	9.81e-06	1.12e-05	9.79e-06	1.12e-05	1.03e-05	4.40e-06
^{32}Si	9.42e-11	8.05e-10	1.77e-10	1.02e-09	3.25e-10	8.08e-08
^{32}P	1.44e-08	1.87e-07	1.47e-08	1.83e-07	1.65e-08	3.20e-06
^{33}P	5.99e-09	1.32e-07	6.08e-09	1.31e-07	8.27e-09	2.04e-06
^{35}S	1.14e-08	1.35e-07	1.17e-08	1.29e-07	1.82e-08	4.64e-06
^{36}Cl	2.73e-08	5.66e-07	2.74e-08	5.49e-07	3.23e-08	4.26e-06
^{37}Ar	1.03e-05	2.35e-05	1.03e-05	2.30e-05	1.03e-05	4.10e-05
^{39}Ar	4.60e-10	5.56e-09	1.77e-09	1.11e-08	2.67e-08	4.59e-07
^{40}K	2.94e-09	3.57e-08	3.31e-09	3.51e-08	1.38e-08	3.58e-07
^{41}Ca	9.15e-06	4.07e-06	9.15e-06	3.99e-06	1.06e-05	6.95e-06
^{44}Ti	2.57e-03	1.33e-05	2.58e-03	1.33e-05	2.87e-03	9.29e-06
^{48}V	9.56e-07	5.98e-08	9.69e-07	5.94e-08	1.45e-06	1.04e-07
^{49}V	2.54e-07	1.86e-07	2.61e-07	1.88e-07	5.02e-07	8.95e-07
^{48}Cr	2.67e-03	3.48e-04	2.66e-03	3.49e-04	2.43e-03	2.38e-04
^{49}Cr	2.01e-05	1.96e-05	2.02e-05	1.95e-05	2.78e-05	2.67e-05
^{51}Cr	1.17e-06	9.24e-07	1.18e-06	9.05e-07	1.45e-06	1.33e-05
^{51}Mn	1.11e-04	4.74e-05	1.11e-04	4.69e-05	1.15e-04	8.55e-05
^{52}Mn	1.78e-06	2.95e-06	1.78e-06	2.95e-06	2.13e-06	4.12e-06
^{53}Mn	1.12e-06	1.86e-05	1.13e-06	1.84e-05	1.54e-06	1.54e-04
^{54}Mn	1.15e-10	1.90e-08	4.65e-10	2.06e-08	1.67e-08	8.36e-07
^{52}Fe	8.90e-04	7.36e-03	8.82e-04	7.38e-03	6.37e-04	5.44e-03
^{53}Fe	1.89e-05	5.20e-04	1.89e-05	5.17e-04	2.04e-05	7.94e-04
^{55}Fe	1.47e-07	2.64e-05	1.58e-07	2.58e-05	6.40e-07	5.17e-04
^{59}Fe	2.59e-09	1.46e-08	2.76e-08	1.49e-07	1.47e-06	3.79e-06
^{60}Fe	1.16e-08	4.22e-08	1.16e-07	4.15e-07	1.69e-06	2.51e-05
^{55}Co	3.03e-05	2.63e-03	3.02e-05	2.60e-03	2.68e-05	5.25e-03
^{56}Co	2.83e-07	9.27e-06	2.92e-07	9.19e-06	6.31e-07	2.57e-05
^{57}Co	7.32e-08	3.48e-06	1.72e-07	3.42e-06	7.17e-06	5.64e-05
^{58}Co	1.12e-09	6.48e-09	1.18e-08	1.03e-08	9.80e-07	2.09e-07
^{60}Co	6.32e-09	1.37e-08	6.23e-08	1.37e-07	9.31e-07	2.68e-06
^{56}Ni	7.50e-05	2.10e-01	7.42e-05	2.10e-01	4.98e-05	1.77e-01
^{57}Ni	6.45e-06	2.03e-03	6.51e-06	2.02e-03	6.95e-06	3.68e-03
^{59}Ni	2.28e-07	2.10e-06	4.91e-07	2.14e-06	1.24e-05	1.32e-05
^{63}Ni	1.47e-09	9.60e-09	1.42e-08	9.27e-08	2.06e-07	4.08e-06
^{62}Zn	6.36e-07	2.54e-05	1.36e-06	2.51e-05	1.34e-05	5.56e-05
^{65}Zn	2.49e-09	7.76e-09	1.69e-08	7.82e-08	2.15e-07	2.15e-07
^{65}Ge	8.95e-09	1.15e-08	1.74e-08	1.15e-08	9.34e-08	1.05e-08

Table A.14: Nucleosynthesis yields (in solar masses) for select radioactive nuclides of Model M08_10 with 0.01, 0.1, and $3 Z_{\odot}$.

	M08_10_001		M08_10_01		M08_10_3	
	He det [M_{\odot}]	core det [M_{\odot}]	He det [M_{\odot}]	core det [M_{\odot}]	He det [M_{\odot}]	core det [M_{\odot}]
^{14}C	2.53e-12	2.17e-09	2.81e-12	1.29e-09	1.15e-11	5.76e-08
^{22}Na	8.66e-09	1.03e-08	8.97e-09	1.04e-08	1.79e-08	7.49e-09
^{26}Al	6.65e-07	6.65e-06	6.63e-07	6.67e-06	7.06e-07	2.76e-06
^{32}Si	2.18e-12	8.20e-10	2.24e-12	4.33e-11	2.54e-12	1.41e-08
^{32}P	2.00e-08	1.19e-07	2.01e-08	1.16e-07	2.14e-08	2.09e-06
^{33}P	1.59e-08	9.33e-08	1.60e-08	9.05e-08	1.70e-08	1.36e-06
^{35}S	1.17e-08	9.64e-08	1.16e-08	9.04e-08	1.18e-08	3.50e-06
^{36}Cl	7.72e-08	4.18e-07	7.66e-08	4.05e-07	7.95e-08	3.24e-06
^{37}Ar	7.83e-06	1.84e-05	7.79e-06	1.81e-05	8.08e-06	3.28e-05
^{39}Ar	6.02e-10	4.02e-09	5.91e-10	3.96e-09	6.93e-10	1.51e-07
^{40}K	4.76e-09	2.83e-08	4.66e-09	2.71e-08	5.58e-09	2.71e-07
^{41}Ca	3.21e-06	3.27e-06	3.21e-06	3.21e-06	4.16e-06	5.64e-06
^{44}Ti	1.78e-03	1.52e-05	1.78e-03	1.52e-05	1.83e-03	1.04e-05
^{48}V	1.01e-06	4.33e-08	1.02e-06	4.29e-08	1.53e-06	8.12e-08
^{49}V	3.26e-07	1.59e-07	3.29e-07	1.59e-07	5.10e-07	7.22e-07
^{48}Cr	3.78e-03	3.68e-04	3.79e-03	3.69e-04	3.92e-03	2.57e-04
^{49}Cr	3.03e-05	2.00e-05	3.06e-05	1.99e-05	4.15e-05	2.83e-05
^{51}Cr	2.49e-06	7.82e-07	2.50e-06	7.66e-07	2.88e-06	1.11e-05
^{51}Mn	2.89e-04	4.88e-05	2.90e-04	4.83e-05	3.09e-04	9.16e-05
^{52}Mn	8.90e-06	2.55e-06	8.96e-06	2.55e-06	1.13e-05	3.71e-06
^{53}Mn	4.78e-06	1.67e-05	4.84e-06	1.65e-05	6.96e-06	1.30e-04
^{54}Mn	3.05e-10	2.43e-08	4.66e-10	2.29e-08	5.57e-09	6.93e-07
^{52}Fe	7.35e-03	7.92e-03	7.36e-03	7.93e-03	7.88e-03	5.96e-03
^{53}Fe	9.18e-05	5.52e-04	9.29e-05	5.48e-04	1.29e-04	8.69e-04
^{55}Fe	9.68e-07	2.18e-05	9.85e-07	2.15e-05	1.73e-06	4.28e-04
^{59}Fe	2.84e-11	1.49e-09	2.75e-10	1.53e-08	6.90e-09	3.33e-07
^{60}Fe	8.26e-11	7.26e-09	8.13e-10	6.97e-08	1.27e-08	9.60e-06
^{55}Co	9.19e-04	2.81e-03	9.21e-04	2.79e-03	9.70e-04	5.87e-03
^{56}Co	3.02e-06	8.91e-06	3.05e-06	8.82e-06	4.15e-06	2.65e-05
^{57}Co	1.07e-06	3.01e-06	1.11e-06	3.02e-06	2.81e-06	4.73e-05
^{58}Co	3.90e-10	5.81e-09	2.39e-09	8.90e-09	1.07e-07	1.71e-07
^{60}Co	1.59e-10	5.96e-09	1.55e-09	5.88e-08	2.97e-08	1.84e-06
^{56}Ni	1.49e-02	3.24e-01	1.49e-02	3.24e-01	1.49e-02	2.78e-01
^{57}Ni	1.29e-03	4.50e-03	1.29e-03	4.47e-03	1.31e-03	7.79e-03
^{59}Ni	9.42e-06	1.28e-05	9.54e-06	1.28e-05	1.61e-05	3.07e-05
^{63}Ni	7.89e-11	3.81e-09	7.46e-10	3.63e-08	1.10e-08	2.66e-06
^{62}Zn	1.24e-04	3.90e-04	1.26e-04	3.84e-04	1.75e-04	1.12e-03
^{65}Zn	2.13e-07	8.52e-09	2.32e-07	6.73e-08	6.21e-07	1.77e-07
^{65}Ge	2.95e-06	2.37e-07	2.95e-06	2.36e-07	2.93e-06	2.15e-07

Table A.15: Nucleosynthesis yields (in solar masses) for select radioactive nuclides of Model M09_03 with 0.01, 0.1, and $3 Z_{\odot}$.

	M09_03_001		M09_03_01		M09_03_3	
	He det [M_{\odot}]	core det [M_{\odot}]	He det [M_{\odot}]	core det [M_{\odot}]	He det [M_{\odot}]	core det [M_{\odot}]
^{14}C	3.68e-08	1.93e-06	3.73e-08	1.83e-06	4.31e-08	3.71e-06
^{22}Na	9.34e-08	1.38e-08	9.78e-08	1.38e-08	2.32e-07	9.36e-09
^{26}Al	1.33e-05	7.04e-06	1.33e-05	7.09e-06	1.45e-05	2.74e-06
^{32}Si	3.09e-10	5.35e-10	5.69e-10	6.89e-10	9.61e-10	5.47e-08
^{32}P	1.00e-08	1.39e-07	1.05e-08	1.36e-07	1.32e-08	2.22e-06
^{33}P	2.57e-09	9.66e-08	2.82e-09	9.56e-08	7.86e-09	1.43e-06
^{35}S	5.02e-09	9.84e-08	5.57e-09	9.44e-08	1.51e-08	3.14e-06
^{36}Cl	1.06e-08	4.32e-07	1.07e-08	4.19e-07	1.48e-08	3.04e-06
^{37}Ar	3.00e-06	2.10e-05	2.99e-06	2.06e-05	3.04e-06	3.82e-05
^{39}Ar	3.54e-10	4.23e-09	2.82e-09	7.54e-09	4.90e-08	2.97e-07
^{40}K	8.71e-10	2.69e-08	1.26e-09	2.63e-08	1.11e-08	2.47e-07
^{41}Ca	1.04e-05	3.82e-06	1.03e-05	3.74e-06	1.10e-05	6.65e-06
^{44}Ti	7.50e-04	1.57e-05	7.47e-04	1.58e-05	6.50e-04	1.12e-05
^{48}V	4.44e-07	5.42e-08	4.50e-07	5.37e-08	6.06e-07	9.88e-08
^{49}V	8.92e-08	1.80e-07	9.15e-08	1.80e-07	1.64e-07	7.95e-07
^{48}Cr	1.25e-04	4.29e-04	1.23e-04	4.30e-04	7.45e-05	3.00e-04
^{49}Cr	3.61e-06	2.32e-05	3.60e-06	2.30e-05	3.00e-06	3.29e-05
^{51}Cr	7.69e-08	8.98e-07	7.77e-08	8.81e-07	9.33e-08	1.27e-05
^{51}Mn	5.40e-06	5.63e-05	5.34e-06	5.58e-05	3.62e-06	1.06e-04
^{52}Mn	1.00e-07	3.34e-06	1.01e-07	3.34e-06	9.94e-08	4.58e-06
^{53}Mn	3.67e-08	2.09e-05	3.81e-08	2.07e-05	1.13e-07	1.53e-04
^{54}Mn	9.17e-11	1.84e-08	6.34e-10	1.94e-08	2.56e-08	7.84e-07
^{52}Fe	5.16e-06	9.49e-03	5.06e-06	9.50e-03	2.75e-06	7.13e-03
^{53}Fe	4.30e-07	6.51e-04	4.26e-07	6.47e-04	2.81e-07	1.03e-03
^{55}Fe	3.58e-09	2.55e-05	7.93e-09	2.49e-05	2.34e-07	4.94e-04
^{59}Fe	4.71e-09	8.35e-09	5.04e-08	8.51e-08	2.48e-06	2.26e-06
^{60}Fe	2.46e-08	2.75e-08	2.44e-07	2.71e-07	2.84e-06	1.66e-05
^{55}Co	2.57e-07	3.34e-03	2.60e-07	3.31e-03	5.27e-07	7.01e-03
^{56}Co	4.61e-09	1.08e-05	6.05e-09	1.07e-05	7.43e-08	3.14e-05
^{57}Co	8.22e-09	3.50e-06	7.74e-08	3.43e-06	4.55e-06	5.49e-05
^{58}Co	7.42e-10	6.24e-09	8.00e-09	8.64e-09	7.18e-07	1.94e-07
^{60}Co	1.77e-08	8.85e-09	1.75e-07	8.88e-08	1.61e-06	1.72e-06
^{56}Ni	7.45e-07	3.43e-01	7.54e-07	3.43e-01	1.26e-06	2.94e-01
^{57}Ni	9.79e-08	4.04e-03	1.06e-07	4.02e-03	4.22e-07	7.22e-03
^{59}Ni	1.12e-08	8.88e-06	8.45e-08	8.85e-06	3.02e-06	2.32e-05
^{63}Ni	1.40e-09	6.59e-09	1.38e-08	6.37e-08	2.81e-07	2.61e-06
^{62}Zn	3.80e-08	1.84e-04	2.97e-07	1.81e-04	2.81e-06	4.16e-04
^{65}Zn	2.98e-10	6.09e-09	2.76e-09	5.40e-08	2.43e-08	1.55e-07
^{65}Ge	4.03e-10	6.83e-08	1.90e-09	6.82e-08	8.78e-09	4.42e-08

Table A.16: Nucleosynthesis yields (in solar masses) for select radioactive nuclides of Model M09_05 with 0.01, 0.1, and $3 Z_{\odot}$.

	M09_05_001		M09_05_01		M09_05_3	
	He det [M_{\odot}]	core det [M_{\odot}]	He det [M_{\odot}]	core det [M_{\odot}]	He det [M_{\odot}]	core det [M_{\odot}]
^{14}C	6.91e-11	2.08e-07	6.95e-11	1.95e-07	5.21e-11	1.18e-06
^{22}Na	1.49e-08	1.41e-08	1.54e-08	1.41e-08	2.93e-08	1.00e-08
^{26}Al	3.04e-06	7.54e-06	3.03e-06	7.58e-06	3.06e-06	2.94e-06
^{32}Si	4.31e-12	2.23e-10	4.13e-12	2.40e-10	4.67e-12	3.72e-08
^{32}P	1.54e-08	1.19e-07	1.54e-08	1.16e-07	1.63e-08	2.06e-06
^{33}P	1.04e-08	8.24e-08	1.04e-08	8.06e-08	1.10e-08	1.22e-06
^{35}S	1.40e-08	9.21e-08	1.39e-08	8.71e-08	1.48e-08	2.98e-06
^{36}Cl	5.00e-08	3.72e-07	4.98e-08	3.61e-07	5.24e-08	2.70e-06
^{37}Ar	9.40e-06	1.79e-05	9.38e-06	1.75e-05	9.50e-06	3.27e-05
^{39}Ar	6.51e-10	3.68e-09	7.05e-10	4.77e-09	2.14e-09	2.27e-07
^{40}K	5.22e-09	2.44e-08	5.25e-09	2.39e-08	8.56e-09	2.28e-07
^{41}Ca	6.35e-06	3.26e-06	6.35e-06	3.20e-06	7.10e-06	5.71e-06
^{44}Ti	1.99e-03	1.65e-05	2.00e-03	1.65e-05	2.13e-03	1.12e-05
^{48}V	1.83e-06	4.56e-08	1.85e-06	4.53e-08	2.54e-06	8.44e-08
^{49}V	4.35e-07	1.54e-07	4.41e-07	1.54e-07	6.76e-07	6.86e-07
^{48}Cr	4.47e-03	4.03e-04	4.49e-03	4.04e-04	4.97e-03	2.84e-04
^{49}Cr	4.06e-05	2.14e-05	4.10e-05	2.13e-05	5.42e-05	3.10e-05
^{51}Cr	3.41e-06	7.68e-07	3.43e-06	7.54e-07	4.14e-06	1.08e-05
^{51}Mn	3.69e-04	5.23e-05	3.71e-04	5.18e-05	4.19e-04	9.97e-05
^{52}Mn	1.03e-05	2.80e-06	1.04e-05	2.80e-06	1.23e-05	3.96e-06
^{53}Mn	6.93e-06	1.76e-05	6.99e-06	1.75e-05	9.00e-06	1.31e-04
^{54}Mn	2.57e-10	1.58e-08	4.91e-10	1.68e-08	8.01e-09	6.71e-07
^{52}Fe	5.08e-03	8.79e-03	5.09e-03	8.80e-03	5.25e-03	6.65e-03
^{53}Fe	1.29e-04	6.03e-04	1.30e-04	5.99e-04	1.63e-04	9.62e-04
^{55}Fe	1.09e-06	2.17e-05	1.11e-06	2.12e-05	1.63e-06	4.21e-04
^{59}Fe	2.81e-10	4.66e-09	2.98e-09	4.79e-08	1.83e-07	1.16e-06
^{60}Fe	1.59e-09	2.06e-08	1.58e-08	2.01e-07	2.61e-07	1.57e-05
^{55}Co	4.11e-04	3.08e-03	4.11e-04	3.05e-03	3.94e-04	6.52e-03
^{56}Co	2.72e-06	1.03e-05	2.74e-06	1.02e-05	3.18e-06	2.94e-05
^{57}Co	6.54e-07	3.11e-06	6.95e-07	3.05e-06	2.95e-06	4.75e-05
^{58}Co	5.51e-10	5.41e-09	4.09e-09	7.77e-09	2.80e-07	1.66e-07
^{60}Co	1.50e-09	9.69e-09	1.43e-08	9.68e-08	2.83e-07	1.81e-06
^{56}Ni	2.13e-03	3.98e-01	2.12e-03	3.98e-01	1.70e-03	3.43e-01
^{57}Ni	1.37e-04	5.79e-03	1.37e-04	5.76e-03	1.27e-04	1.00e-02
^{59}Ni	2.90e-06	1.82e-05	3.09e-06	1.80e-05	1.17e-05	3.98e-05
^{63}Ni	6.78e-10	6.72e-09	6.50e-09	6.48e-08	8.20e-08	2.91e-06
^{62}Zn	1.29e-05	5.82e-04	1.35e-05	5.73e-04	2.72e-05	1.63e-03
^{65}Zn	1.15e-08	7.67e-09	3.72e-08	5.04e-08	4.48e-07	1.33e-07
^{65}Ge	1.14e-07	3.45e-07	1.27e-07	3.44e-07	4.07e-07	2.90e-07

Table A.17: Nucleosynthesis yields (in solar masses) for select radioactive nuclides of Model M09_10 with 0.01, 0.1, and $3 Z_{\odot}$.

	M09_10_001		M09_10_01		M09_10_3	
	He det [M_{\odot}]	core det [M_{\odot}]	He det [M_{\odot}]	core det [M_{\odot}]	He det [M_{\odot}]	core det [M_{\odot}]
^{14}C	3.84e-12	2.80e-13	4.47e-12	1.73e-13	2.36e-11	3.61e-11
^{22}Na	7.85e-09	5.73e-09	8.22e-09	5.68e-09	1.83e-08	6.08e-09
^{26}Al	9.78e-08	1.84e-06	9.91e-08	1.84e-06	1.43e-07	7.96e-07
^{32}Si	1.93e-12	4.35e-10	2.03e-12	7.81e-11	2.34e-12	3.41e-09
^{32}P	1.52e-08	7.62e-08	1.55e-08	7.39e-08	1.65e-08	1.07e-06
^{33}P	1.22e-08	6.01e-08	1.25e-08	5.81e-08	1.32e-08	8.09e-07
^{35}S	3.80e-09	5.22e-08	3.78e-09	4.92e-08	3.93e-09	1.55e-06
^{36}Cl	6.30e-08	2.80e-07	6.30e-08	2.71e-07	6.46e-08	1.91e-06
^{37}Ar	3.56e-06	1.41e-05	3.53e-06	1.39e-05	3.70e-06	2.59e-05
^{39}Ar	1.60e-10	2.51e-09	1.57e-10	2.40e-09	2.07e-10	4.74e-08
^{40}K	1.23e-09	1.80e-08	1.20e-09	1.70e-08	1.52e-09	1.45e-07
^{41}Ca	1.14e-06	2.59e-06	1.15e-06	2.54e-06	1.74e-06	4.55e-06
^{44}Ti	8.70e-04	1.81e-05	8.71e-04	1.81e-05	9.07e-04	1.15e-05
^{48}V	4.23e-07	3.68e-08	4.30e-07	3.63e-08	7.18e-07	6.74e-08
^{49}V	1.98e-07	1.37e-07	2.00e-07	1.35e-07	3.03e-07	5.57e-07
^{48}Cr	1.88e-03	3.73e-04	1.88e-03	3.74e-04	1.99e-03	2.62e-04
^{49}Cr	2.02e-05	1.95e-05	2.05e-05	1.93e-05	2.77e-05	2.84e-05
^{51}Cr	2.06e-06	6.40e-07	2.05e-06	6.28e-07	2.05e-06	8.69e-06
^{51}Mn	2.65e-04	4.81e-05	2.64e-04	4.77e-05	2.48e-04	9.26e-05
^{52}Mn	3.70e-06	2.42e-06	3.73e-06	2.42e-06	4.78e-06	3.45e-06
^{53}Mn	2.77e-06	1.54e-05	2.81e-06	1.52e-05	3.99e-06	1.06e-04
^{54}Mn	2.38e-10	1.56e-08	3.08e-10	1.72e-08	3.64e-09	5.43e-07
^{52}Fe	3.98e-03	8.09e-03	3.98e-03	8.11e-03	4.08e-03	6.14e-03
^{53}Fe	5.77e-05	5.54e-04	5.83e-05	5.50e-04	8.01e-05	8.92e-04
^{55}Fe	3.69e-07	1.69e-05	3.88e-07	1.66e-05	1.24e-06	3.32e-04
^{59}Fe	2.72e-11	1.07e-10	2.05e-10	1.07e-09	8.18e-10	2.42e-08
^{60}Fe	1.38e-11	1.92e-09	9.32e-11	1.18e-08	4.44e-10	1.89e-06
^{55}Co	3.68e-04	2.87e-03	3.69e-04	2.84e-03	3.82e-04	6.16e-03
^{56}Co	1.01e-06	1.00e-05	1.02e-06	9.96e-06	1.47e-06	2.78e-05
^{57}Co	5.21e-07	2.67e-06	5.43e-07	2.62e-06	1.39e-06	3.86e-05
^{58}Co	1.53e-10	4.51e-09	1.02e-09	6.04e-09	3.38e-08	1.36e-07
^{60}Co	1.28e-11	1.21e-09	1.05e-10	1.17e-08	1.56e-09	5.26e-07
^{56}Ni	2.60e-02	4.93e-01	2.60e-02	4.93e-01	2.65e-02	4.28e-01
^{57}Ni	2.40e-03	8.62e-03	2.40e-03	8.57e-03	2.42e-03	1.45e-02
^{59}Ni	7.59e-05	3.31e-05	7.56e-05	3.29e-05	6.49e-05	6.60e-05
^{63}Ni	5.55e-12	5.83e-10	4.89e-11	5.31e-09	6.79e-10	6.46e-07
^{62}Zn	1.65e-04	1.19e-03	1.65e-04	1.17e-03	1.63e-04	3.45e-03
^{65}Zn	2.41e-07	1.03e-08	2.43e-07	4.42e-08	3.06e-07	1.62e-07
^{65}Ge	4.13e-06	8.10e-07	4.13e-06	8.08e-07	3.88e-06	7.19e-07

Table A.18: Nucleosynthesis yields (in solar masses) for select radioactive nuclides of Model M10_02 with 0.01, 0.1, and $3 Z_{\odot}$.

	M10_02_001		M10_02_01		M10_02_3	
	He det [M_{\odot}]	core det [M_{\odot}]	He det [M_{\odot}]	core det [M_{\odot}]	He det [M_{\odot}]	core det [M_{\odot}]
^{14}C	9.13e-09	4.82e-07	9.25e-09	4.55e-07	1.07e-08	1.09e-06
^{22}Na	4.63e-08	7.63e-09	4.85e-08	7.62e-09	1.15e-07	5.23e-09
^{26}Al	6.68e-06	4.05e-06	6.69e-06	4.08e-06	7.41e-06	1.57e-06
^{32}Si	9.92e-11	2.11e-10	1.67e-10	2.53e-10	2.82e-10	2.52e-08
^{32}P	4.98e-09	8.29e-08	5.13e-09	8.09e-08	5.94e-09	1.31e-06
^{33}P	1.26e-09	5.62e-08	1.33e-09	5.51e-08	2.79e-09	8.13e-07
^{35}S	2.55e-09	6.27e-08	2.74e-09	5.95e-08	6.27e-09	1.94e-06
^{36}Cl	5.32e-09	2.60e-07	5.39e-09	2.52e-07	7.63e-09	1.82e-06
^{37}Ar	1.96e-06	1.45e-05	1.96e-06	1.42e-05	2.17e-06	2.80e-05
^{39}Ar	1.42e-10	2.70e-09	1.08e-09	3.69e-09	1.89e-08	1.44e-07
^{40}K	4.62e-10	1.74e-08	6.79e-10	1.69e-08	6.00e-09	1.51e-07
^{41}Ca	4.61e-06	2.77e-06	4.61e-06	2.71e-06	5.17e-06	5.02e-06
^{44}Ti	5.72e-04	1.99e-05	5.72e-04	1.99e-05	5.54e-04	1.27e-05
^{48}V	2.60e-07	4.18e-08	2.64e-07	4.15e-08	3.83e-07	7.60e-08
^{49}V	5.38e-08	1.38e-07	5.52e-08	1.38e-07	1.08e-07	5.80e-07
^{48}Cr	2.53e-04	4.32e-04	2.51e-04	4.33e-04	1.95e-04	3.05e-04
^{49}Cr	3.59e-06	2.24e-05	3.61e-06	2.22e-05	4.19e-06	3.28e-05
^{51}Cr	1.01e-07	6.76e-07	1.02e-07	6.65e-07	1.30e-07	9.60e-06
^{51}Mn	1.09e-05	5.49e-05	1.09e-05	5.43e-05	9.73e-06	1.06e-04
^{52}Mn	1.46e-07	2.87e-06	1.47e-07	2.87e-06	1.91e-07	4.00e-06
^{53}Mn	6.49e-08	1.76e-05	6.64e-08	1.74e-05	1.29e-07	1.20e-04
^{54}Mn	5.15e-11	1.37e-08	3.21e-10	1.44e-08	1.25e-08	5.87e-07
^{52}Fe	2.91e-05	9.49e-03	2.87e-05	9.51e-03	1.93e-05	7.21e-03
^{53}Fe	1.22e-06	6.44e-04	1.22e-06	6.40e-04	1.19e-06	1.04e-03
^{55}Fe	1.08e-08	1.86e-05	1.37e-08	1.82e-05	1.51e-07	3.72e-04
^{59}Fe	2.37e-09	2.82e-09	2.54e-08	2.89e-08	1.23e-06	8.06e-07
^{60}Fe	1.27e-08	1.21e-08	1.26e-07	1.19e-07	1.41e-06	9.11e-06
^{55}Co	1.27e-06	3.32e-03	1.27e-06	3.29e-03	1.32e-06	7.14e-03
^{56}Co	1.81e-08	1.21e-05	1.97e-08	1.20e-05	8.33e-08	3.24e-05
^{57}Co	1.04e-08	2.94e-06	6.76e-08	2.90e-06	3.05e-06	4.34e-05
^{58}Co	4.09e-10	4.69e-09	4.36e-09	6.07e-09	3.61e-07	1.45e-07
^{60}Co	8.52e-09	5.15e-09	8.40e-08	5.15e-08	7.48e-07	1.09e-06
^{56}Ni	1.80e-06	5.59e-01	1.80e-06	5.59e-01	1.79e-06	4.86e-01
^{57}Ni	2.90e-07	9.28e-03	2.97e-07	9.23e-03	4.86e-07	1.58e-02
^{59}Ni	1.85e-08	3.47e-05	6.98e-08	3.44e-05	2.07e-06	6.96e-05
^{63}Ni	7.22e-10	3.78e-09	7.13e-09	3.65e-08	1.41e-07	1.52e-06
^{62}Zn	5.05e-08	1.27e-03	2.17e-07	1.26e-03	1.84e-06	3.69e-03
^{65}Zn	1.82e-10	9.79e-09	1.43e-09	3.76e-08	1.42e-08	9.24e-08
^{65}Ge	8.47e-10	8.36e-07	2.07e-09	8.34e-07	6.04e-09	7.22e-07

Table A.19: Nucleosynthesis yields (in solar masses) for select radioactive nuclides of Model M10_03 with 0.01, 0.1, and $3 Z_{\odot}$.

	M10_03_001		M10_03_01		M10_03_3	
	He det [M_{\odot}]	core det [M_{\odot}]	He det [M_{\odot}]	core det [M_{\odot}]	He det [M_{\odot}]	core det [M_{\odot}]
^{14}C	8.73e-10	6.33e-08	8.84e-10	5.84e-08	8.62e-10	3.51e-07
^{22}Na	1.96e-08	7.01e-09	2.04e-08	6.99e-09	4.12e-08	4.96e-09
^{26}Al	5.01e-06	3.83e-06	5.00e-06	3.85e-06	5.07e-06	1.49e-06
^{32}Si	7.27e-12	9.32e-11	8.88e-12	9.69e-11	1.12e-11	1.72e-08
^{32}P	1.43e-08	6.92e-08	1.43e-08	6.73e-08	1.50e-08	1.13e-06
^{33}P	8.37e-09	4.71e-08	8.35e-09	4.59e-08	8.74e-09	6.75e-07
^{35}S	1.41e-08	5.25e-08	1.41e-08	4.95e-08	1.57e-08	1.62e-06
^{36}Cl	3.95e-08	2.21e-07	3.94e-08	2.14e-07	4.22e-08	1.54e-06
^{37}Ar	7.91e-06	1.30e-05	7.89e-06	1.28e-05	7.92e-06	2.50e-05
^{39}Ar	5.67e-10	2.20e-09	7.15e-10	2.55e-09	3.91e-09	1.10e-07
^{40}K	4.48e-09	1.46e-08	4.61e-09	1.42e-08	1.00e-08	1.27e-07
^{41}Ca	6.33e-06	2.52e-06	6.32e-06	2.48e-06	6.70e-06	4.54e-06
^{44}Ti	1.05e-03	2.01e-05	1.05e-03	2.02e-05	1.17e-03	1.24e-05
^{48}V	4.48e-07	3.68e-08	4.52e-07	3.66e-08	6.26e-07	6.81e-08
^{49}V	1.12e-07	1.24e-07	1.16e-07	1.24e-07	2.21e-07	5.16e-07
^{48}Cr	1.71e-03	4.03e-04	1.71e-03	4.03e-04	1.55e-03	2.85e-04
^{49}Cr	1.13e-05	2.06e-05	1.13e-05	2.05e-05	1.36e-05	3.06e-05
^{51}Cr	4.72e-07	6.15e-07	4.75e-07	6.07e-07	5.91e-07	8.57e-06
^{51}Mn	6.03e-05	5.08e-05	6.04e-05	5.03e-05	6.14e-05	9.90e-05
^{52}Mn	9.08e-07	2.59e-06	9.08e-07	2.59e-06	9.37e-07	3.64e-06
^{53}Mn	5.24e-07	1.60e-05	5.27e-07	1.59e-05	6.62e-07	1.08e-04
^{54}Mn	8.14e-11	1.25e-08	3.24e-10	1.33e-08	9.76e-09	5.31e-07
^{52}Fe	7.31e-04	8.74e-03	7.24e-04	8.75e-03	5.12e-04	6.66e-03
^{53}Fe	1.22e-05	5.93e-04	1.22e-05	5.89e-04	1.16e-05	9.63e-04
^{55}Fe	5.64e-08	1.70e-05	6.23e-08	1.68e-05	3.26e-07	3.31e-04
^{59}Fe	6.53e-10	1.77e-09	6.99e-09	1.82e-08	4.26e-07	4.55e-07
^{60}Fe	3.80e-09	9.38e-09	3.79e-08	9.12e-08	5.80e-07	7.94e-06
^{55}Co	1.74e-05	3.06e-03	1.73e-05	3.02e-03	1.40e-05	6.61e-03
^{56}Co	1.14e-07	1.19e-05	1.16e-07	1.18e-05	1.97e-07	3.06e-05
^{57}Co	2.59e-08	2.85e-06	6.87e-08	2.82e-06	3.40e-06	3.94e-05
^{58}Co	5.28e-10	4.33e-09	5.48e-09	5.66e-09	4.94e-07	1.31e-07
^{60}Co	2.93e-09	5.03e-09	2.90e-08	5.02e-08	5.19e-07	9.67e-07
^{56}Ni	6.95e-05	6.10e-01	6.85e-05	6.11e-01	4.25e-05	5.32e-01
^{57}Ni	3.37e-06	1.11e-02	3.37e-06	1.10e-02	3.09e-06	1.86e-02
^{59}Ni	9.35e-08	4.59e-05	2.81e-07	4.55e-05	9.02e-06	8.90e-05
^{63}Ni	1.08e-09	3.39e-09	1.04e-08	3.26e-08	1.26e-07	1.45e-06
^{62}Zn	2.42e-07	1.69e-03	5.20e-07	1.67e-03	4.01e-06	4.81e-03
^{65}Zn	2.87e-09	1.15e-08	2.59e-08	3.40e-08	3.17e-07	7.87e-08
^{65}Ge	4.42e-09	1.10e-06	7.68e-09	1.10e-06	2.61e-08	9.23e-07

Table A.20: Nucleosynthesis yields (in solar masses) for select radioactive nuclides of Model M10_05 with 0.01, 0.1, and $3 Z_{\odot}$.

	M10_05_001		M10_05_01		M10_05_3	
	He det [M_{\odot}]	core det [M_{\odot}]	He det [M_{\odot}]	core det [M_{\odot}]	He det [M_{\odot}]	core det [M_{\odot}]
^{14}C	1.41e-12	1.03e-08	1.64e-12	9.76e-09	8.35e-12	4.47e-08
^{22}Na	3.59e-09	7.16e-09	3.71e-09	8.19e-09	7.09e-09	6.42e-09
^{26}Al	1.11e-07	3.88e-06	1.11e-07	3.89e-06	1.24e-07	1.64e-06
^{32}Si	2.44e-12	8.01e-10	2.54e-12	8.60e-11	2.90e-12	6.30e-09
^{32}P	1.97e-08	9.13e-08	2.00e-08	8.83e-08	2.12e-08	1.50e-06
^{33}P	1.59e-08	7.06e-08	1.61e-08	6.81e-08	1.71e-08	1.02e-06
^{35}S	5.37e-09	7.25e-08	5.33e-09	6.83e-08	5.50e-09	2.46e-06
^{36}Cl	7.84e-08	3.19e-07	7.82e-08	3.09e-07	8.05e-08	2.47e-06
^{37}Ar	5.40e-06	1.49e-05	5.35e-06	1.46e-05	5.59e-06	2.71e-05
^{39}Ar	2.36e-10	3.24e-09	2.30e-10	3.12e-09	2.63e-10	8.73e-08
^{40}K	1.86e-09	2.33e-08	1.82e-09	2.21e-08	2.17e-09	2.12e-07
^{41}Ca	1.84e-06	2.74e-06	1.84e-06	2.69e-06	2.42e-06	4.77e-06
^{44}Ti	7.79e-04	2.42e-05	7.80e-04	2.43e-05	8.10e-04	1.37e-05
^{48}V	4.79e-07	5.44e-08	4.86e-07	5.40e-08	7.56e-07	8.20e-08
^{49}V	1.85e-07	1.43e-07	1.87e-07	1.43e-07	2.72e-07	6.16e-07
^{48}Cr	2.06e-03	3.95e-04	2.06e-03	3.96e-04	2.15e-03	2.75e-04
^{49}Cr	2.03e-05	2.02e-05	2.05e-05	2.01e-05	2.61e-05	2.96e-05
^{51}Cr	1.07e-06	6.55e-07	1.07e-06	6.49e-07	1.27e-06	9.06e-06
^{51}Mn	1.47e-04	4.98e-05	1.47e-04	4.93e-05	1.58e-04	9.63e-05
^{52}Mn	4.23e-06	2.81e-06	4.27e-06	2.80e-06	5.45e-06	3.80e-06
^{53}Mn	2.40e-06	1.60e-05	2.43e-06	1.59e-05	3.42e-06	1.11e-04
^{54}Mn	2.78e-10	1.38e-08	3.49e-10	1.58e-08	3.43e-09	5.76e-07
^{52}Fe	4.02e-03	8.42e-03	4.03e-03	8.43e-03	4.36e-03	6.39e-03
^{53}Fe	5.53e-05	5.75e-04	5.59e-05	5.71e-04	7.56e-05	9.27e-04
^{55}Fe	4.09e-07	1.77e-05	4.22e-07	1.74e-05	1.08e-06	3.47e-04
^{59}Fe	9.45e-12	6.17e-10	7.11e-11	6.38e-09	6.18e-10	1.31e-07
^{60}Fe	7.26e-12	3.88e-09	6.09e-11	3.51e-08	7.48e-10	4.85e-06
^{55}Co	4.77e-04	2.96e-03	4.78e-04	2.93e-03	4.93e-04	6.37e-03
^{56}Co	1.33e-06	1.51e-05	1.34e-06	1.50e-05	1.84e-06	3.30e-05
^{57}Co	4.61e-07	2.97e-06	4.83e-07	2.92e-06	1.43e-06	4.05e-05
^{58}Co	1.54e-10	4.61e-09	1.00e-09	7.07e-09	4.24e-08	1.46e-07
^{60}Co	1.07e-11	3.41e-09	1.00e-10	3.36e-08	2.27e-09	1.05e-06
^{56}Ni	8.32e-03	5.56e-01	8.31e-03	5.57e-01	8.07e-03	4.84e-01
^{57}Ni	5.75e-04	1.01e-02	5.75e-04	1.00e-02	5.71e-04	1.69e-02
^{59}Ni	5.36e-06	4.35e-05	5.39e-06	4.31e-05	7.93e-06	8.35e-05
^{63}Ni	6.77e-12	1.58e-09	6.42e-11	1.51e-08	1.06e-09	1.34e-06
^{62}Zn	5.98e-05	1.57e-03	6.04e-05	1.55e-03	8.24e-05	4.48e-03
^{65}Zn	6.44e-08	1.57e-08	6.96e-08	6.41e-08	1.93e-07	1.95e-07
^{65}Ge	1.52e-06	1.26e-06	1.52e-06	1.25e-06	1.51e-06	1.10e-06

Table A.21: Nucleosynthesis yields (in solar masses) for select radioactive nuclides of Model M10_10 with 0.01, 0.1, and $3 Z_{\odot}$.

	M10_10_001		M10_10_01		M10_10_3	
	He det [M_{\odot}]	core det [M_{\odot}]	He det [M_{\odot}]	core det [M_{\odot}]	He det [M_{\odot}]	core det [M_{\odot}]
^{14}C	3.58e-14	7.47e-16	7.04e-14	7.84e-16	1.08e-12	2.09e-15
^{22}Na	1.25e-08	3.21e-13	1.22e-08	3.20e-13	6.93e-09	1.65e-10
^{26}Al	8.09e-07	1.46e-10	7.98e-07	1.50e-10	5.20e-07	5.55e-11
^{32}Si	4.10e-13	2.13e-13	5.85e-13	2.19e-13	5.18e-13	6.99e-12
^{32}P	3.87e-09	1.77e-09	3.93e-09	1.78e-09	4.29e-09	1.01e-08
^{33}P	1.58e-09	1.12e-09	1.63e-09	1.12e-09	1.78e-09	9.16e-09
^{35}S	8.28e-10	8.03e-10	8.54e-10	7.88e-10	9.10e-10	5.69e-09
^{36}Cl	8.25e-09	7.97e-09	8.24e-09	7.82e-09	8.67e-09	3.00e-08
^{37}Ar	1.63e-06	1.66e-06	1.62e-06	1.63e-06	1.65e-06	4.09e-06
^{39}Ar	4.45e-11	6.70e-11	4.50e-11	6.45e-11	5.23e-11	4.16e-10
^{40}K	3.04e-10	4.33e-10	3.00e-10	4.18e-10	3.91e-10	1.70e-09
^{41}Ca	3.19e-07	4.10e-07	3.21e-07	4.03e-07	4.78e-07	8.56e-07
^{44}Ti	2.68e-04	2.04e-05	2.68e-04	2.04e-05	2.78e-04	1.25e-05
^{48}V	1.28e-07	2.54e-08	1.28e-07	2.54e-08	2.28e-07	2.60e-08
^{49}V	4.58e-08	8.20e-08	4.62e-08	8.14e-08	7.37e-08	1.66e-07
^{48}Cr	5.30e-04	4.14e-04	5.32e-04	4.14e-04	5.96e-04	3.00e-04
^{49}Cr	9.11e-06	2.00e-05	9.16e-06	1.99e-05	1.11e-05	3.16e-05
^{51}Cr	3.81e-07	2.28e-07	3.79e-07	2.23e-07	4.86e-07	2.04e-06
^{51}Mn	8.48e-05	4.88e-05	8.46e-05	4.83e-05	7.91e-05	1.02e-04
^{52}Mn	1.10e-06	2.52e-06	1.11e-06	2.52e-06	1.47e-06	3.11e-06
^{53}Mn	1.66e-06	1.32e-05	1.67e-06	1.31e-05	2.55e-06	3.98e-05
^{54}Mn	1.71e-09	1.37e-09	1.76e-09	1.50e-09	1.12e-08	6.67e-08
^{52}Fe	1.96e-03	9.26e-03	1.97e-03	9.28e-03	2.05e-03	7.19e-03
^{53}Fe	5.34e-05	6.10e-04	5.36e-05	6.06e-04	6.39e-05	1.03e-03
^{55}Fe	1.77e-06	3.22e-06	1.80e-06	3.00e-06	3.65e-06	8.56e-05
^{59}Fe	7.84e-13	3.86e-10	5.87e-12	8.77e-16	4.55e-11	6.54e-11
^{60}Fe	1.60e-13	1.57e-09	9.65e-13	2.09e-17	1.60e-12	3.40e-11
^{55}Co	2.50e-04	3.16e-03	2.51e-04	3.13e-03	2.74e-04	7.15e-03
^{56}Co	7.09e-07	1.24e-05	7.17e-07	1.23e-05	9.47e-07	3.08e-05
^{57}Co	3.22e-07	1.17e-06	3.30e-07	1.12e-06	6.31e-07	1.19e-05
^{58}Co	3.28e-10	4.92e-10	4.63e-10	4.41e-10	5.09e-09	1.61e-08
^{60}Co	2.96e-13	6.85e-11	2.26e-12	4.86e-14	3.61e-11	7.93e-11
^{56}Ni	3.95e-02	7.45e-01	3.95e-02	7.45e-01	3.89e-02	6.52e-01
^{57}Ni	1.37e-03	1.41e-02	1.37e-03	1.40e-02	1.50e-03	2.49e-02
^{59}Ni	5.24e-05	6.09e-05	5.19e-05	6.04e-05	3.69e-05	1.41e-04
^{63}Ni	1.41e-13	2.85e-09	1.19e-12	4.59e-13	2.23e-11	1.61e-10
^{62}Zn	9.91e-05	2.25e-03	9.89e-05	2.21e-03	9.57e-05	6.05e-03
^{65}Zn	2.51e-08	1.19e-08	2.52e-08	1.19e-08	2.77e-08	1.01e-08
^{65}Ge	3.17e-06	1.42e-06	3.16e-06	1.42e-06	2.97e-06	1.13e-06

Table A.22: Nucleosynthesis yields (in solar masses) for select radioactive nuclides of Model M11_05 with 0.01, 0.1, and $3 Z_{\odot}$.

	M11_05_001		M11_05_01		M11_05_3	
	He det [M_{\odot}]	core det [M_{\odot}]	He det [M_{\odot}]	core det [M_{\odot}]	He det [M_{\odot}]	core det [M_{\odot}]
^{14}C	1.02e-12	1.39e-16	1.15e-12	1.46e-16	5.25e-12	4.72e-16
^{22}Na	7.64e-09	1.36e-13	7.56e-09	1.35e-13	6.16e-09	6.06e-10
^{26}Al	2.78e-07	3.39e-11	2.75e-07	3.48e-11	2.00e-07	1.71e-11
^{32}Si	5.17e-13	3.42e-14	5.32e-13	6.53e-14	6.65e-13	9.46e-13
^{32}P	5.12e-09	4.12e-10	5.18e-09	4.19e-10	5.77e-09	2.17e-09
^{33}P	1.91e-09	2.25e-10	1.94e-09	2.35e-10	2.18e-09	1.75e-09
^{35}S	1.04e-09	1.92e-10	1.05e-09	1.93e-10	1.18e-09	1.37e-09
^{36}Cl	1.24e-08	2.21e-09	1.24e-08	2.17e-09	1.36e-08	8.57e-09
^{37}Ar	3.56e-06	8.71e-07	3.56e-06	8.60e-07	3.93e-06	1.93e-06
^{39}Ar	6.85e-11	2.07e-11	6.88e-11	2.01e-11	8.86e-11	1.39e-10
^{40}K	6.61e-10	1.70e-10	6.62e-10	1.65e-10	8.37e-10	6.83e-10
^{41}Ca	9.97e-07	2.58e-07	1.00e-06	2.55e-07	1.30e-06	4.85e-07
^{44}Ti	1.53e-04	2.05e-05	1.53e-04	2.05e-05	1.74e-04	1.15e-05
^{48}V	9.25e-08	1.90e-08	9.44e-08	1.90e-08	1.85e-07	1.77e-08
^{49}V	6.15e-08	5.94e-08	6.21e-08	5.90e-08	9.53e-08	1.12e-07
^{48}Cr	7.16e-04	3.52e-04	7.19e-04	3.53e-04	8.03e-04	2.57e-04
^{49}Cr	1.38e-05	1.62e-05	1.39e-05	1.61e-05	1.66e-05	2.67e-05
^{51}Cr	2.25e-07	1.57e-07	2.29e-07	1.56e-07	4.43e-07	8.98e-07
^{51}Mn	3.12e-05	4.00e-05	3.14e-05	3.96e-05	3.59e-05	8.71e-05
^{52}Mn	8.78e-07	1.91e-06	8.86e-07	1.91e-06	1.17e-06	2.26e-06
^{53}Mn	2.42e-06	9.85e-06	2.44e-06	9.79e-06	3.72e-06	2.33e-05
^{54}Mn	4.42e-09	7.53e-10	4.64e-09	1.09e-09	1.98e-08	2.86e-08
^{52}Fe	2.04e-03	7.79e-03	2.04e-03	7.80e-03	2.23e-03	6.09e-03
^{53}Fe	6.94e-05	5.06e-04	6.97e-05	5.03e-04	7.79e-05	8.74e-04
^{55}Fe	4.55e-06	1.85e-06	4.60e-06	1.89e-06	7.97e-06	3.42e-05
^{59}Fe	5.94e-12	1.69e-17	4.37e-11	1.60e-16	1.46e-10	5.21e-11
^{60}Fe	2.83e-12	9.92e-20	1.68e-11	3.32e-18	1.14e-11	2.51e-11
^{55}Co	2.10e-04	2.63e-03	2.10e-04	2.61e-03	2.24e-04	6.11e-03
^{56}Co	8.28e-07	1.23e-05	8.35e-07	1.23e-05	1.04e-06	2.63e-05
^{57}Co	5.44e-07	1.13e-06	5.51e-07	1.15e-06	1.01e-06	5.85e-06
^{58}Co	9.70e-10	2.38e-10	1.16e-09	3.29e-10	7.19e-09	6.47e-09
^{60}Co	2.78e-12	4.02e-15	1.80e-11	1.46e-14	7.02e-11	5.90e-11
^{56}Ni	1.24e-02	8.47e-01	1.23e-02	8.48e-01	1.14e-02	7.46e-01
^{57}Ni	3.03e-04	1.77e-02	3.03e-04	1.76e-02	2.99e-04	3.35e-02
^{59}Ni	4.36e-06	7.82e-05	4.30e-06	7.76e-05	3.04e-06	2.24e-04
^{63}Ni	6.87e-13	8.60e-15	5.30e-12	8.55e-14	4.06e-11	1.12e-10
^{62}Zn	2.09e-05	3.08e-03	2.10e-05	3.04e-03	2.24e-05	7.57e-03
^{65}Zn	2.04e-09	1.43e-08	2.15e-09	1.43e-08	5.73e-09	1.12e-08
^{65}Ge	8.14e-07	2.04e-06	8.07e-07	2.04e-06	6.46e-07	1.53e-06